

ARCHIVES

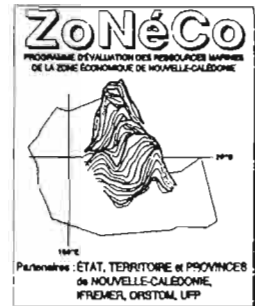
SCIENCES DE LA MER

OCÉANOGRAPHIE PHYSIQUE

N° 11

1999

ZoNéCo et l'environnement physique :  
Impacts du phénomène El Niño / Southern  
Oscillation (ENSO) dans le sud-ouest Pacifique  
et Upwelling Néo-Calédonien



Christian HENIN

**ARCHIVES**

**SCIENCES DE LA MER**

**OCÉANOGRAPHIE PHYSIQUE**

**N° 11**

**1999**

**ZoNéCo et l'environnement physique :  
Impacts du phénomène El Niño / Southern Oscillation  
(ENSO) dans le sud-ouest Pacifique et Upwelling  
Néo-Calédonien**

**Christian HENIN**



**Institut de recherche  
pour le développement**

© IRD, Nouméa, 1999

/Henin, C.

ZoNéCo et l'environnement physique : Impacts du phénomène El Niño / Southern Oscillation (ENSO) dans le sud-ouest Pacifique et Upwelling Néo-Calédonien

Nouméa : IRD. juillet 1999. 72 p.  
Archives : *Sci. Mer ; Océanogr. Phys* ; 11

EAU DE MER ; CARACTERISTIQUE CHIMIQUE ; CARACTERISTIQUE PHYSIQUE ; ZONE ECONOMIQUE EXCLUSIVE ; SURVEILLANCE ; TEMPERATURE ; SALINITE / NOUVELLE CALEDONIE

**ZoNéCo et l'environnement physique :  
Impacts du phénomène  
El Nino / Southern Oscillation (ENSO)  
dans le sud-ouest Pacifique  
et Upwelling Néo-Calédonien.**

**Christian Hénin**  
Centre IRD (ex ORSTOM) de Nouméa

## INTRODUCTION

L'océan Pacifique est le plus grand des océans dont la superficie est égale à celle des terres immergées de la planète. En zone tropicale il couvre une distance zonale de 20 000 km c'est à dire environ la moitié de la circonférence du globe. Cette dimension et la distribution de la température de surface font que l'océan Pacifique est un des éléments clés du climat du globe, spécialement aux échelles de temps interannuelles en relation avec le phonème ENSO (El Nino - Southern Oscillation).

Ce phénomène ENSO se manifeste dans la région du sud-ouest Pacifique où se trouve la Nouvelle-Calédonie par une variabilité marquée des pluies, du régime des vents, des courants océaniques, de la température et de la salinité des eaux marines. La figure 1 présente l'évolution de l'Indice d'Oscillation Australe (SOI pour Southern Oscillation Index) qui utilise la différence de pression atmosphérique entre Tahiti (Polynésie Française) et Darwin (Australie). Les années de SOI négative, inférieure à -1, sont nommées années El Nino (par exemple 1972, 1982-83, 1987, 1992, 1997) et les années de valeur positive de SOI sont des années La Nina (par exemple 1988-89, 1998 etc.). A l'échelle globale cet indice est très utilisé pour définir la situation climatique.

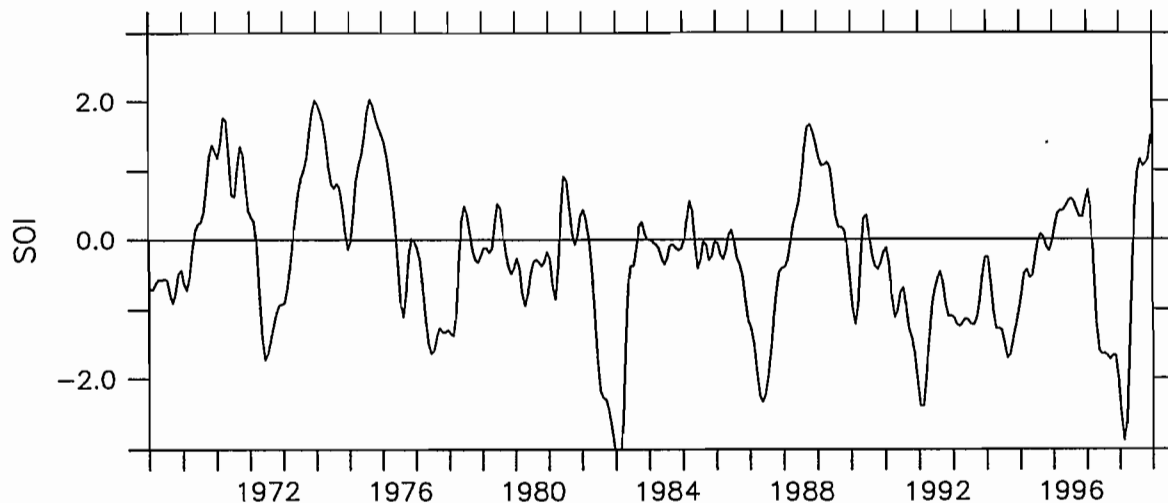


Figure 1 : Indice d'Oscillation Australe;  
les valeurs mensuelles ont été lissées par un filtre Hanning de 3 mois.

### AMELIORATION DES RESEAUX D'OBSERVATION

Afin d'étudier le phénomène ENSO, les océanographes du centre ORSTOM de Nouméa ont mis en place depuis 1969 un réseau d'observations de surface (seau météorologique) par navires de commerce (Donguy et Hénin, 1976) dans le Pacifique intertropical. Les observations se sont étendues à la subsurface en 1979 lorsque les XBT (Expendable Bathymographs) ont été installés sur ces navires grâce à une collaboration entre la Scripps Institution of Oceanography (Californie), l'IFREMER (Brest) et l'ORSTOM (Nouméa). Ces réseaux ont été modernisés en 1990 par l'installation de systèmes de mesures automatiques de la température et de la salinité (thermosalinographies) (Henin et Grelet, 1996). Parallèlement des observations automatiques de T et S en des stations côtières ont été mises en place (Henin et Grelet, 1992) tout en maintenant les observations quotidiennes manuelles par des observateurs.

Le programme ZoNeCo participe activement aux observations systématiques réalisées dans la zone économique de la Nouvelle-Calédonie. C'est ainsi que le programme prend en charge une partie du financement de sondes XBT lancées chaque année dans la zone 10°S-30°S / 155°E-180°. D'autre part les nouvelles stations côtières automatiques mises en place autour de la Nouvelle-Calédonie ont bénéficié d'un financement ZoNéCo pour leur installation et leur fonctionnement annuel. Enfin, un navire de commerce assurant des liaisons maritimes entre les îles Loyautés, l'Île des Pins, et Nouméa a été équipé d'un thermosalinomètre grâce à un financement exclusif ZoNéCo en 1995.

## RESULTATS SCIENTIFIQUES :

Les observations réalisées en zone néo-calédonienne dans le cadre du programme ZoNeCo font partie intégrante de l'effort international CLIVAR (Climate Variability and Prediction) permettant d'entreprendre des recherches afin de comprendre les mécanismes océaniques responsables du climat au sens large. Au niveau régional elles permettent d'expliquer les « anomalies » observées dans le domaine du climat, de la circulation océanique et de la pêche hauturière. Par ces observations la Nouvelle-Calédonie non seulement permet d'améliorer la connaissance de son environnement mais également contribue aux progrès accomplis en matière climatique et océanographique.

Le Pacifique sud-ouest a fait l'objet de recherches sur le phénomène ENSO (El Nino - Southern Oscillation) depuis une vingtaine d'années par les océanographes du Centre ORSTOM de Nouméa basées sur les rares observations disponibles telles que celles des campagnes de recherche. Depuis la mise en place des réseaux d'observation et le lancement de satellites instrumentés la recherche a beaucoup progressé.

Une grande partie des observations obtenues dans le cadre de ZoNéCo et/ou aux environs de la Nouvelle-Calédonie a été utilisée dans des articles publiés et/ou proposés dans les revues océanographiques spécialisées traitant du phénomène ENSO. Les dernières observations ont plus particulièrement traité de l'événement El Nino de 1997-98 et La Nina qui s'est mis en place en mai 1998.

Sont présentés ci après les articles suivants publiés, soumis ou en fin de rédaction de l'équipe de recherche du programme ECOP (Etudes Climatiques de l'Océan Pacifique) de l'IRD-Nouméa. Il s'agit principalement travaux sur le phénomène ENSO dans le Pacifique tropical sud-ouest, mais également de la mise en évidence du phénomène purement côtier de l'upwelling calédonien.

-Delcroix T., O. Lenormand, 1997. ENSO signals in the vicinity of New-Caledonia, south-western Pacific. *Oceanologica Acta* , 20, N°2, 1-11.

-Hénin C., Y. duPenhoat, M.Ioualalen, 1998. Observations of Sea Surface Salinity in the Western Pacific fresh Pool : Large-scale changes during 1992-1995 *Journal of Geophysical Research* , Vol 103, C4, 7523-7536

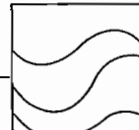
- Delcroix T., L. Gourdeau et C. Hénin, 1998. Sea surface salinity changes along the Fiji-Japan shipping track during the 1996 La Niña and 1997 El Niño period. *Geophys. Res. Letter*, 25, 3169-3172.
- Ioualalen M and C. Hénin, Thermohaline variability of the western tropical Pacific during 1998 : on the erosion / reconstitution of the fresh pool (*Soumis à Geophysical Research Letter*)
- Hénin C., Stations côtières de Nouvelle-Calédonie et variabilité thermique. Mise en évidence d'un upwelling côtier (*Version provisoire*)

## BIBLIOGRAPHIE

Enfin un certain nombre de travaux, antérieurs au programme ZoNéCo et/ou financés en dehors de ce programme mais traitant de la variabilité climatique du Pacifique sud-ouest et de la circulation océanique régionale sont référencés ci après:

- Alory G. and T. Delcroix, 1999, Climatic variability in the vicinity of Wallis, Futuna and Samoa islands (13°S-15°S / 180°-170°W). *Oceanologica Acta* (sous presse)
- Crowley T. J., T. M. Quinn, F.W. Taylor, C. Hénin and P. Joannot, 1997. Evidence for a volcanic cooling signal in a 335-year coral record from New Caledonia. *Paleoceanography*, Vol 12, N°5, 633-639
- Delcroix Th and C.Hénin, 1989 : Mechanisms of subsurface thermal structure and sea-surface thermohaline variabilities in the southwestern tropical Pacific during 1979-85. *Journal of Marine Research*, 47, 777-812
- Delcroix T., C. Hénin, V. Porte and P. Arkin, 1996, Precipitation and sea-surface salinity in the tropical Pacific. *Deep Sea Research*, 43, 1123-1141.
- Delcroix T., 1998, Observed surface oceanic and atmospheric variability in the Tropical Pacific at seasonal and ENSO time scales : a tentative overview. *J. Geophys. Res.*, 103, 18611-18633.
- Delcroix T. and J. Picaut , 1998, Zonal displacement of the western Pacific fresh pool. *J. Geophys. Res.* , 103, 1087-1098.
- Hénin C., JM Guillerm, L.Chabert, 1984. Circulation superficielle autour de la Nouvelle-Calédonie. *Océanographie Tropicale*, 19 (2), 113-126
- Hénin C., J. Grelet, 1996, A Merchant Ship Thermosalinograph Network in the Pacific Ocean. *Deep Sea Resarch*, Vol 43, Iss 11-12, pp 1833-1855

- Morliere A. and JP Rébert, 1986. Rainfall shortage and El Nino Southern Oscillation in New Caledonia, southwestern Pacific. *Mon Weather Rev.*, **114**, 1131-1137.
- Quinn T.M., T.J. Crowley, F.W. Taylor, C.Hénin, P.Joannot, Y. Join, 1998. A multicentury stable isotope record from a New Caledonia coral : Interannual and decadal SST variability in the southwest Pacific since 1657. *Paleoceanography* , Vol 13, N°4, pp 412-426



El Niño  
Southern Oscillation  
New Caledonia

El Niño  
Oscillation Australe  
Nouvelle Calédonie

# ENSO signals in the vicinity of New Caledonia, South Western Pacific

Thierry DELCROIX <sup>a</sup> and Olivier LENORMAND <sup>b</sup>

<sup>a</sup> Groupe SURTROPAC, Institut Français de Recherche Scientifique pour le Développement en Coopération (ORSTOM), BP A5, Nouméa Cedex, New Caledonia.

<sup>b</sup> Centre d'Océanologie de l'Université d'Aix-Marseille II, Campus de Luminy, case 901, F 13288 Marseille Cedex 9, France  
et École Supérieure d'Ingénieurs de Marseille (ESIM), Institut Méditerranéen de Technologie, Technopole de Château-Gombert, F 13451 Marseille Cedex 20, France.

Received 28/09/95, in revised form 05/07/96, accepted 12/07/96.

## ABSTRACT

Data collected in an area enclosing New Caledonia are analysed both for the open ocean ( $17^{\circ}\text{S}$ - $27^{\circ}\text{S}$ ,  $160^{\circ}\text{E}$ - $170^{\circ}\text{E}$ ; 1972-1992) and for one point in its lagoon (1967-1993), in order to improve our knowledge of the regional environment, with emphasis on seasonal and interannual (*i.e.* ENSO) variability. Long-term means and seasonal changes in surface wind, sea-surface temperature and salinity, and 0-400 m temperature, salinity and zonal geostrophic current are first described to set the context. Through comparisons with the Southern Oscillation Index (SOI), it is demonstrated that there are signals in these parameters that are connected with ENSO. During the warm phase of ENSO (SOI < 0, El Niño), we observed saltier-than-average anomalies in sea-surface salinity ( $\sim 0.2$ ), 0-50 m cold temperature anomalies ( $\sim 0.5^{\circ}\text{C}$ ) contrasting with the well-known warm eastern equatorial Pacific anomalies, together with westerly ( $\sim 10 \text{ m}^2 \text{ s}^{-2}$ ) and southerly ( $\sim 4 \text{ m}^2 \text{ s}^{-2}$ ) wind anomalies over a large part of the studied area. Conversely, anomalies of similar magnitude but of opposite sign were detected during the cold phase of ENSO (SOI > 0; La Niña). The mechanisms which connect these regional anomalies to ENSO evolution at low-latitudes are qualitatively discussed.

## RÉSUMÉ

### De la signature d'ENSO au voisinage de la Nouvelle Calédonie.

Un ensemble de données, collectées au voisinage de la Nouvelle Calédonie ( $17^{\circ}\text{S}$ - $27^{\circ}\text{S}$ ,  $160^{\circ}\text{E}$ - $170^{\circ}\text{E}$ ) et dans son lagon au cours des 20 à 30 dernières années, est analysé afin d'améliorer notre connaissance de l'environnement régional et de sa variabilité à l'échelle saisonnière et interannuelle (ENSO). Les structures moyennes et les variations saisonnières du vent de surface, de la température de la mer, de la salinité et du courant géostrophique zonal entre 0 et 400 m sont d'abord décrites. Les anomalies liées à ENSO sont ensuite identifiées pour chaque paramètre par comparaison à l'indice d'oscillation australe. Au cours des événements El Niño, la salinité de surface présente des anomalies positives de l'ordre de 0,2, la couche 0-50 m se refroidit d'environ  $0,5^{\circ}\text{C}$  (contrairement au fort réchauffement observé dans le Pacifique équatorial est), la composante méridienne du vent s'intensifie ( $\sim 4 \text{ m}^2 \text{ s}^{-2}$ ) alors que la composante zonale diminue ( $\sim 10 \text{ m}^2 \text{ s}^{-2}$ ). Les anomalies observées pendant les événements El Niño sont de signes contraires pendant les événements La Niña. Les mécanismes liant les anomalies régionales aux anomalies observées au voisinage de l'équateur sont discutés qualitativement.

*Oceanologica Acta*, 1997, 20, 3, 481-491.

## INTRODUCTION

The Southern Oscillation (SO) refers to a seesaw in surface pressure anomalies between the Austral-Asian region and the southeastern tropical Pacific. It was first surmised in the work of Hildebrandsson (1897) who evidenced an out-of-phase relationship between surface pressure anomalies at Sydney, Australia, and Buenos-Aires, Argentina. The landmark papers of Walker (1923, 1924) then described the SO-related salient features of surface pressure, temperature and precipitation changes over the tropical Indian and Pacific oceans. Later, a significant new dimension of the SO was provided by Berlage (1966), Bjerknes (1966) and Wyrtki (1975), who documented the remarkable link between interannual Sea Surface Temperature (SST) changes along the Peru and Ecuador coast, previously attributed to the "local" El Niño phenomenon, and the SO-related changes in large-scale precipitation and wind regime. In 1975, Wyrtki postulated that the interannual SST changes in the eastern equatorial Pacific result from a remote response to equatorial winds in the western and central Pacific. Wyrtki's work revealed the dynamic coupling between El Niño and the SO. This ocean-atmosphere coupling was further confirmed by results of equatorial models (McCreary and Anderson, 1991). Nowadays, the label ENSO (El Niño Southern Oscillation) denotes a basin-scale ocean-atmosphere phenomenon.

The tropical regions are the area of the globe most directly affected by ENSO: the associated meteorological and oceanographic changes have been documented for the tropical Atlantic Ocean (*e.g.* Delecluse *et al.*, 1994), for the tropical Indian Ocean (*e.g.* Cadet, 1985), and abundantly for the tropical Pacific Ocean (*e.g.* Rasmusson and Carpenter, 1982). On a global basis, the relationships between ENSO and large-scale precipitation, surface air and sea-surface temperature patterns were discussed by Ropelewski and Halpert (1987), Halpert and Ropelewski (1992) and Trenberth and Hoar (1996). These authors demonstrated that the strongest relationships indeed occur in the tropics, although ENSO signals clearly show up in some sub-tropical regions. In particular, and in contrast with several other regions of the globe, they pointed out that the south central and western Pacific region experiences air and sea-surface temperature anomalies that are out of phase with other regions affected by ENSO. Specifically, in an area extending approximately from 10°S-40°S, 160°E-150°W, the air and sea-surface temperatures appear anomalously cold during warm episodes (El Niño, negative Southern Oscillation Index) and anomalously warm during cold episodes (La Niña, positive SOI).

The south central and western Pacific region, alluded to earlier, is located roughly south of the mean SPCZ (South Pacific Convergence Zone) position and encompasses several island nations and territories, including New Caledonia, Fiji, Vanuatu, part of New Zealand and French Polynesia, all of which suffer economically and ecologically from ENSO effects. In this region, several studies have already highlighted the link between ENSO and regional atmospheric and oceanic anomalies, such as air temperature, rainfall, wind speed and direction, SST,

Sea Surface Salinity (SSS), and zonal surface current (*e.g.* Gordon, 1986; Morlière and Rébert, 1986, Delcroix and Hénin, 1989). As a complement to these earlier works, and given the regional ENSO peculiarity, the aim of the present study is to analyse the ENSO signature in the New Caledonia sector. This will be based on extensive observational data sets including SST, SSS, subsurface temperature and salinity profiles and surface wind.

The organization of the paper is as follows. In the next section, the data and data processing will be presented. Then, long-term averages will be discussed in order to set the context, and seasonal changes will be examined since they generally account for a large part of the variability in sub-tropical regions: this section also provides a convenient summary of the knowledge gained from past regional studies. In the following section, emphasis will be put on ENSO-related anomalies in order to identify the signature of ENSO, if any, upon the analysed parameters. Conclusion and discussion will be given in the last section.

## DATA AND DATA PROCESSING

The oceanic surface measurements (SST and SSS) were derived from sea-water samples collected as part of an ORSTOM ship-of-opportunity programme (SOP) operated from Nouméa, New Caledonia, since 1969 (see the article by Donguy, 1987, and its references). Although quoted as "surface" measurements, it should be noted that the SST and SSS data are in fact representative of the water layer between the surface and about 8 m, depending on the ship draft and load. The ORSTOM-SOP measurements have already been used in the literature, for example, in the analysis of seasonal and interannual variations of SSS and SST in the tropical Pacific (Delcroix and Hénin, 1991; Delcroix, 1993). As detailed in these last references, measurements of SST and SSS are routinely validated before entering the ORSTOM data base, through procedures that check for flagrant errors, internal consistency of data pertaining to each voyage and climatic limits. The expected accuracy of a given measurement is of the order of 0.1 for SSS and of 0.3 °C for SST.

In the vicinity of New Caledonia (17°S-27°S, 161°E-171°E; Fig. 1a), the ORSTOM-SOP collected about 12,000 SST and SSS data during the 1972-1992 period. Details concerning the time-space distribution of these data are given in Lenormand (1995). Following the routine subjective validation, additional validation tests were applied to the selected values of Figure 1a. Spurious measurements were detected through objective criteria based on multiples ( $\pm 5$ ,  $\pm 4$ , and  $\pm 3.5$ ) of sample standard deviations computed in 1° latitude bands. The resulting assumed spurious measurements (< 1%) were rejected. Based on the validated data, maps of the long-term mean SST and SSS (1972-1992) are displayed in Figure 2a,b; they will be discussed in the following section. At this stage, we note that the spatial SST and SSS changes are generally greater in the meridional than in the zonal direction.

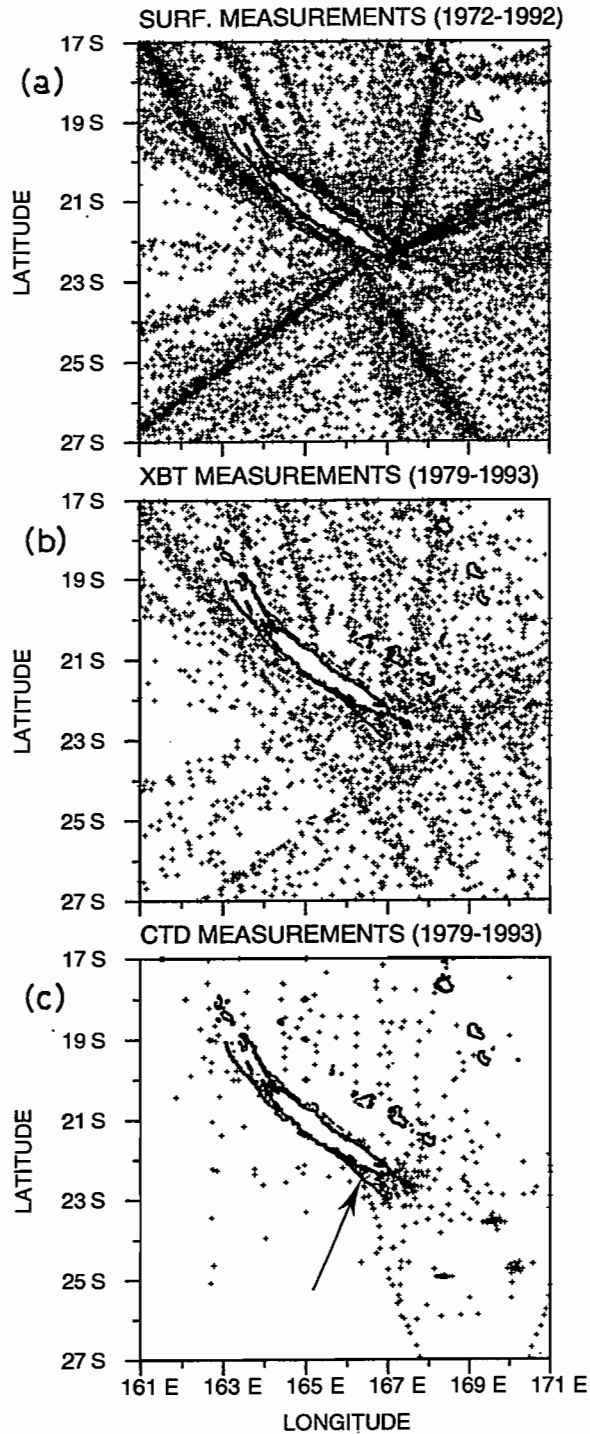


Figure 1

Spatial distribution of (a) sea-surface temperature and salinity, (b) XBT, and (c) subsurface temperature and salinity measurements collected in the vicinity of New Caledonia during the reported time periods. The arrow in (c) indicates the location of the Amédée Lighthouse.

In order to analyse changes in SST and SSS fields, the irregularly-distributed longitude-latitude-time SST and SSS data were interpolated (or averaged, as appropriate) on to a regular 1-month by 1°-latitude grid, from 27°S to 17°S and from January 1972 to December 1992. This was performed through an objective interpolation scheme (Laplacian method), in a manner similar to Delcroix and Hénin (1991).

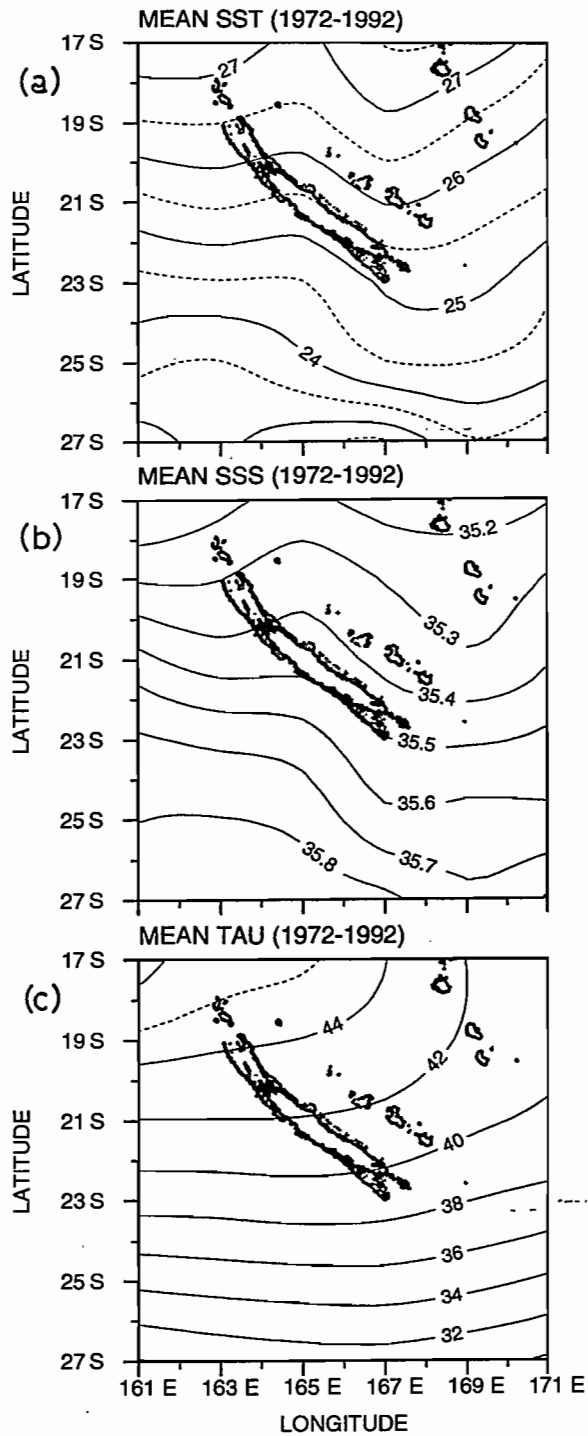


Figure 2

Mean (a) sea-surface temperature, (b) sea-surface salinity, and (c) pseudo wind stress modulus. Units are °C and  $m^2 s^{-2}$  in (a) and (c), respectively. All values are averaged over the 1972-1992 period.

This latitude-time gridding procedure was done ignoring the longitude of measurements within 161°E-171°E, on the grounds that the information lost does not severely bias the gridded fields given the tendency for meridional gradients to dominate zonal gradients (Fig. 2a,b) and the 15° zonal decorrelation scale in SST (White *et al.*, 1985). On an average, a gridded value represents 4.3 observations collected during a given month, within a 1° latitude band and within 161°E-171°E longitude. The rms error is thus

roughly reduced by  $4.3^{1/2}$  and we believe that the overall accuracy of one gridded value is better than 0.1 for SSS and  $0.3^{\circ}\text{C}$  for SST.

A more comprehensive SST and SSS data set is available at Amédée Lighthouse ( $22^{\circ}29'\text{S}$ - $166^{\circ}28'\text{E}$ ) which is located in the lagoon close to a pass through the reef barrier, about twelve nautical miles south of Nouméa, New Caledonia (see Fig. 1c). Such a data set enables us to compare open-ocean and lagoon waters as far as seasonal and ENSO signals are concerned. It consists of daily observations taken between 5 and 9 AM during the period 1967-1994. When necessary, values of SST have been extrapolated to 7 AM based on a mean diurnal cycle which indicates an almost linear increase of  $0.1^{\circ}\text{C}$  per hour between 5 AM and 3 PM (C. Hénin, pers. comm., 1995). Seven-day median and Hanning filters (Bendat and Piersol, 1971) were applied to the daily SST and SSS time series to suppress high-frequency variations, and the filtered values were monthly averaged.

Regarding subsurface measurements, about 3800 temperature and 610 salinity profiles were collected in the studied region during the 1979-1993 period. The temperature profiles were obtained from eXpendable Bathymeterograph (XBT, 83%), hydrocast and Conductivity Temperature Depth (CTD) measurements (Fig. 1b, c), the latter providing the salinity profiles. The XBT drops were made from ships-of-opportunity along shipping routes (Meyers and Donguy, 1980) and the two other types of measurements originate from 53 research cruises carried out by ORSTOM scientists. In combining XBT, hydrocast and CTD profiles, the XBT depths were multiplied by a correction factor ( $C = 1.0336$ ) to account for the new depth equation for XBT (Hanawa *et al.*, 1994).

The temperature and salinity profile data were submitted to a validation test similar to the one performed for SST and SSS. For each profile, temperature and salinity were first linearly interpolated at intervals of 5 m, from the surface down to 400 m. Then, at each level, spurious values were detected through standard deviation criteria ( $\pm 5$ ,  $\pm 4$ , and  $\pm 3.5$ ) over  $2^{\circ}$  latitude bands. Out of the complete file, 6.5% of the profiles were rejected. The irregularly-distributed longitude-latitude-time temperature values were interpolated (or averaged, as appropriate) on to a regular 1-month by  $2^{\circ}$ -latitude by 5 m depth grid, following the technique detailed in Delcroix and Hénin (1991). On average, each grid point represents 3.3 temperature measurements collected during a given month (from January 1979 to December 1993), within a  $2^{\circ}$  latitude band (from  $27^{\circ}\text{S}$  to  $17^{\circ}\text{S}$ ), within a 5 m depth interval (from 0 to 400 m) and within  $161^{\circ}\text{E}$ - $171^{\circ}\text{E}$  longitude. This gridding procedure was not possible for the salinity profiles given the poor time-space distribution: only the long-term mean latitude-depth salinity will be discussed in the following section.

As for surface winds, they are derived from the monthly Florida State University (FSU) pseudo-stress fields which are available on a  $2^{\circ}$  latitude by  $2^{\circ}$  longitude grid over the tropical Pacific (Goldenberg and O'Brien, 1981). Monthly values from January 1972 to December 1992, from  $17^{\circ}\text{S}$  to  $27^{\circ}\text{S}$  and averaged within  $160^{\circ}\text{E}$ - $170^{\circ}\text{E}$  longitude were

used to derive 1-month by  $2^{\circ}$  latitude grids of pseudo-stress moduli (hereafter referred to as  $|\tau|$ ), zonal pseudo-stress ( $\tau^x$ ), and meridional pseudo-stress ( $\tau^y$ ) in  $\text{m}^2 \text{s}^{-2}$  unit.

## MEANS AND SEASONAL VARIATIONS

Maps of long-term mean SST, SSS and  $|\tau|$  (1972-1992) are displayed in Figure 2a, b, c. The mean SST increases equatorward from about  $23^{\circ}\text{C}$  at  $27^{\circ}\text{S}$  latitude to  $27.5^{\circ}\text{C}$  at  $17^{\circ}\text{S}$ . The surface isotherms are almost zonally oriented with, however, about  $0.5^{\circ}\text{C}$  difference at the same latitude between the western and eastern side of New Caledonia (east being warmer). In contrast to the mean SST, the mean SSS decreases equatorward from about 35.8 at  $27^{\circ}\text{S}$  latitude to 35.2 at  $17^{\circ}\text{S}$ . The surface isohalines are also almost zonally oriented with again a small difference ( $< 0.1$ ) between the eastern and western sides of New Caledonia (east being fresher). It is worth noting that the 35.4 isohaline and  $25.5\text{-}26^{\circ}\text{C}$  isotherm parallel the eastern coast of New Caledonia's main island, reflecting the likely role of advection by the coastal *Courant du Vauban* which flows south-eastward between the main island and the Loyalty Islands (Hénin *et al.*, 1984, 1995). The average direction of the wind (not shown here) is E-SE, reflecting the dominance of the trade winds in the region. The mean pseudo-stress modulus ranges from less than  $32 \text{ m}^2 \text{s}^{-2}$  at  $27^{\circ}\text{S}$  latitude to  $41\text{-}46 \text{ m}^2 \text{s}^{-2}$  at  $17^{\circ}\text{S}$ . It is virtually unaffected by longitude in the southern half of the region, but increases westward in the northern half. The tendency for  $|\tau|$  to be weaker in the east than in the west of New Caledonia is consistent with the tendency for SST to be warmer and for SSS to be fresher in the east than in the west, reflecting the possible effects of evaporative cooling, wind mixing and evaporation.

Mean monthly values in SST, SSS, and  $|\tau|$ , averaged over the  $161^{\circ}\text{E}$ - $171^{\circ}\text{E}$  band, are displayed in Figure 3a, b, c between  $27^{\circ}\text{S}$  and  $17^{\circ}\text{S}$  latitudes (see also Hénin, 1982). The warm water pool ( $\text{SST} > 28^{\circ}\text{C}$ ) of climatic significance (Lukas and Webster, 1992) penetrates south of  $19^{\circ}\text{S}$  for about three months, reaching the latitude of Port-Vila, Vanuatu, from January to April. As expected, the SST is warmest (coldest) in February-March (August-September), *i.e.* by the end of the austral summer (winter), reflecting the remarkable effect of surface thermal forcing in governing extra-equatorial SST. As discussed below, the annual variations of SST are the dominant features since they represent more than 80% of the total variance.

The mean monthly values in SSS (Fig. 3b) present relatively strong changes in the northern *versus* the southern part of the region. Maximum (minimum) SSS takes place around September (March) from  $17^{\circ}\text{S}$  to  $27^{\circ}\text{S}$ , with an annual amplitude of the order of 0.15 at  $17^{\circ}\text{S}$  latitude, decreasing to almost-zero at  $27^{\circ}\text{S}$ . Looking at the northern part of the region only, the seasonal SSS cycle is out of phase with the seasonal precipitation cycle (see Morlière and Rébert, 1986; Lenormand, 1995) and in phase with the seasonal  $|\tau|$  cycle (Fig. 3c). Namely, the September maximum in SSS roughly corresponds to a minimum in precipitation and to a minimum in  $|\tau|$ , suggesting the

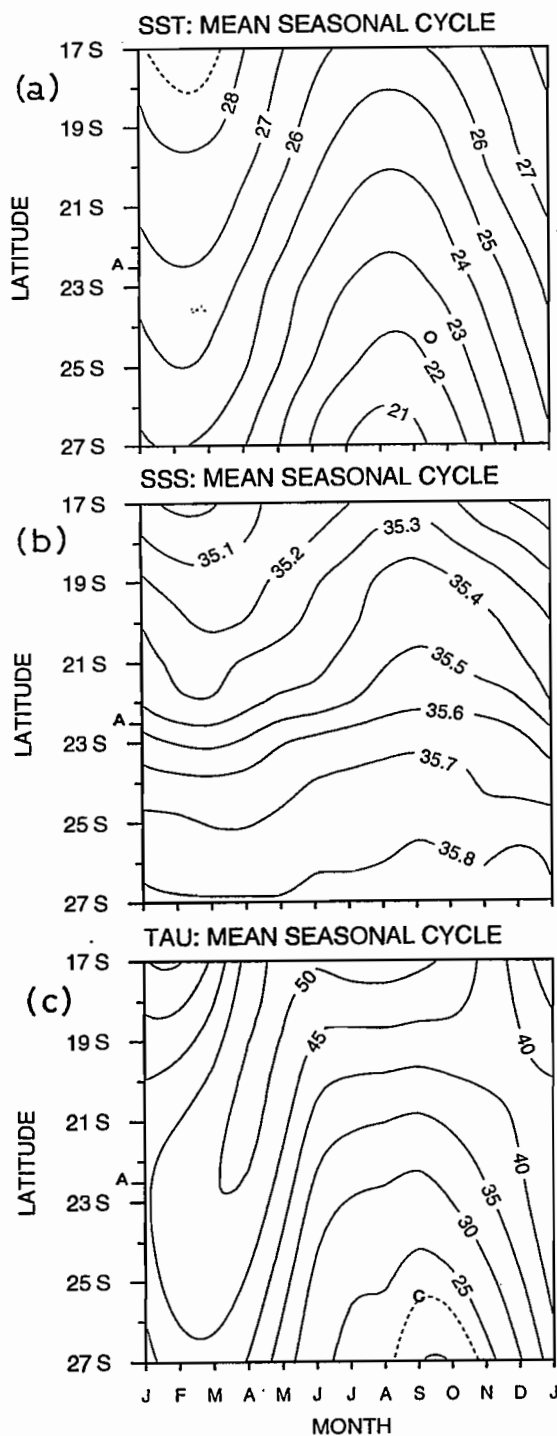


Figure 3

Mean monthly values of (a) sea-surface temperature, (b) sea-surface salinity, and (c) pseudo wind stress modulus. Units are  $^{\circ}\text{C}$  and  $\text{m}^2 \text{s}^{-2}$  in (a) and (c), respectively. All values are averaged over 1972–1992 and within  $160^{\circ}\text{E}$ – $170^{\circ}\text{E}$ . The letter “A” in the vertical axis indicates the latitude of the Amédée Lighthouse.

combined role of evaporation and precipitation (P) in modulating SSS. Contrary to SST, it should be noted that the annual SSS, P and  $|\tau|$  cycles represent less than 20, 30 and 40% of the total variance, respectively (Lenormand, 1995).

As mentioned in the section above, a longer and finer resolution SST and SSS data set has been collected at

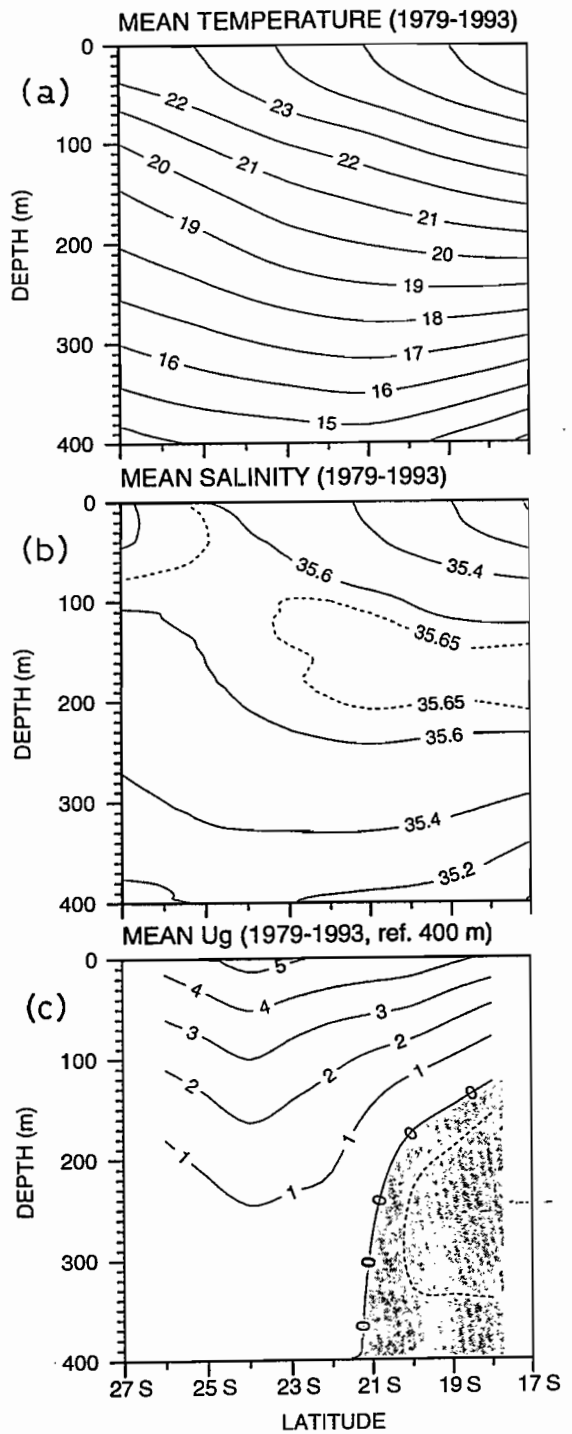


Figure 4

Mean latitude-depth distributions of (a) temperature, (b) salinity, and (c) zonal geostrophic current relative to 400 m. Units are  $^{\circ}\text{C}$  and  $\text{cm s}^{-1}$  in (a) and (c), respectively. Negative (shaded) current denotes westward flow. All values are averaged over 1979–1993 and within  $160^{\circ}\text{E}$ – $170^{\circ}\text{E}$ .

the Amédée lighthouse, in the lagoon off Nouméa. At the Amédée lighthouse, on the average, the lagoon waters are about  $1.5^{\circ}\text{C}$  colder and 0.2 saltier than in the open ocean (Table 1, Fig. 2), in agreement with a similar comparison mentioned by Hénin *et al.* (1984). Seasonal change in SST ranges from  $25.8^{\circ}\text{C}$  in March to  $21.0^{\circ}\text{C}$  in August, with monthly standard deviations of the order of  $0.6^{\circ}\text{C}$

Table 1

Monthly means, annual mean and standard deviations ( $\sigma$ ) for Sea Surface Temperature (SST) and Salinity (SSS) at Amédée Lighthouse ( $22^{\circ}29'S$ ,  $166^{\circ}28'E$ ). Values are based on daily measurements made during the 1967-1994 period for SST and 1974-1994 for SSS.

	Jan.	Feb.	Mar.	Apr.	May	June	July	Aug.	Sept.	Oct.	Nov.	Dec.	Mean
SST	25.6	25.6	25.8	24.6	23.4	22.4	21.4	21.0	21.4	22.5	23.6	24.6	23.5
$\sigma_{\text{SST}}$	0.6	0.7	0.7	0.7	0.5	0.5	0.4	0.5	0.6	0.6	0.7	0.7	1.7
SST	35.7	35.6	35.5	35.6	35.7	35.7	35.8	35.8	35.9	35.9	35.8	35.8	35.7
$\sigma_{\text{SSS}}$	0.3	0.3	0.3	0.3	0.2	0.2	0.2	0.2	0.2	0.2	0.2	0.2	0.2

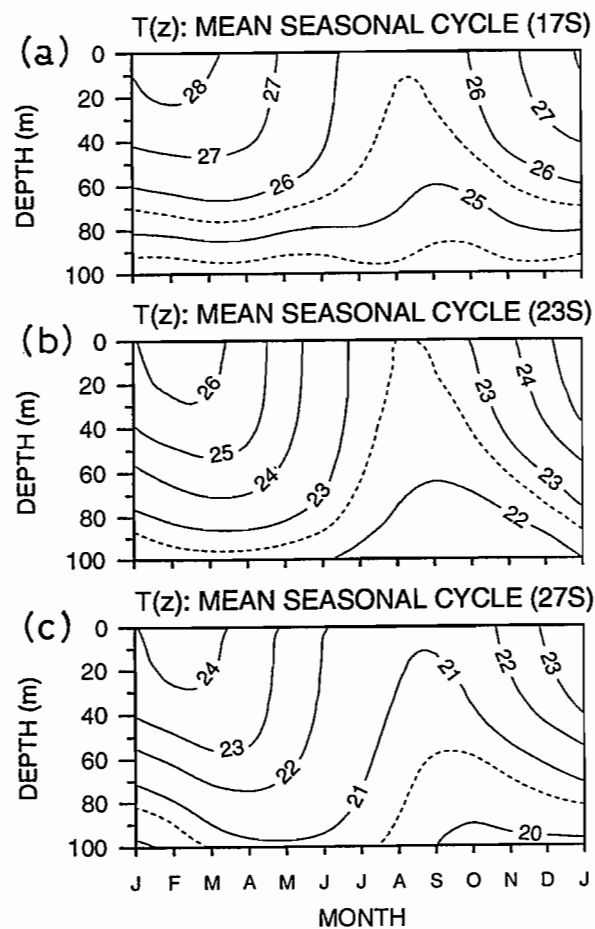


Figure 5

Mean monthly values of temperature ( $^{\circ}\text{C}$ ) as a function of depth, for three selected latitudes, (a)  $17^{\circ}\text{S}$ , (b)  $23^{\circ}\text{S}$ , and (c)  $27^{\circ}\text{S}$ . Monthly values have been calculated from data collected during 1979-1993 and within  $160^{\circ}\text{E}-170^{\circ}\text{E}$ .

(Table 1). Seasonal change in SSS ranges from 35.5 in March to 35.9 in October, with monthly standard deviations of the order of 0.2-0.3. The amplitude of the seasonal variations is thus similar in magnitude inside and outside the lagoon for SST, and twice as much for SSS (Table 1, Fig. 3). The origin of the differences between the lagoon and open-ocean waters is unclear. It may reflect river runoff, local upwelling (the trade winds parallel the reef), strong vertical mixing close by the reef, and/or enhanced evaporation due to the existence of diurnal wind: all these processes but river runoff would consistently bring colder and saltier water close by the reef.

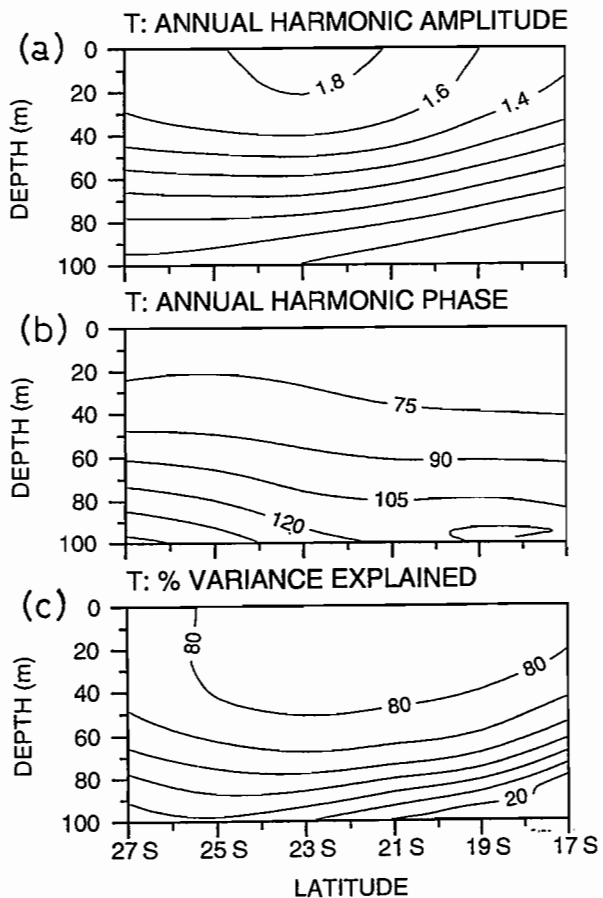


Figure 6

Annual harmonic of  $160^{\circ}\text{E}-170^{\circ}\text{E}$  averaged temperature as a function of latitude and depth: (a) amplitude ( $^{\circ}\text{C}$ ), (b) year-day phase of warmest sea-surface temperature, and (c) per-cent of total variance explained by the annual harmonic.

We now turn our attention to subsurface measurements. The 1979-1993 mean latitude-depth distributions of temperature and salinity, averaged over the  $161^{\circ}\text{E}-171^{\circ}\text{E}$  band, are displayed in Figure 4a,b, together with the derived zonal geostrophic current relative to 400 m (Fig. 4c). In the northern part of the region, deepening of the upper isotherms ( $> 19^{\circ}\text{C}$ ) and rising of the lower isotherms characterize the appearance of the equatorial thermocline found farther to the north. This spreading of isotherms reflects a 0-150 m eastward geostrophic current flowing above a weak westward current characterizing the southern edge of the South Equatorial Current. The zero isothach located at  $21^{\circ}\text{S}$  below 200 m reaches the surface near  $15^{\circ}\text{S}$ .

(see Delcroix and Hénin, 1989, their Fig. 10), it denotes the large-scale South Pacific anticyclonic gyre axis. In the southern part of the region, an almost-constant vertical temperature gradient ( $2.3 \times 10^{-2} \text{ }^{\circ}\text{C.m}^{-1}$ ) can be seen on Figure 4a, with all the isotherms rising toward the surface. This upward movement of isotherms induces a 0-400 m eastward geostrophic current: it was referred to as the South Tropical Countercurrent (Merle *et al.*, 1969) and characterizes the northern side of the eastward flow which extends as far as the Antarctic Circumpolar Current. Figure 4b shows a low salinity water ( $S < 35.4$ ) near the surface equatorward of 21°S, above a tongue of high salinity ( $S > 35.65$ ) located around 160 m, in agreement with the results of Rougerie and Donguy (1975). The high salinity water characterizes the south Pacific tropical water formed further east in the vicinity of French Polynesia (Wyrtki, 1962). High salinity waters are also found near the surface south of 25°S; they partly originate from intrusions of Bass Strait waters into the Tasman Sea (Tomczak, 1981).

Mean monthly values of 0-100 m temperature are displayed in Figure 5a,b,c for three selected latitudes, 17°S, 23°S and 27°S. (Note that 100-400 m temperature and 0-400 m zonal geostrophic current are not discussed here because the seasonal changes are very weak.) Significant seasonal cycles exist in the first 100 m with the warmest temperature in February/March at the surface and progressively later in the year at depth (e.g. in May-June at 100 m, 27°S). For the three selected latitudes, Figure 5a,b,c shows the development of a seasonal thermocline in summer and, *a contrario*, a well-mixed temperature layer in winter. Through a Fourier analysis, computation of the annual harmonic enabled us to assess how representative was the annual temperature cycle out of the total temperature signal. The amplitude and phase (*i.e.* year-day phase of warmest temperature) of the annual harmonic, together with the percent of variance explained by the annual harmonic are shown in Figure 6a,b,c as a function of depths and latitudes. The annual amplitude of 1.4-1.8 °C near the surface, accounting for more than 80 % of the total variance, declines rapidly to less than 0.5 °C at 100 m depth where it represents 20 to 40% of the total variance. The date of the annual temperature maximum is delayed with depth, from mid-March (day 75) in the upper 30 m to early May (day 120) at 100 m. All the above patterns characterize a mid-latitude open ocean where an ENSO signal is not generally seen.

## THE SIGNATURE OF ENSO

Bearing in mind this overview of the average conditions and of the seasonal changes, we then asked ourselves the following question: what is the signature of ENSO, if any, on the analysed surface and subsurface parameters? To answer this question, we calculated monthly anomalies relative to the long-term means (1972-1992 for the surface parameters; 1979-1993 for the subsurface temperature), and we filtered the resulting time series in time with a 12-month Hanning filter (half length) in order to remove annual and shorter-period variations. The potential impact of ENSO

was examined by comparing the interannual anomalies and the SOI which was also filtered with a 12-month Hanning filter. The comparison was guided by lagged correlation analysis.

The interannual anomalies of SST, SSS, and  $\tau^y$  (1972-1992, 17°S-27°S) are shown in Figure 7a,b,c, together with the SOI in Figure 7d. Periods of warm (cold) SST anomalies of the order of 0.5 °C have a clear tendency to appear during La Niña (El Niño) events when the SOI is positive (negative). Namely, the warm SST anomalies occur during the 1973-1975 (not in the southern half of the region in 1973-74) and 1988-1989 La Niña and, conversely, the cold SST anomalies occur during the 1982-1983, 1987 and 1991 El Niño (not during the 1977 El Niño). Such correspondence still applies between SSS anomalies and the SOI. Fresher-than-average (saltier-than-average) SSS anomalies ranging within 0.1-0.3 are clearly associated with La Niña (El Niño) events over almost the full latitudinal range. Of particular interest in this regard is the penchant for the peak SSS anomalies, regardless of the sign, to arise a few months after the SOI peak, with the time delay increasing with latitude. The meridional pseudo-stress anomalies ( $\tau^y$ ) are also related to the SOI, in agreement with the results of Van Loon and Shea (1985). Southerly wind anomalies coincide to a large extent with El Niño episodes in 1972, 1977, 1982-1983, 1987, and 1991-1992, and northerly anomalies are observed during the two La Niña periods in 1973-1975 and 1988. The zonal pseudo-stress ( $\tau^x$ ) and pseudo-stress modulus ( $|\tau|$ ) anomalies are consistent with the SOI mainly north of 19°S latitude (not shown here; *see* Lenormand, 1995), with magnitudes of the order of -5 and +5  $\text{m}^2 \text{s}^{-2}$  during El Niño events, respectively; the signs of the anomalies are reversed during La Niña events.

Tables 2 and 3 present the zero-lag and maximum correlation between the SST, SSS,  $|\tau|$ ,  $\tau^y$ , and  $\tau^x$  anomalies and the SOI. In addition to the preceding qualitative comparisons, it appears that the observed anomalies in SST and pseudo-stresses are significantly correlated with the SOI in the northern part of our domain, at almost zero-lag, with values ranging in magnitude between 0.43 and 0.85. Regarding SSS anomalies, they also are significantly correlated with the SOI but now over the full domain ( $R < -0.7$ ). Furthermore, as noted previously, SSS anomalies seem to migrate southward with 8-month delay at 17°S and 13-month delay at 27°S as compared to the SOI. Thus, not all but a significant part of the interannual variability in the surface parameters is related to ENSO.

The relationships between SST and SSS anomalies still exist at the Amédée lighthouse, inside the New Caledonian lagoon. Cold (warm) SST anomalies and saltier-than-average (fresher-than-average) SSS anomalies clearly have a propensity for arising during warm El Niño (cold La Niña) episodes (Fig. 8), with magnitude similar to, or greater than, that which is observed in the open ocean (Fig. 7a,b). Specifically, we note the very contrasted SSS conditions encountered in 1989 during La Niña and in 1992 during El Niño, with peak-to-peak values reaching as much as 0.7. Such extremes are of major interest and probably

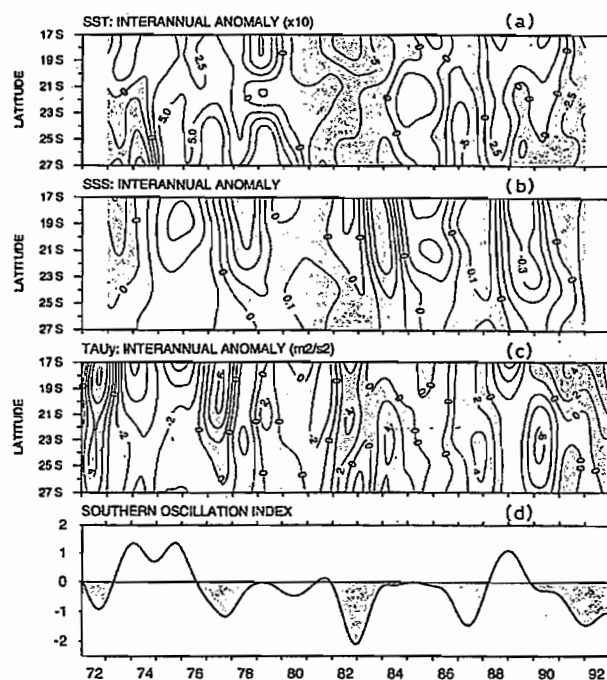


Figure 7

Interannual anomalies of 160°E-170°E averaged (a) sea-surface temperature ( $^{\circ}\text{C} \times 10$ ), (b) sea-surface salinity, and (c) meridional pseudo-stress ( $\text{m}^2 \text{s}^{-2}$ ; positive to the north). All values are relative to the 1972-1992 period. The bottom panel (d) represents the Southern Oscillation Index which is filtered in time with a 12-month Hanning filter. Shaded areas indicate negative anomalies in (a) and (d), and positive anomalies in (b) and (c).

of concern for local fishing and aquaculture activities. For the time series as a whole, SST and SSS anomalies versus the SOI are highly correlated with values of 0.61 (3-month lag) and 0.66 (9-month lag), respectively (Table 2) (note that the zero-lag correlation for SST is 0.57 which is not statistically different from 0.61). Hence, the ENSO signal does exist inside the New Caledonian lagoon. Moreover, we observe a cooling trend of  $-0.4^{\circ}\text{C}$  over 10 years. Such a trend is also detected in open-ocean measurements ( $-0.3^{\circ}\text{C}$  over 10 years within 17°S-27°S), and may be related to the excess of positive versus negative SOI in the first half of the analysed period as compared to the excess of negative versus positive SOI in the second half.

Table 2

Simultaneous ( $R_0$ ) and maximum ( $R_1$ ) correlations ( $\times 100$ ) at given lag (months) between interannual anomalies of sea-surface temperature (SST) and sea-surface salinity (SSS) versus the Southern Oscillation Index (SOI). A positive lag indicates that the SOI leads the anomalies. SST and SSS anomalies between 17°S and 27°S are averaged within 160°E-170°E. The Amédée Lighthouse is located at 22°29'S-166°28'E. Only correlations significantly different from zero at 95% confidence level are reported.

Location	SST			SSS		
	$R_0$	$R_1$	lag	$R_0$	$R_1$	lag
17°S	55	55	-1	-43	-74	8
18°S	54	54	0	-43	-78	8.5
19°S	43	43	0	-47	-82	9
20°S	58	58	-1	-79	10	
21°S				-77	10	
22°S				-78	11	
23°S	43	43	0	-71	12	
24°S				-69	13	
25°S				-73	14.5	
26°S				-71	13	
27°S				-45	-72	13
Amédée Lighthouse	57	61	-3	-36	-66	9

We then focused our attention on subsurface temperatures which are available over 15 years, from 1979 to 1993. Despite the length of the time series, it is rather short to test for significant correlations between interannual anomalies and the SOI. In fact, the Hanning filter used to derive interannual anomalies reduces the number of effectively independent values and further diminishes the time series by two years (1979 and 1993). Basically, the time between independent values is about one year and only correlation coefficients greater than 0.5 are significantly non-zero at the 95% level of confidence. With this caveat in mind, Figure 9 presents the latitude-depth distribution of zero-lag correlation coefficients between the interannual temperature anomalies and the SOI. The positive sign of correlations confirms that cold anomalies emerge during warm El Niño events ( $\text{SOI} < 0$ ), whereas warm anomalies come out during cold La Niña events ( $\text{SOI} > 0$ ). These points underline once again that regional temperature anomalies

Table 3

Simultaneous ( $R_0$ ) and maximum ( $R_1$ ) correlations ( $\times 100$ ) at given lag (months) between interannual anomalies of pseudo wind stress modulus ( $|\tau|$ ), zonal pseudo wind stress ( $\tau^x$ ), meridional pseudo wind stress ( $\tau^y$ ) versus the Southern Oscillation Index (SOI). A positive lag indicates that the SOI leads the anomalies.  $|\tau|$ ,  $\tau^x$  and  $\tau^y$  anomalies are averaged within 160°E-170°E. Only correlations significantly different from zero at 95% confidence level are reported.

Location	$ \tau $			$\tau^x$			$\tau^y$		
	$R_0$	$R_1$	lag	$R_0$	$R_1$	lag	$R_0$	$R_1$	lag
17°S	-67	-67	0	53	53	1	-85	-85	0
19°S	-60	-60	1	44	46	2	-77	-77	0
21°S							-61	-61	0
23°S							-46	-46	0
25°S									
27°S									

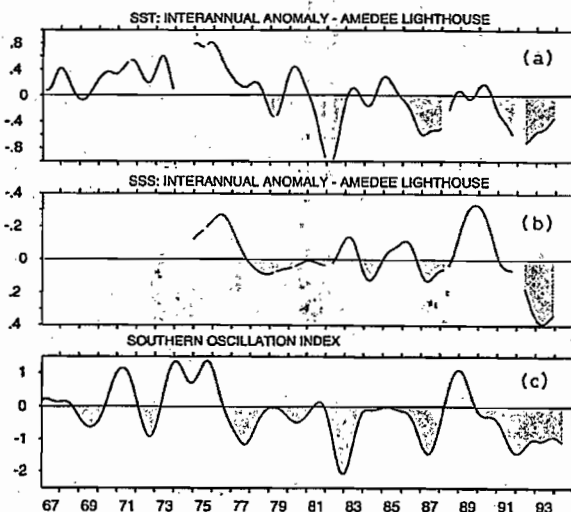


Figure 8

Interannual anomalies of  $160^{\circ}\text{E}$ - $170^{\circ}\text{E}$  averaged (a) sea-surface temperature ( $^{\circ}\text{C}$ ), and (b) sea-surface salinity at the Amédée lighthouse ( $22^{\circ}29'\text{S}$ ,  $166^{\circ}28'\text{E}$ ). All values are relative to the respective duration of the time series. The bottom panel (c) represents the Southern Oscillation Index which is filtered in time with a 12-month Hanning filter. Shaded areas indicate negative anomalies in (a) and (c), and positive anomalies in (b).

0-400 m temperature time series and mean T-S curves (see Figure 4a,b). In the absence of salinity time series below the surface, it is worth pointing out that this T-S procedure neglects the strong ENSO-related salinity changes as identified in Figure 7b for SSS. Combined with the assumption that 400 m can be meaningfully used as a reference level, the resulting error is of the order of  $\pm 2 \text{ cm s}^{-1}$  (Delcroix *et al.*, 1987), *i.e.* about 50% of the mean zonal geostrophic current in the upper 0-20 m layer and over 100% below 100 m (Fig. 4). Investigating the 0-20 m layer only (where signal/noise  $\sim 2$ ), we found a hint that the eastward-flowing geostrophic current, averaged within  $26^{\circ}\text{S}$ - $18^{\circ}\text{S}$ , diminished by about  $2 \text{ cm s}^{-1}$  during a 1-year period, one year after the 1982-1983 and 1987 El Niño. Such a decrease is consistent with the southward displacement of the anticyclonic gyre axis observed during the 1982-83 El Niño (Delcroix and Hénin, 1989). However, the  $2 \text{ cm s}^{-1}$  decrease did not appear in 1992 and, furthermore, no increase was detectable during the 1988 La Niña. Hence, given the weakness of the possible ENSO-related signal ( $\sim 2 \text{ cm s}^{-1}$ ) and considering that the interannual anomalies of zonal geostrophic current (not shown here) are not significantly correlated with the SOI ( $R < 0.5$ ), this precludes a definite conclusion as to whether or not the zonal geostrophic circulation is systematically affected by ENSO in the studied region.

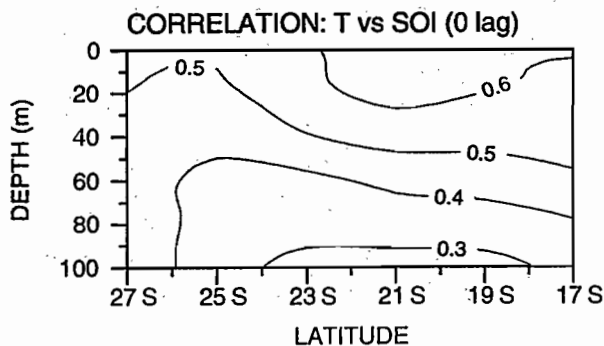


Figure 9

Latitude-depth distribution of zero-lag correlation coefficients between the Southern Oscillation Index, filtered in time with a 12-month Hanning filter, and the interannual anomalies of  $160^{\circ}\text{E}$ - $170^{\circ}\text{E}$  averaged temperature over the 1979-1993 period. Values greater than 0.5 are significant at 95%.

are out of phase with those in the eastern and central equatorial Pacific. It is worth noting that the correlations are maximum at zero-lag in the 0-100 m layer (this is not true below 100 m where the correlations are not significant), and their values at the surface are similar to those obtained with bucket measurements (Table 2). Quantitatively, the magnitude of the temperature anomalies (not shown here) associated with ENSO ranges from about  $0.5^{\circ}\text{C}$  at the surface, as in Figure 7 for SST, to almost-zero below 100 m depth. Figure 9 indicates clearly that ENSO-related temperature anomalies appear mainly in the near-surface, decreasing regularly with depth. We shall return to the implications of this result in the following section.

Time series of zonal geostrophic current relative to 400 m were calculated at each latitude and depth, using the

## CONCLUSION AND DISCUSSION

In this paper, an attempt was made to identify the signature of ENSO in oceanic and wind data collected for years in the south western Pacific ( $17^{\circ}\text{S}$ - $27^{\circ}\text{S}$ ;  $160^{\circ}\text{E}$ - $170^{\circ}\text{E}$ ), within an area centred on New Caledonia. This region is of interest since past studies indicated that it presents ENSO-related anomalies out of phase with most of the other regions of the globe. Following a detailed analysis of long-term means and seasonal changes, the link between ENSO and anomalies in SST, SSS, 0-400 m temperature and zonal geostrophic current, and surface wind ( $\tau$ ) was investigated through comparisons with the Southern Oscillation Index (SOI).

During the warm phase of ENSO ( $\text{SOI} < 0$ ; El Niño), we observed saltier-than-average SSS anomalies, cold temperature anomalies that extended at least to 50 m depth, together with westerly and southerly wind anomalies over a large part of the studied area. Interestingly, anomalies of opposite sign were detected during the cold phase of ENSO ( $\text{SOI} > 0$ ; La Niña). We must however bear in mind that the ENSO-signals are relatively weak: the ranges of the interannual SST and  $\tau$  anomalies are only 20-30% of the corresponding mean seasonal ranges. The exception is for SSS which experiences ENSO-related anomalies of similar magnitude as, or greater than, the mean seasonal changes. Furthermore, SSS anomalies are not in phase with the SOI, unlike SST and  $\tau$  anomalies, but rather present a time lag that increases from 8 months at  $17^{\circ}\text{S}$  to 13 months at  $27^{\circ}\text{S}$  (SSS after SOI). It was also noted that SST and SSS anomalies do exist inside the lagoon of New Caledonia. Modification of the zonal geostrophic circulation in relation

to ENSO was not ascertained, mainly due to the weakness of possible related anomalies *versus* the accuracy of the calculated geostrophic current.

We shall now propose tentative explanations for the observed regional ENSO-related anomalies. During the warm phase of ENSO (El Niño, SOI < 0), the Warm Pool with SST warmer than 28–29°C is displaced from the western to the central equatorial Pacific (Picaut and Delcroix, 1995). Lowering pressure in the central equatorial Pacific produces anomalous Walker and Hadley circulation, and, as a conceivable consequence, the regional SE geostrophic trade winds veer clockwise, generating the observed westerly and southerly wind anomalies. The reverse situation appears during the cold phase of ENSO (La Niña, SOI > 0) when the warm pool is displaced toward the far western equatorial Pacific. Regarding near-surface temperature fluctuations, they can be due to anomalies in air-sea heat exchange and/or to modifications in heat transport by anomalous ocean currents. These two mechanisms, which cannot be rigorously quantified with our data set, may work in concert during both phases of ENSO. In fact, the cold temperature anomalies during the warm phase are consistent with: 1) an increase in the wind speed ( $\tau$ ) which induces evaporative cooling (Meyers *et al.*, 1986); 2) the occurrence of southerly wind anomalies bringing dryer and cooler air from the south; and 3) the import of relatively cold water coming from the east due to both anomalous westward Ekman transport related to southerly wind anomalies and possibly to the southern displacement of the large-scale anticyclonic gyre axis (Wyrtki and Wenzel, 1984; Delcroix and Hénin, 1989, their Fig. 12). The warm near-surface temperature anomalies during the cold phase of ENSO are in accord with the reverse processes. As for SSS anomalies, saltier-than-average SSS during the warm phase of ENSO are remarkably consistent with the reduced precipitation

observed 9 to 13 months after the peak SOI in the region of New Caledonia (Ropelewski and Halpert, 1987; their Fig. 3d). Of possible importance is also the enhanced evaporation due to an increase in the wind speed, as well as the income of saltier water from the east in response to the circulation change just discussed above. The 8–13 months delay between the SSS anomalies and the SOI suggests, however, that these anomalies are mainly governed by precipitation changes.

Hence, there is no doubt that ENSO is one of the major factors influencing interannual climate variations in the vicinity of New Caledonia. We have suggested several consistent causes that can account for the regional ENSO-related anomalies, and that connect these anomalies to ENSO evolution at low-latitudes. Model simulations and/or altimetric measurements should provide the complementary information needed to assess and/or to discriminate the relative magnitude of the mechanisms identified.

## Acknowledgements

Special thanks go to the many ORSTOM scientists and/or colleagues involved in the collection of data gathered under the ship-of-opportunity programme and oceanic cruises. The FSU wind data was supplied by James J. O'Brien and co-workers. We wish to thank Christian Hénin and Pierre Rual for their suggestions and helpful comments during the course of this study. For one of us (OL), this investigation is part of a *Mémoire de Diplôme d'Études Approfondies de l'Université d'Aix-Marseille-II*, and a *Mémoire de Stage de l'École Supérieure d'Ingénieurs de Marseille*, performed while visiting the ORSTOM Center in Nouméa. Support from this Institute has been greatly appreciated.

## REFERENCES

- Bendat J., A. Piersol (1971). Random Data: analysis and measurement procedures. Wiley-Interscience, 407 p.
- Berlage H.P. (1966). The Southern Oscillation and world weather. *K. Ned. Met. Inst., Meded. Verh.* **88**, 152 p.
- Bjerknes J. (1966). A possible response of the atmospheric Hadley circulation to equatorial anomalies of ocean temperature. *Tellus* **18**, 820–829.
- Cadet D. (1985). The Southern Oscillation over the Indian Ocean. *J. Climatol.* **5**, 189–212.
- Delcroix T., G. Eldin, C. Hénin (1987). Upper ocean water masses and transports in the western tropical Pacific (165°E). *J. Phys. Oceanogr.* **17**, 2248–2262.
- Delcroix T., C. Hénin (1989). Mechanisms of subsurface thermal structure and sea surface thermohaline variabilities in the southwestern tropical Pacific during 1979–1985. *J. Mar. Res.* **47**, 777–812.
- Delcroix T., C. Hénin (1991). Seasonal and interannual variations of sea-surface salinity in the tropical Pacific Ocean. *J. Geophys. Res.* **96**, 22135–22150.
- Delcroix T. (1993). Seasonal and interannual variability of sea-surface temperatures in the tropical Pacific, 1969–1991. *Deep-Sea Res.* **40**, 2217–2228.
- Delecluse P., J. Servain, C. Levy, K. Arpe, L. Bengtsson (1994). On the connection between the 1984 Atlantic warm event and the 1982–1983 ENSO. *Tellus* **46**, 448–464.
- Donguy J.R. (1987). Recent advances in the knowledge of the climatic variations in the tropical Pacific Ocean. *Prog. Oceanogr.* **19**, 49–85.
- Goldenberg S., J. O'Brien (1981). Time and space variability of tropical wind stress. *Mon. Weather Rev.* **109**, 1190–1207.
- Gordon N. (1986). The Southern Oscillation and New Zealand weather. *Mon. Weather Rev.* **114**, 371–387.
- Halpert M., C. Ropelewski (1992). Surface temperature patterns associated with the Southern Oscillation. *J. Climate* **5**, 577–593.
- Hanawa K., P. Rual, R. Bailey, A. Sy, M. Szabados (1994). Calculation of new depth equations for expendable bathythermograph using a temperature-error-free method (Application to Sippican/TSK T-7, T-6 and T-4 XBTs). IOC technical series 42, UNESCO.

- Hénin C.** (1982). Caractéristiques des températures et salinités de surface et leurs variabilités dans le Pacifique sud-ouest. Rapports Scientifiques et Techniques, Centre ORSTOM de Nouméa, Nouvelle Calédonie, **28**, 18 p.
- Hénin C., J.M. Guillerm, L. Chabert** (1984). Circulation superficielle autour de la Nouvelle Calédonie. *Océanogr. Trop.* **19**, 113-126.
- Hénin C., F. Gallois, M.J. Langlade** (1995). Rapport des données physiques de la campagne ZoNéCo-2 à bord du N.O. L'ATALANTE du 2 au 21 août. Rapports de missions, Sciences de la mer, Océanographie physique, Centre ORSTOM de Nouméa, Nouvelle Calédonie, **15**, 40 p.
- Hildebrandsson H.H.** (1897). Quelques recherches sur les centres d'action de l'atmosphère. *Kongl. Svenska Vetenskaps-Akademien Handlingar.*, Bandet 29, 3, 36 p.
- Lenormand O.** (1995). Les anomalies climatiques associées à ENSO ont-elles une influence au voisinage de la Nouvelle Calédonie ? Mémoire de DEA, sciences de la mer, océanographie physique, centre ORSTOM de Nouméa, 52 p.
- Lukas R., P. Webster** (1992). TOGA-COARE, Tropical Ocean Global Atmosphere program and Coupled Ocean Atmosphere Response Experiment. *Oceanus* **35**, 62-65.
- McCreary J., D. Anderson** (1991). An overview of coupled ocean-atmosphere models of El Niño and the Southern Oscillation. *J. Geophys. Res.* **96** suppl., 3125-3151.
- Merle J., H. Rotschi, B. Voituriez** (1969). Zonal circulation in the tropical western south Pacific. In: "Perspectives in Fisheries Oceanography". *Jap. Soc. Fish. Oceanogr.*, Prof. Uda's special number, 91-98.
- Meyers G., J.R. Donguy** (1980). An XBT network with merchant ships. *Trop. Ocean-Atmos. Newslett.* **2**, 6-7.
- Meyers G., J.R. Donguy, R.K. Reed** (1986). Evaporative cooling of the western equatorial Pacific Ocean by anomalous winds. *Nature* **323**, 523-526.
- Morlière A., J.P. Rébert** (1986). Rainfall shortage and El Niño Southern Oscillation in New Caledonia, southwestern Pacific. *Mon. Weather Rev.* **114**, 1131-1137.
- Picaut J., T. Delcroix** (1995). Equatorial wave sequence associated with the warm pool displacement during the 1986-1989 El Niño and La Niña. *J. Geophys. Res.* **100**, 18398-18408.
- Rasmusson E.M., T.H. Carpenter** (1982). Variations in tropical sea surface temperature and surface wind field associated with the Southern Oscillation/El Niño. *Mon. Weather Rev.* **110**, 354-384.
- Ropelewski C. F., M. S. Halpert** (1987) Global and regional scale precipitation patterns associated with the El Niño/Southern Oscillation. *Mon. Weather Rev.* **115**, 1606-1626.
- Rougerie F., J.R. Donguy** (1975). La mer du Corail en régime d'alizé de sud-est. *Cah. ORSTOM*, sér. *Océanogr.* **13**, 49-67.
- Tomczak M.** (1981). Bass Strait water intrusions in the Tasman Sea and mean temperature-salinity curves. *Aust. J. Mar. Freshwater Res.* **32**, 699-708.
- Trenberth K., T. Hoar** (1996). The 1990-1995 El Niño Southern oscillation event: longest on record. *Geophys. Res. Lett.* **23**, 57-60.
- van Loon H., Shea J.** (1985). The Souther Oscillation. IV. The precursors south of 15°S to the extremes of the Oscillation. *Mon. Weather Rev.* **113**, 2063-2074.
- Walker G.T.** (1923). Correlation in seasonal variations of weather, VIII: a preliminary study of world weather. *Mem. Indian Meteor. Dep.* **24**, 75-131.
- Walker G.T.** (1924). Correlation in seasonal variations of weather, IX: a further study of world weather. *Mem. Indian Meteor. Dep.* **24**, 275-332.
- White W., G. Meyers, J.R. Donguy, S. Pazan** (1985). Short-term climatic variability in the thermal structure of the Pacific Ocean during 1979-1982. *J. Phys. Oceanogr.* **15**, 917-935.
- Wyrtki K.** (1962). The subsurface water masses in the western south Pacific Ocean. *Aust. J. Mar. Freshwater Res.* **13**, 18-48.
- Wyrtki K.** (1975). El Niño - the dynamic response of the equatorial Pacific ocean to atmospheric forcing. *J. Phys. Oceanogr.* **5**, 572-584.
- Wyrtki K., J. Wenzel** (1984). Possible gyre-gyre interaction in the Pacific ocean. *Nature* **309**, 538-540.



# Observations of sea surface salinity in the western Pacific fresh pool: Large-scale changes in 1992–1995

Christian Hénin, Yves du Penhoat,<sup>1</sup> and Mansour Ioualalen<sup>2</sup>

Centre ORSTOM, Noumea, New Caledonia

**Abstract.** This paper investigates the variability of sea surface salinity (SSS) in the western equatorial Pacific fresh pool. For this purpose, we processed data collected from thermosalinographs embarked on merchant ships. Two main cross-equatorial shipping lines that are representative of the oceanic conditions in the western tropical Pacific were selected: the Japan-Tarawa-Fiji line that crosses the equator near 173°E (eastern track) and the New-Caledonia-Japan line that crosses the equator near 156°E (western track). We show that there is a strong SSS variability in the region at monthly as well as interannual timescales. This high variability is attributed to the successive passages of a zonal salinity front, trapped in the  $(5^{\circ}\text{N}-5^{\circ}\text{S})$  equatorial band and migrating in phase with the southern oscillation index. We also found the eastern track to be more variable in SSS because it is more exposed to these SSS front incursions. We carried out a detailed study of the mechanisms responsible for this variability; it revealed that the rainfall input acts as a source of freshwater responsible for the existence of a contrasted distribution of SSS (mainly high-salinity waters in the central Pacific and low-salinity waters in the western Pacific). However, the main mechanism responsible for the SSS variability is zonal advection that makes the two distinct masses of water converge, resulting in a salinity front which shifts back and forth in the equatorial band.

## 1. Introduction

The western equatorial Pacific is a region of net freshwater input for the ocean because of the excess of precipitation over evaporation: it is a region of active deep atmospheric convection where low wind conditions usually prevail [Donguy, 1994; Webster and Lukas, 1992]. These particular conditions have a significant potential impact on the dynamics and thermodynamics of the western Pacific warm pool through their effect on salinity and density. The salinity effect on density can be as large as the temperature effect in the surface mixed layer, whose depth cannot be determined by temperature alone. Variations of salinity with depth created by downward freshwater fluxes lead to the appearance of a distinct stable layer near the surface. The layer between the base of the mixed layer and the top of the thermocline is called the barrier layer, as proposed by Lukas [1988]. Several studies have investigated the presence of a barrier layer. For example, Lukas and Lindstrom [1991] found that during Western Equatorial Pacific Ocean Circulation Study (WEPOCS) cruises, a barrier layer was present most of the time in the warm pool, and Sprintall and Tomczak [1992] showed that a barrier layer is detectable on climatological data. Delcroix *et al.* [1992] noticed the presence of a barrier layer along the 165°E meridian during Survey of Tropical Pacific (SURTROPAC) cruises. This concept of barrier layer is important to understand the heat budget of the warm pool and thus raises questions about possible salinity

contribution in El Niño-Southern Oscillation (ENSO) dynamics. The thin surface lens of relatively fresh waters that we call Western Pacific Fresh Pool seems to behave as if it slides on top of the region, responding to wind changes within days [Lukas, 1988].

Close to the equator, horizontal distribution of sea surface salinity (SSS) is also potentially significant as it reveals a surface salinity front at the eastern edge of the warm pool. The front marks a boundary between western and central Pacific surface waters. The western equatorial and tropical waters are characterized by low surface salinity due to excess of precipitation over evaporation most of the time, while evaporation dominates east of the fresh pool leading to saltier waters in the central Pacific enhanced by equatorial upwelling processes. In climatologies, salinity data show evidence of the front [Levitus, 1982], but no such evidence can be derived from wind forcing, buoyancy, or temperature data.

Under wind convergence zones, SSS distribution is mainly driven by the evaporation-minus-precipitation budget, with a time lag of a few months. This process does not prevail in the western equatorial Pacific [Delcroix *et al.*, 1996]. Sprintall and McPhaden [1994] discussed the importance of zonal advection of salinity along the equator using long moored time series data from 0°, 165°E. The role of zonal advection was recently emphasized by Shinoda and Lukas [1995], Hénin *et al.* [1995] and Picaut *et al.* [1996]. Positive advection of low-salinity water from the western Pacific is a result of eastward currents in the equatorial band, due to eastward jets generated either by westerly wind bursts or by positive horizontal zonal salinity gradients, i.e., “fresh equatorial jets” which have already been observed near the date line in the western Pacific [Roemmich *et al.*, 1994].

Several studies have emphasized the influence of salinity on tropical ocean model simulations [Cooper, 1988] and the influ-

<sup>1</sup>Now at Groupement de Recherche en Géodésie Spatiale, Toulouse, France.

<sup>2</sup>Now at Laboratoire d'Océanographie Dynamique et du Climat, Université Pierre et Marie Curie, Paris.

Copyright 1998 by the American Geophysical Union.

Paper number 97JC01773.  
0148-0227/98/97JC-01773\$09.00

ence of rainfall anomalies linked to ENSO events on global ocean circulation models [Reason, 1992]. Vialard and Delecluse [1998a, b] respectively investigated the formation and maintenance of the barrier layer in the western Pacific using an ocean global circulation model. R. W. Reynolds (personal communication, 1996) noticed the role of salinity on sea level simulation using an operational ocean model with temperature profile assimilation. These studies stress the dynamical impact of salinity in the warm pool region.

While sea surface temperature distribution is well documented through in situ and satellite observations, salinity observations are still scarce. However, a few SSS studies using data provided mainly by merchant ships and sampled with meteorological buckets, have shown that SSS distribution is related to Pacific ocean circulation and rainfall patterns at annual and interannual timescales [Hines and Montgomery, 1972; Rochford, 1977; Donguy and Hénin, 1976; Delcroix and Hénin, 1991]. SSS observations were also used by Kessler and Taft [1987] to improve the calculation of geostrophic tropical transports in the central Pacific.

In order to improve the data quality and reliability of SSS measurements, ORSTOM initiated, and have been developing since 1992, a thermosalinograph network based on voluntary observing ships (VOS). This network makes it possible to observe more intensively and with improved accuracy the structures of surface temperature and salinity along shipping routes [Hénin and Grelet, 1996]. This network and its data are described in section 2. It consists mainly of two cross-equatorial merchant shipping lines, one in the western part and the other in the eastern part of the warm pool. The period of observation (1992–1995) was also more heavily sampled as it covers the Tropical Ocean and Global Atmosphere/Coupled Ocean-Atmosphere Response Experiment (TOGA-COARE) [Webster and Lukas, 1992]. In particular, we also used limited time series at several locations in the western equatorial Pacific where moorings are equipped with thermosalinographs. All these data yield information on the temporal and spatial evolutions of SSS (section 3). SSS distribution presents contrasted patterns between El Niño and La Niña periods [Delcroix and Picaut, 1998]. Picaut et al. [1996], using SSS data provided by bucket sampling in 1982–1989 (but not really adequate to monitor salinity fronts) and model results found that, at interannual timescale, advection of SSS was responsible for the displacement of this front. However, even though our period of interest covers the extended ENSO event of 1991–1994 and the 1995 La Niña event, it presented strong changes in SSS at a timescale of one to three months, as discussed in section 4. In the conclusion we state that zonal advection was the dominant mechanism for the observed SSS variability during the 1992–1995 period. The result is derived from observations and in particular the estimation of each contribution in the salt budget equation. We also stress that the TSG network is a powerful tool in monitoring the zonal SSS front, and that it can provide a useful indicator of ENSO.

## 2. Data and Methods

Since 1969, ORSTOM has carried out from Noumea (New Caledonia) a program of systematic observations of sea surface temperature (SST) and SSS in the Pacific, Atlantic, and Indian oceans, using surface water samples collected on merchant ships by the “meteorological bucket technique.” Measurements taken in these conditions can easily be inaccurate due to

several hard-to-assess parameters. The water sample is placed in an airtight container, to be analyzed later in the laboratory. On certain routes, a ship may call at Noumea only once every 4 months, and the preservation of the samples in good condition becomes questionable. Evaporation may become a problem depending on the quality and condition of the sample bottles, and current estimates indicate that accuracy in such surface salinity measurements is of the order of 0.2 (see Reverdin et al. [1994] for discussion on water modification during collection). Furthermore, this technique is becoming harder and harder to put into practice, since modern vessels have a higher bridge and operate with smaller crews than in the past. These vessels increasingly make use of automated equipment for their other data-gathering needs, and it had become clear that our original and often imprecise sampling technique needed to be upgraded. This was made possible in 1992 when we started to equip commercial vessels with SBE 21 thermosalinographs (hereafter called TSG) manufactured by Seabird Electronics Inc. The accuracy of measurements given by both thermosalinograph and bucket sampling techniques was compared and assessed along cruise tracks with conductivity temperature depth (CTD) casts in the tropical western Pacific. The mean discrepancy in salinity between TSG measurements and CTD is an order of magnitude smaller (0.00–0.03) than that between buckets and CTDs (−0.13 to +0.07). The dispersion of measurements is also smaller using TSGs (standard deviation of 0.01–0.02 versus 0.09–0.19 for the bucket technique; see Hénin and Grelet [1996]).

Since the beginning of the monitoring, the effort has been focused on the western and central tropical Pacific. The observation area extends from Japan to New Zealand, and from southeastern Asia to French Polynesia. In spite of difficulties encountered during the experimental period and of the limited number of ships, we have been able to demonstrate that intensive automated sea surface monitoring with TSGs is indeed possible and that it substantially improves the accuracy of the data and the density of coverage along the routes [Hénin and Grelet, 1996; Hénin, 1996].

Our present data set consists mainly in data provided by this intensive sampling along the New Caledonia–Japan shipping line (referred to as the Western Track or WT hereafter) and the Japan–Tarawa–Fiji shipping line (referred to as the Eastern Track or ET hereafter). These two lines cross the equator near 156°E and 173°E respectively (Figure 1). The period of observation started in March 1992 for the WT and June 1992 for the ET. Regular commercial vessels operated these lines every 2 months at the beginning of the period of study and then every month from mid-1995. Note that the WT began to be less frequently sampled after June 1995 when shipping lines moved westward toward Hong Kong. The temporal coverage of the 4-year period (1992–1995) is satisfactory with 20 and 23 voyages made along WT and ET, respectively. Additional transects (5°N–5°S) during the COARE—Période d’Observations Intensives (COARE-POI) cruise [Eldin et al., 1994] along 156°E as well as occasional observations were also used.

The TOGA-COARE experiment covers part of the 1992–1995 period. Some of the Tropical Atmosphere Ocean (TAO) moorings [Hayes et al., 1991; McPhaden, 1993] and some additional moorings deployed during the enhanced monitoring phase of the experiment were equipped with salinity sensors at the equator at different depths (in a joint effort between the University of Hawaii, National Oceanic and Atmospheric Administration/Pacific Marine Environmental Laboratory

(NOAA/PMEL), and ORSTOM). We use part of these data to infer the temporal variability of SSS at a time scale shorter than one or two months which is not resolved with the VOS-TSG network. The longest time series is at the equator (160.5°E, between the two tracks) and covers the period from May 1992 till the end of April 1994. The autocorrelation time function shows a zero crossing at 58 days, but this value might depend on the period. However, this confirms the pertinence of the one/two month TSG sampling. The thermal structure variability is derived from XBT measurements from VOS on the same tracks (Global Subsurface Data Center, Brest, France).

To relate SSS variability and surface circulation, we use a complementary data set derived from satellite-tracked surface drifters to estimate surface currents in the equatorial band. The drifters were deployed from both Research Vessels and VOS during the WOCE-TOGA Surface Velocity Program (SVP). They all have a drogue centered at 15 m depth and are used to calculate the average characteristics of the surface circulation in the tropical Pacific [Niiler et al., 1996]. The period 1992–1995 was the most heavily sampled period of the SVP experiment during the «TOGA decade» in the tropical western Pacific, mainly due to the TOGA-COARE experiment. Raw data locations computed by Service ARGOS were interpolated to 6-hour intervals via an experimentally determined Kriging function [Hansen and Poulain, 1996]. The Lagrangian autocorrelation timescales for zonal velocity and meridional velocity were found to be 10 and 5 days, respectively (K. Bi and P. P. Niiler, The equatorial Pacific responses to the 1991–1992 El Niño-Southern Oscillation as observed with Lagrangian mixed layer drifting buoys, submitted to *Journal of Geophysical Research*, 1996). For our study, we sampled the data at a monthly mean on a 3° latitude by 5° longitude grid centered on the equator. The grid size is large enough so that the drifters do not cross it on the timescale of Lagrangian autocorrelations. Some areas were poorly sampled especially near the dateline where westward currents prevail under influence of southerly trade winds; these induce a divergent flow at the surface near the equator. Near 140°E where drifters are scarce and are sometimes captured by coastal currents near Papua-New Guinea, interpretation of the monthly average as the large-scale drift is questionable.

SSS evolution is strongly influenced by the evaporation-minus-precipitation budget (E-P). This budget is dominated by rainfall changes over the western Pacific Ocean characterized by heavy precipitations [Delcroix et al., 1996]. Previous estimates of rainfall and evaporation result in a net freshwater flux of 1–2 m yr<sup>-1</sup> [e.g., Donguy, 1987; Lukas, 1988; Webster and Lukas, 1992]. However, there is a strong rainfall variability linked to the development of ENSO anomalies. For example, during our period of study, winds were more frequently westerlies than is usual in the western equatorial Pacific. During these westerly burst episodes, rainfall tends to increase consistently with the occurrence of anomalous deep atmospheric convection. The location of maximum deep convection, usually west of 180°, also shifts zonally in accordance with wind events. Estimating rainfall over the ocean is a great challenge. Satellite measurements hold the best promise for estimating precipitation since they provide a synoptic coverage. The two most common methods of estimating rainfall rate are based on electromagnetic radiation in the infrared and microwave frequency bands. However, it is difficult to determine errors associated with the different methods, because either the empirical relations or models used to convert the signal to rainfall rates are

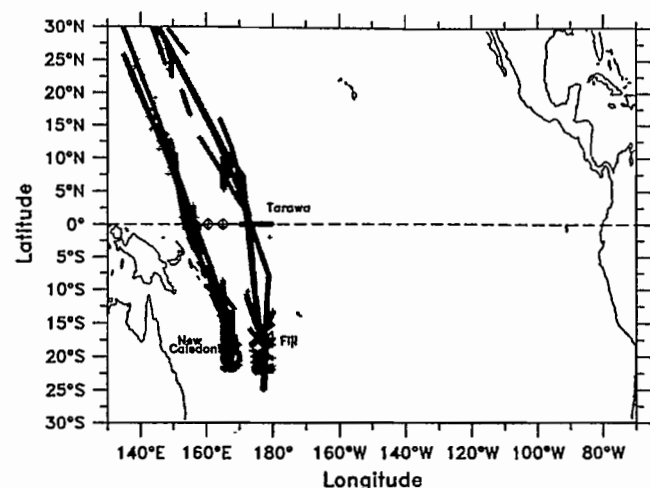


**Figure 1.** Selected thermosalinograph sampling tracks (10° longitude wide) along the two main shipping routes. The western track crosses the equator near 156°E; the eastern track crosses the equator near 173°E. Equatorial moorings (156°E, 160.5°E, and 165°E) are marked by diamonds.

incomplete or based on physical assumptions and approximations which are subject to question. In our study, we used data from the Defense Meteorological Satellite Program (DMSP), special sensor microwave imager (SSM/I) instrument. Ferraro and Marks [1995] developed an algorithm to retrieve instantaneous rainfall rate with an error of approximately 10%. The monthly rainfall product is then generated through several steps on a 2.5° × 2.5° grid from January 1992 to December 1995 but with no error estimates.

### 3. Large-Scale Evolution of Sea Surface Salinity

#### 3.1. Sea Surface Salinity Mean Conditions and Interannual Changes

SSS climatology of the tropical Pacific roughly reflects the mean E-P distribution, in a sense that low-salinity distribution is found under the average position of the Intertropical Convergence Zone (ITCZ) in the northern hemisphere all across the basin and under the South Pacific Convergence Zone (SPCZ) in the southern hemisphere, which is limited to the western part of the basin [Donguy and Hénin, 1978; Delcroix et al., 1996]. This appears clearly on the SSS climatology (Plate 1a) constructed using observations of the ORSTOM bucket network [Delcroix et al., 1996] during the 1974–1989 period. Approximately 150,000 surface salinity observations were used. Plate 1a shows the contrast between low-salinity waters of the western equatorial Pacific ( $S < 35.0$ ) spreading under the wind convergence zones (ITCZ and SPCZ), and the high-salinity waters of the central south Pacific ( $S > 36.0$ ) where rainfall is more scarce, and evaporation exceeds precipitation.

However, SSS data are very scarce and restricted to VOS tracks only. Mapping SSS can lead to uncertain interpolation, and SSS time variability needs regular monitoring. Thanks to meridional oceanographic transects along the 165°E meridian, we were able to observe large-scale temporal changes in the western Pacific Ocean between 20°S and 10°N. Data were provided by French, United States-People's Republic of China, Japanese, and Russian oceanographic cruises. During the 1984–1992 period, a total of 39 sections were completed at

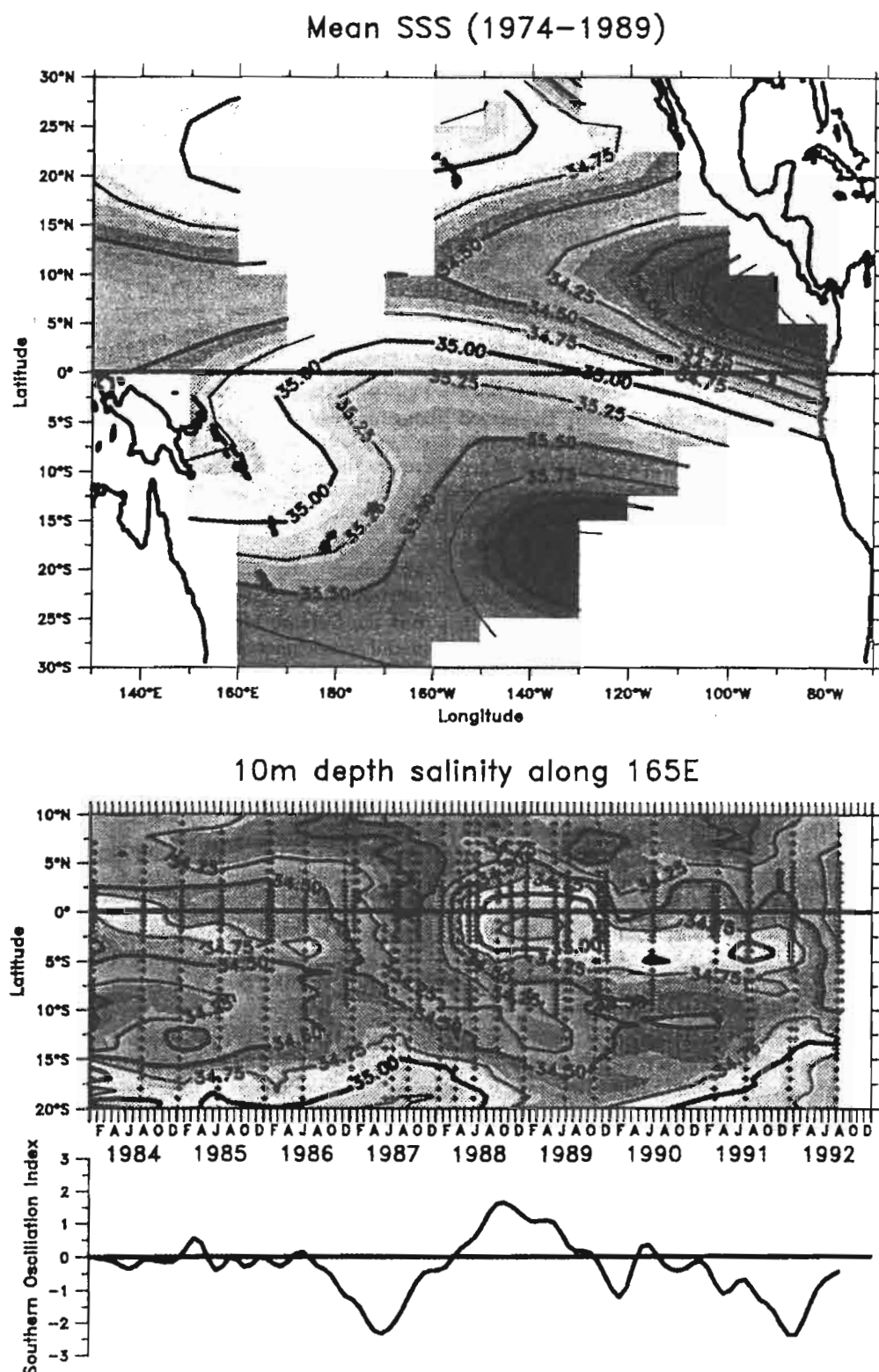


**Plate 1.** (a) Basin-wide mean sea surface salinity on a  $5^\circ \times 2^\circ$  longitude-latitude grid over the 1974–1989 period. Salinity data are provided by bucket sampling on ORSTOM/Noumea ships of opportunity network. (b) Time-latitude salinity at ten meter depth from oceanographic cruises along the  $165^\circ\text{E}$  meridian for the 1984–1992 period. CTD casts are marked (cross). (c) Southern Oscillation index (SOI) filtered with a 6-month Hanning filter over the same period.

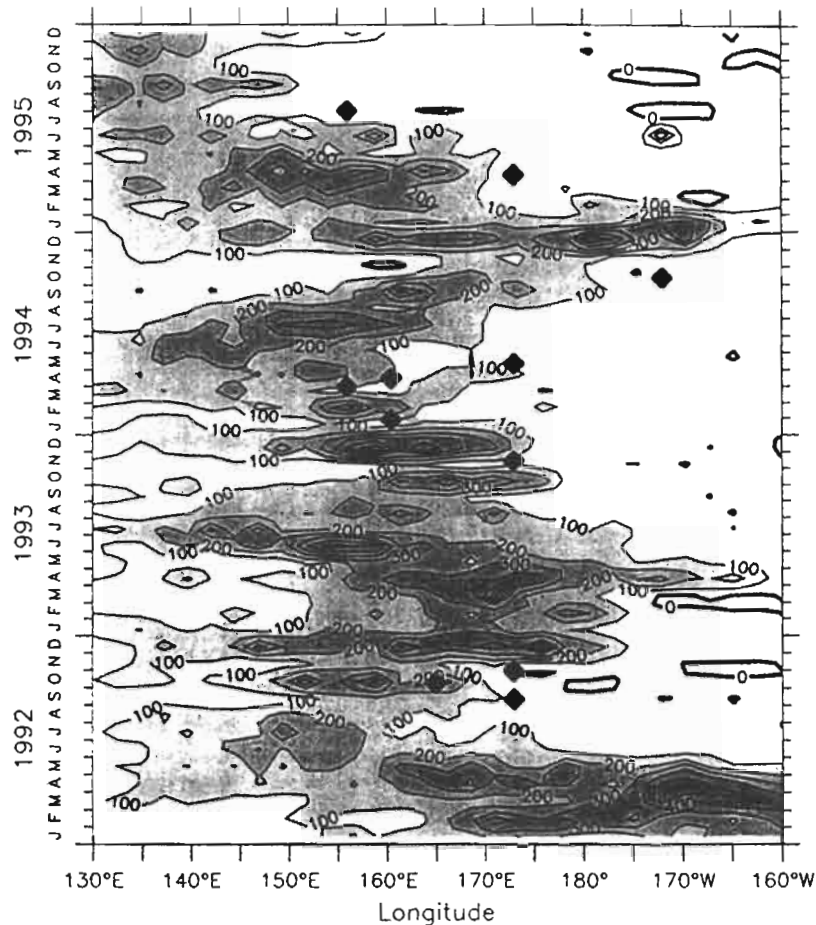


**Figure 2.** Special sensor microwave imager (SSM/I), rainfall estimates along the equator from 1992 to 1995. Data are in  $\text{mm month}^{-1}$ . Diamonds mark positions of zonal sea surface salinity front.

low frequency (2 per year) for the first 3 years (1984–1986) then at higher frequency during the 1987–1989 period when El Niño and La Niña events prevailed. Plate 1b shows the latitude-time distribution of salinity measured from CTD at 10 m depth. Plate 1c presents the southern oscillation index (SOI) in order to indicate the noticeable 1987 and 1992 El Niño and 1988–1989 La Niña events.

In the equatorial band ( $4^\circ\text{N}$ – $4^\circ\text{S}$ ), during the 1987 and 1992 El Niño events, low salinities ( $S < 34.2$ ) prevailed. They corresponded to the drain of western surface waters toward the central Pacific associated with a general eastward drift when SOI reached its lowest value ( $<-2$ ). In contrast, high-salinity waters ( $S > 35.0$ ) were found during 1988–1989. This corresponds to an invasion of high-salinity surface waters carried by the westward South Equatorial Current (SEC) which is particularly strong during a La Niña period [Delcroix *et al.*, 1992; Delcroix and Picaud, 1998a, b].

By contrast, south of  $15^\circ\text{S}$ , high-salinity surface waters ( $S > 35.0$ ) were present during the 1987 and 1992 El Niño events when an equatorward shift of the SPCZ was observed. The increase of salinity was associated with a rainfall deficit and large evaporation due to wind reinforcement [Delcroix and Hénin, 1989], leading to severe droughts in the surrounding islands and northern Australia.

Under the convergence zones, surface waters are less salty than the waters near the equator and south of  $15^\circ\text{S}$ . The  $4^\circ\text{S}$ – $15^\circ\text{S}$  band presents more interannual variability in SSS (and in

heat content computed from XBTs as well [Villain, 1995] than the  $4^\circ\text{N}$ – $10^\circ\text{N}$  region. This is linked to larger meridional shifts of SPCZ as compared to the ITCZ and a more intermittent eastward transport by the South Equatorial Countercurrent (SECC) than by the North Equatorial Countercurrent (NECC). The SECC, usually situated between  $5^\circ\text{S}$  and  $10^\circ\text{S}$ , is well developed during the La Niña periods and is not observed during El Niño events.

These interannual changes were mainly observed on the equator and south of the equator and were nearly in phase with the SOI although there was a 2–3 month lag between atmospheric conditions and SSS variability due to oceanic circulation. (Plate 1c). In the ITCZ region, north of the equator, there was no noticeable interannual surface salinity change. A seasonal surface salinity variability could have been present, but it was not discernable given the density of observations.

### 3.2. Sea Surface Salinity Variability During the 1992–1995 Period

The two TSG tracks cover the 1992–1995 period which was characterized by a long period of warm conditions over the tropical Pacific. An El Niño event started in late 1991 and peaked in March 1992. Kessler and McPhaden [1995a], focusing on the ocean variations in the central Pacific, date the beginning of the event in September 1991 when observations could be interpreted unambiguously as El Niño. They detected Madden-Julian intraseasonal events in the western Pacific, en-

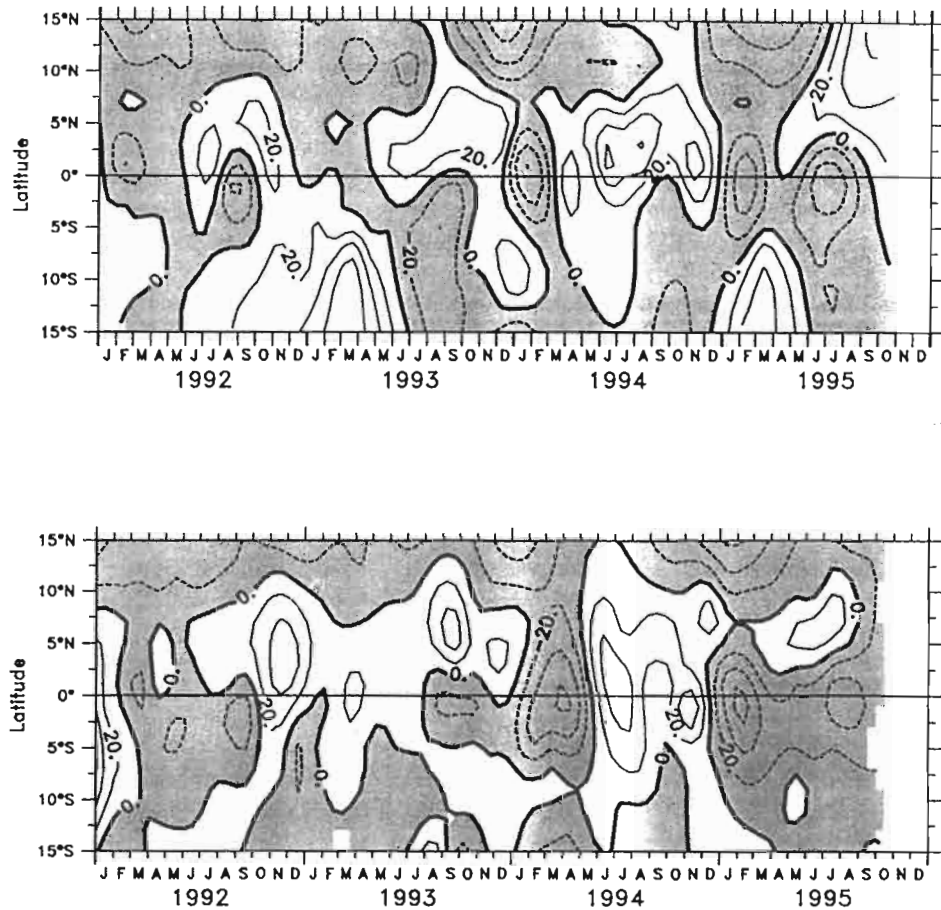


**Figure 3.** Latitude-time distribution of zonal currents (in  $\text{cm s}^{-1}$ ) from surface drifting buoys in 1992–1995: (top) along the western track and (bottom) along the eastern track. Westward currents are negative (and grey), and eastward currents are positive (and white).

hanced atmospheric convection and westerly wind bursts west of the dateline. January–April 1992 represented the peak of the 1991–1993 warm event with a displacement toward the central Pacific of the maximum convection zone (Figure 2). The return to normal condition seems to have occurred in mid-1992 as the SEC strengthened (Figure 3), although an SST warm anomaly was still present at 165°E (CAC Bulletin). In late 1992 to early 1993, the maximum convection zone shifted again close to the dateline when westerly winds prevailed. This appeared again in late 1994 to early 1995 when the maximum of rainfall migrated to a maximum eastward position near the dateline. The SOI remained negative until mid-1995 and presented two minima, one in the first half of 1993 and another in mid-1994, then presented a relative return to normal at the end of 1995. The maximum rainfall was then west of 150°E, as had already been observed during the 1988–1989 La Niña event. Surface currents (see Figure 4) presented also, near the equator, a succession of westward and eastward drifts in phase with the displacements of the position of maximum rainfall.

Vertical temperature distributions of the two tracks at the equator (Figure 5) show that the thermocline rose up abruptly in early 1992 (from 120 to 60–70 meter depth) in relation with Kelvin wave activity [Kessler and McPhaden, 1995b]. The thermocline was subject to several up and down movements (in the 90–110 m range) until the end of 1994 to early 1995. In 1995 the thermocline deepened as observed on XBT data and TAO

moorings. At the surface, a positive SST anomaly remained west of 165°E while a negative SST anomaly prevailed in the central Pacific (CAC Bulletin).

**3.2.1. Time variability.** The SSS variability along the two tracks (WT and ET) is presented in Plate 2. The 165°E cruise track described above is located between these two tracks. In agreement with the SSS evolution at 165°E, the two tracks presented low-salinity distribution ( $\text{SSS} < 34.5$ ) in the western tropical Pacific until early 1995 as suspected for El Niño conditions. In early 1992, high-salinity waters were present, i.e.,  $S > 34.5$ , on the equator (on the WT) and  $S > 35.0$  south of 10°S (on WT and ET). The presence of these high-salinity waters was discernable as early as the end of 1991, on the 165°E longitude (Plate 1b). Around the equator and at the end of the warm event in 1995 when SOI recovered normal values, intrusion of high-salinity waters ( $S > 35.0$ ) appeared on the two tracks, but with a time lag of about 4 months on the WT. No clear seasonal variability appears in our data.

The main difference between the two tracks consists of the incursions of high-salinity surface waters in the equatorial band 5°S–5°N along the ET which do not reach the WT. For instance, SSS reached a maximum of 34.8 in October 1992 and between February and April 1993. SSS values higher than 35.0 during December 1993 to April 1994 were observed on the ET but do not have a signature on the WT where SSS remained low (between 33.7 and 34.2). Either the westward displacement

of high-salinity water was too weak to reach the WT or it reached the WT for a short time only and was therefore not detected by the two-month TSG sampling. As mentioned above, high-salinity equatorial waters invaded the western equatorial Pacific and reached 173°E (ET) in early 1995 and 156°E (WT) in mid-1995.

Salinity measurements on equatorial moorings do not cover the overall period but give some indications on SSS time variability. Despite day-to-day variability due to local atmospheric conditions (isolated heavy rainfall), the low-frequency changes and incursions of high-salinity waters generally agree with TSG equatorial measurements (Figure 6).

These features are summarized in Figure 7, which represents the latitude distribution of mean and standard deviation of SSS along the two tracks. The ET high-salinity waters ( $S > 34.5$ ) are trapped in the 5°N–15°S equatorial band, while no maximum is detectable in the WT. Outside of this 5°N–5°S band there is no difference in WT and ET mean SSS. The SSS variability shown on the standard deviation (Figure 7b) is similar on the two tracks north of 5°N. South of this latitude, the ET variability is stronger than on the WT. Maximum is observed near the equator (0.41 on the WT and 0.54 on the ET). South of the equator the large variability observed on the ET might be due to the large variability of the position of the SPCZ. By contrast, there is no difference in mean SSS and in standard deviation between the two tracks near the mean ITCZ position (6°N–10°N).

**3.2.2. Zonal distribution.** During the oceanographic FLUPAC cruise of R/V *L'Atalante* [LeBorgne et al., 1995] along the equator in October 1994, the thermosalinograph record highlighted a sharp zonal SSS front (Figure 8a) separating the central equatorial Pacific waters ( $S > 35.0$ ) from the western equatorial Pacific waters ( $S < 34.5$ ). The spatial resolution of TSG data gives an estimate of this sharp gradient as more than 0.5 in 200 km near 173°W, i.e., 1500 km east of ET. This front seemed also to delineate two different regimes of salinity variation: west of the front the variation exhibited high frequency and high amplitude due to frequent rainfall, while east of the front evaporation dominated and thus SSS presented a more stable zonal distribution. In ocean simulations such a front seems to be a permanent feature and is subject to strong zonal displacement in relation with winds, zone of maximum convection and currents [Picaud et al., 1996; Vialard and Delecluse, 1998a, b]. This front had a signature in depth as a strong vertical salinity gradient within the temperature mixed layer, indicating the presence of a barrier layer near the date line.

The zonal displacements of this SSS front can be large. For example, waters of salinity higher than 35.0 were also encountered on ET (173°E) in February 1994 (Figure 8b), indicating that the SSS front was west of 173°E at this time. These high-salinity waters extended on both sides of the equator and SSS distribution presented sharp meridional gradients of more than 1.5 over 200 km near 5°N and 5°S. These high-salinity values cannot be attributed to equatorial upwelling of high-salinity water which is generally situated in the top of the thermocline. The thermocline was too deep at that time (around 70 m as shown by TOGA-TAO moorings) to modify the surface salinity. These high-salinity waters were central Pacific waters as already shown above; and they were also detected on equatorial moorings (Figure 6): in early January 1994, high-salinity peaks were visible at different longitudes, 173°E, 160.5°E, and 156°E. They lasted about 4 months at

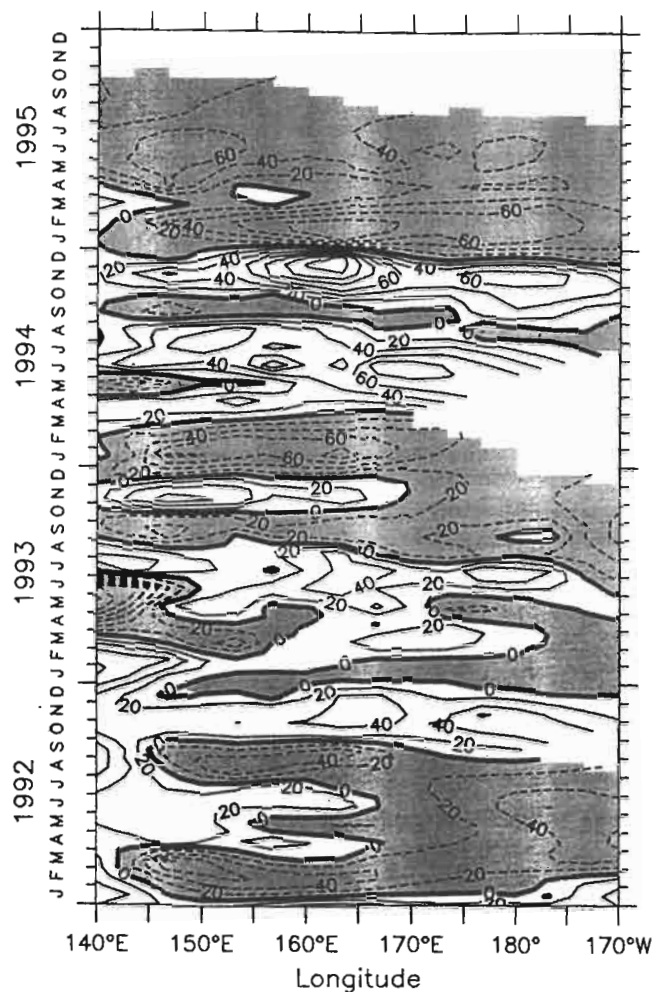
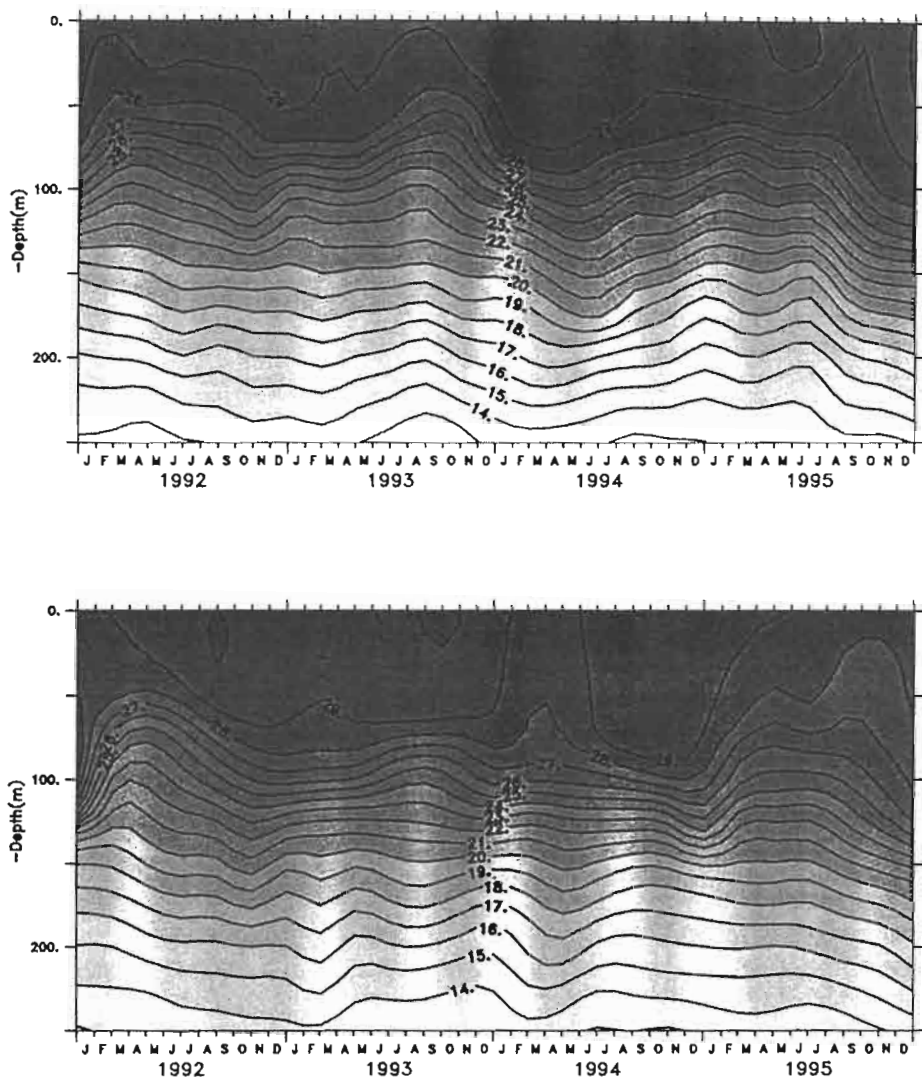


Figure 4. Monthly averaged zonal currents (in  $\text{cm s}^{-1}$ ) along the equator from surface drifting buoys in 1992–1995. Westward currents are negative (and grey), and eastward currents are positive (and white).

173°E, about 3 months at 160.5°E, and about 1 month at 156°E but were not detected with 2-month TSG sampling frequency on the western track. This suggests that the salinity front had reached 156°E, where it remained shortly, and had a zonal displacement of more than 30° of longitude (3300 km). Two other occurrences of such zonal displacement of the front are visible on our data: in October 1992 although of lower amplitude since no SSS greater than 35.0 can be seen at 156°E (the front does not seem to have reached this point), and during 1995 when the front crossed 173°E in April and reached 156°E in September 1995. These incursions of high salinity were trapped between 5°N and 5°S (Plate 2 and Figure 8b) suggesting specific SSS variability in the equatorial band. Similar abrupt changes in salinity have already been observed in the western Pacific. Sprintall and McPhaden [1994] described the invasion of high-salinity surface waters ( $>35.0$ ) over a 100-m-thick layer at 165°E, during the 1988–1989 La Niña event, which were abruptly replaced in November 1989 by low-salinity waters. SSS decreased from 35.3 to 34.3 in 1 month. McPhaden et al. [1992] argued that this abrupt salinity change was the result of meridional advection.

The speed of the eastward and westward displacements of such a front has been estimated for the 1992–1995 period using



**Figure 5.** Time-depth plot of temperature at the equator sampled with XBT probes (top) at 156°E, western track, and (bottom) at 173°E, eastern track during 1992–1995.

daily salinity averages from Seacats thermosalinographs on moorings and more roughly with TSG observations. It is in the range of 20–60 cm/s to the west or to the east.

#### 4. Discussion

The large-scale variability of SSS is due either to variations of E-P, of mixing rate or to surface currents which advect salinity. The standard mixed layer formulation for salinity evolution can be written as

$$\frac{\partial S}{\partial t} + \mathbf{U} \cdot \nabla S = \frac{S}{h} (E - P) - \frac{w_e}{h} \frac{\Delta S}{S} \quad (1)$$

where  $S$  is the mixed layer salinity,  $\mathbf{U}$  the surface current,  $E - P$  the evaporation minus precipitation term, and  $w_e$  the vertical entrainment at the base of the mixed layer of thickness  $h$ . The last term in the right-hand side of the equation represents the vertical mixing and  $w_e$  is given by  $W_e = \partial h / \partial t + \nabla \cdot h \mathbf{U}$  when the mixed layer deepens and  $w_e = 0$  when the mixed layer is shoaling. The problem of determining  $h$  is beyond the scope of this study.

The contributions of vertical advection and turbulent mixing

cannot be obtained rigorously with our observations alone and only numerical simulations at such large scales (annual and interannual changes) can give the magnitude of these terms in the salt budget [Vialard and Delecluse, 1998a, b]. From our observations during the period 1992–1995 we can, however, discuss the contributions of some mechanisms responsible for the SSS variability.

In the warm pool region, at the equator, air-sea conditions (high SST, low surface winds, and high atmospheric convection activity) make the evaporation term quite uniform in longitude and in time, at a monthly timescale with the exception of high wind episodes (Zhang et al. [1995]: however, at 165°E–8°N, Zhang and McPhaden, [1995], found a significant seasonal variation in latent heat flux). This is confirmed by our estimation of the evaporation term using TAO mooring data in the warm pool at a monthly timescale. Evaporation range is between 100 and 140 mm/month and quite uniform between 156°E and 165°E in 1992–1995. On the other hand, rainfall estimates from SSM/I have a range between near 0 and 680 mm/month. This makes precipitation the dominant term in E-P variability.

Figure 2 displays the SSM/I rainfall estimations in the near equatorial band (2°N–2°S) and the location of the salinity front

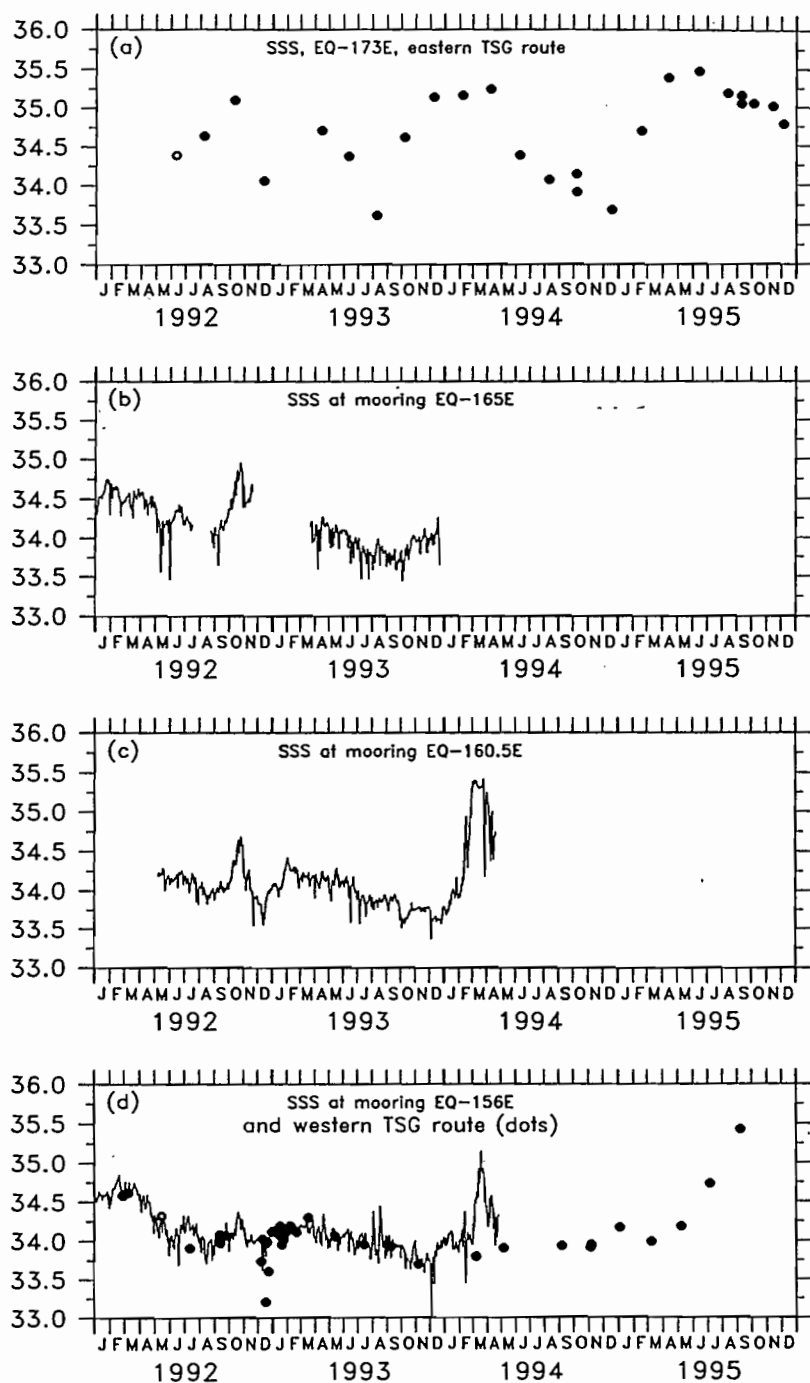


**Figure 6.** Sea surface salinity time series at the equator in 1992–1995: (a) at 173°E (TSG), (b) at 165°E (mooring), (c) at 160.5°E (mooring), and (d) at 156°E (solid line: mooring, dots: TSG).

(arbitrarily located by the 35.0 isohaline separating central equatorial Pacific high-salinity waters and western equatorial Pacific low-salinity waters as already stated) derived from TSG and mooring data. The salinity front is always located near the eastern edge of the maximum rainfall region and migrates with it. This indicates that the salinity front delineates two distinct regions: low salinity in the western region where maximum rainfall is located and high salinity in the east where rainfall is more sparse and where evaporation processes dominate precipitation. The two distinct regimes of rainfall are responsible for SSS mean distribution under the two associated regions, but the region of the front is more likely to behave in relation

with oceanic circulation dynamics [Picaud *et al.*, 1996; Vialard and Delecluse, 1998a]. Note that from January to October 1993, Figure 2 does not indicate the zonal SSS front which was supposed to have drifted east of the monitored area.

Delcroix *et al.* [1996] established that the thickness of the homogeneous layer is approximately  $h = 31$  m in the western equatorial Pacific. Ando and McPhaden [this issue] stated that in the western Pacific, west of 160°E, the mixed layer is 40–50 m deep. The ratio  $S/h$  being roughly equal to 1 ( $S \approx 35$ ), the local change in salinity (in month $^{-1}$ ) of the homogeneous layer due to rainfall is approximately equal to  $-P$ . Figure 9 shows the monthly local rate of change in SSS due to precipitation

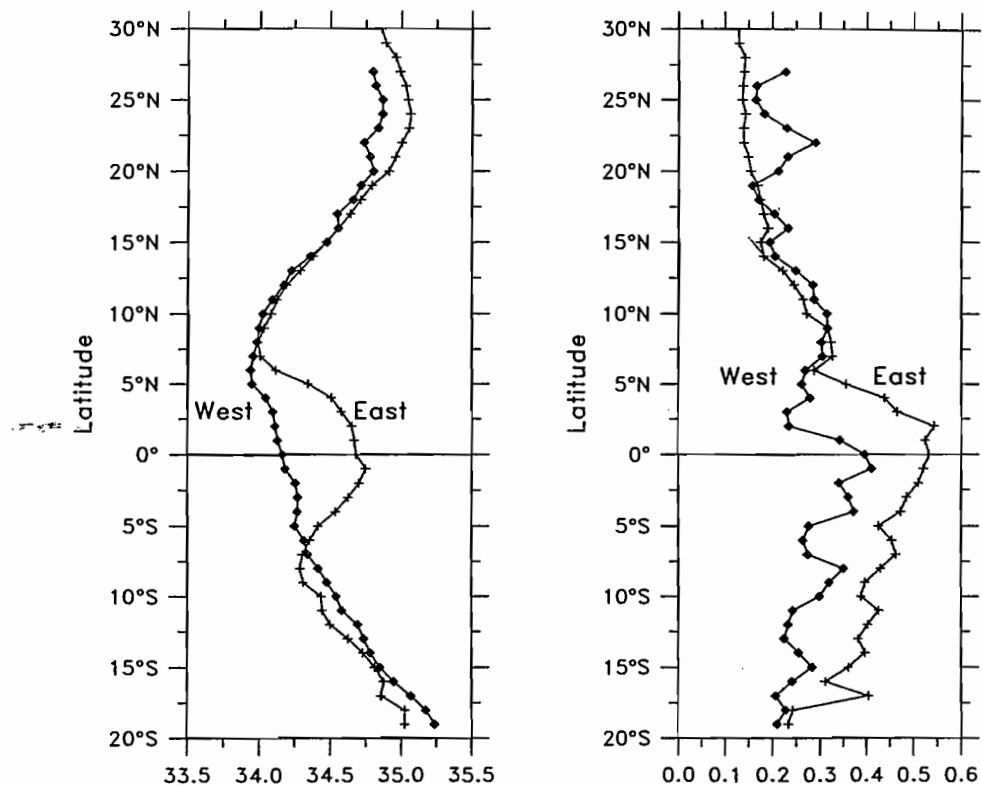


**Figure 7.** (left) Meridional mean sea surface salinity and (right) associated standard deviation over the period 1992–1995 for both western (diamonds) and eastern tracks (crosses).

(stars) and the local variation of salinity (circles) estimated over 2 months at 0°–173°E from TSG data. The monthly local change in salinity due to precipitation appears to be of the order 0 to –0.3 per month while observed changes in salinity are of the order of –0.4 to +0.5 per month. The time evolution of the influence of precipitation is smoother than the observed local rate of SSS changes which present abrupt events. We note that in July–August 1993, September–December 1993, April–May 1994, December 1994 to March 1995 the term E-P cannot explain the strong changes in SSS (decreases or increases; Figure 9). We then argue that rainfall patterns act only as a fresh water input but are not responsible for some strong observed SSS variations in the western equatorial Pacific. At our scale of time and space, the oceanic processes that may contribute to the SSS variability might be therefore horizontal and/or vertical advection (equation (1)).

Systematic observations of the vertical haline structure are scarce in the ocean, and this is also true for our observational period in the western Pacific. The few moorings available did not provide enough information on the subsurface haline distribution between the surface and 200 m: the 165°E mooring did not provide observations during the arrivals of the salinity maxima because of technical mooring failures and, at 160.5°E, only the 30-m upper layer was sampled. The mean vertical salinity distribution reveals that the isohaline 35.0 is generally located in the upper thermocline (around 100 m depth) as seen from cruises at 165°E [Gourion and Toole, 1993; Delcroix and Eldin, 1995]. An increase of surface salinity to 35.0 by upwelling processes would imply a vertical rise of the upper thermocline from 100 m. TAO moorings (equator 156°E; 165°E; 170°E; 180° and 2°S–165°E) indicated a deepening of the thermocline of 30–40 m depth during the equatorial

“salty” episodes (October 1992, February–March 1994, and during 1995; Plate 2). These deepenings of the thermocline indicate that there was no influence of deep salty waters on SSS during these episodes. It is worthwhile noting that during thermocline deepening (in February–March 1994 and the whole of 1995 at 180°E on TAO mooring), a 1°–2°C cooling was observed in the first 120 m surface layer. This cooling was likely due to horizontal advection of cooler water and/or evaporative cooling.

High-salinity waters were trapped in the near-equatorial band (Figure 8b). This suggests that meridional advection was small at our timescale (2 month); otherwise, the meridional fronts would move in latitude. This maintenance of high salinity on the equator also excluded equatorward meridional advection as a major process in SSS variability because the only waters that would shift equatorward would be low-salinity waters that were present under the ITCZ and SPCZ (see Plate 2, <5°–10°N and <5°–10°S bands). The abrupt SSS increases in waters occasionally trapped near the equator (and explained neither by E-P nor by vertical and meridional advects) were mainly driven by zonal advection (Figure 4; Plate 2).

In order to investigate the role of zonal advection in the SSS variability, mainly illustrated by the displacements of the salinity front, we reported (Figure 3) the zonal current field derived from SVP data along the two cross-equatorial transects WT and ET. There is a clear correlation in time, mainly on the ET, between these fields and the SSS displayed in Plate 2. Usually, an increase of SSS in the near equatorial band corresponds to a westward drift carrying high-salinity waters and a decrease of SSS corresponds to an eastward drift carrying low salinity waters. The magnitudes of the associated zonal currents ( $\pm 20$  to  $\pm 60$  cm/s) are in agreement with the rough estimate of the speed of the zonal displacements of the salinity

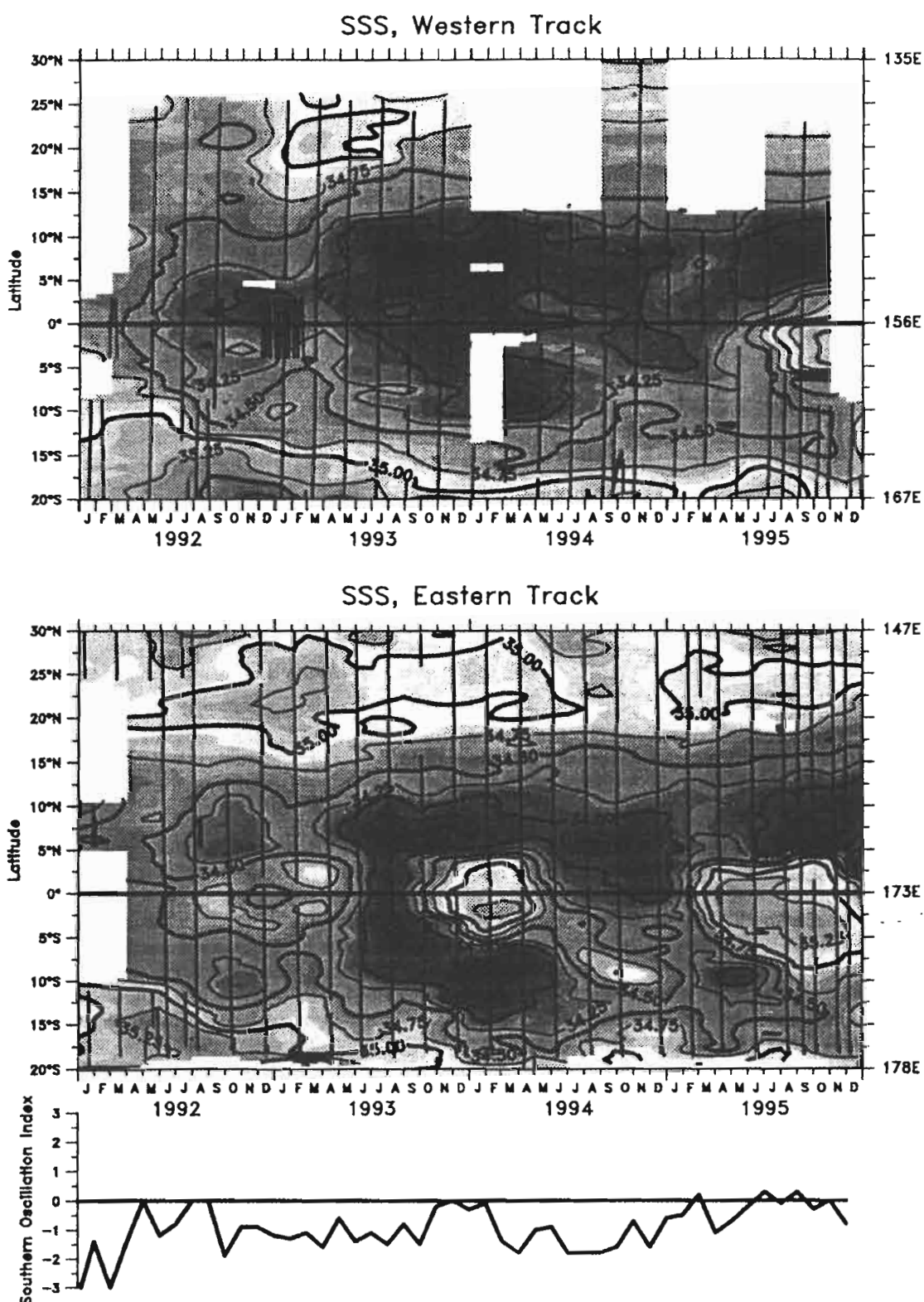


**Plate 2.** Time-latitude sea surface salinity measured by thermosalinograph for the 1992–1995 period, along the (top) western track, (middle) along the eastern track. The different voyages are indicated by lines. (bottom) SOI filtered with a 6-month Hanning filter over the same period.

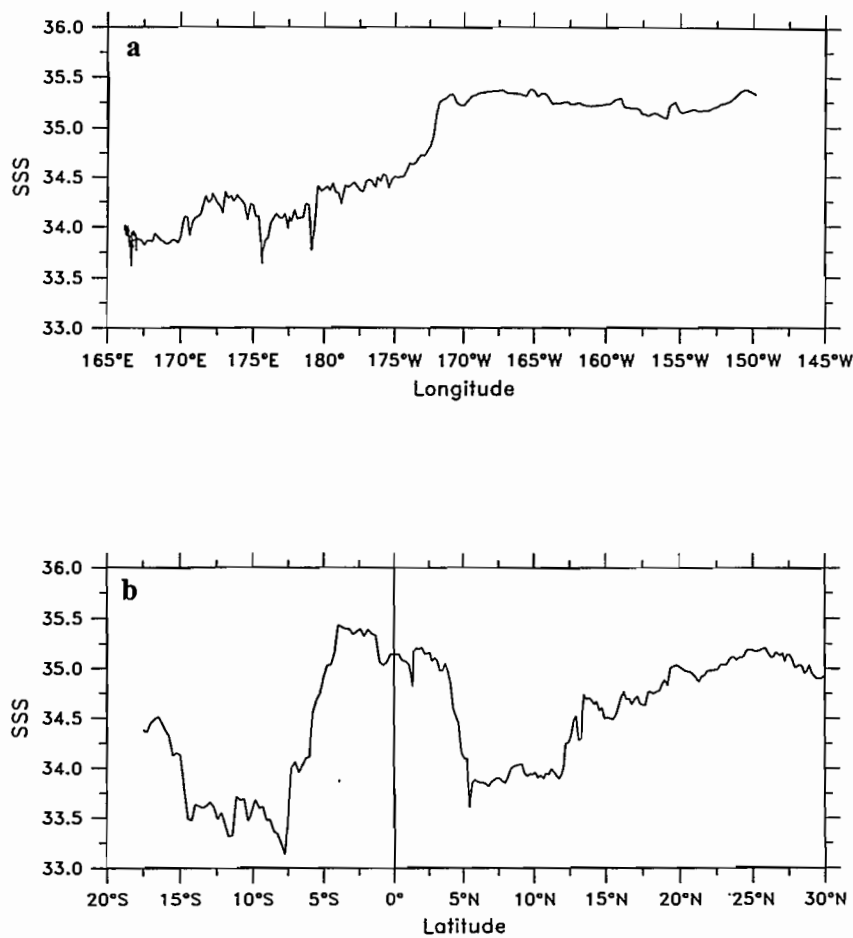


**Figure 8.** (a) Zonal sea surface salinity distribution observed during FLUPAC cruise along the equator (October 2–22, 1994). (b) Meridional sea surface salinity distribution observed along the eastern track by the VOS Pacific Islander (January 30 to February 11, 1994).

front calculated in the preceding section. Geostrophic current anomalies computed from TOPEX-POSEIDON data (C. Menkes, personal communication, 1996) confirm the increase in strength of the South Equatorial Current in early 1994 (January–April) and during 1995 which was associated with equatorial high-salinity waters. Figure 4 displays the time variations of the zonal currents along the equator. The surface currents present numerous abrupt reversals over a wide area which can be as large as  $50^{\circ}$  longitude. Eastward drift and episodic occurrences of equatorial jets near the equator during westerly wind bursts are linked with low SSS near the equator on the two tracks. For our period of interest, the surface currents were more often eastward in the western part of the area of the study, and more often westward in the eastern part. Therefore, the SSS zonal front was often found between the two tracks during our period of observation (Figure 2). If we consider that the 35.0 isohaline separates the central and western equatorial surface waters, climatology indicates that its position was around  $170^{\circ}\text{E}$  (Plate 1a).

The main results of this study can be summarized in a conceptual view along the equator as proposed in Figure 10. Atmospheric convection is maximum in the western Pacific. The associated rainfall forces the ocean through an input of fresh water that accumulates in the mixed layer maintaining low-salinity waters, i.e., the fresh pool. The maximum atmospheric convection is situated near the eastern edge of the fresh pool

and induces a strong zonal gradient with a region further east where, on the average, convection is weak. West of the maximum, convection decreases more slowly. This leads to a contrasted distribution of SSS along the equator: high-salinity waters in the central east equatorial Pacific and low salinity waters in the western equatorial Pacific separated by a sharp SSS front as described above, and an inversion of SSS gradient on the western side of the fresh pool. This fresh pool lies at the top of the warm pool, thus forming stable low-density waters that can be easily shifted back and forth along the equator by zonal advection. The frontal zone is therefore linked with a convergence between westward advection of Central Pacific waters and occurrences of eastward advection of western Pacific freshwater. This convergence zone is due to large-scale wind forcing [Vialard and Delecluse, 1998b] and moves zonally in phase with the southern oscillation index [Picaud et al., 1996]. During the period of observations, ET was crossed several times by the SSS front which explains the observed abrupt SSS changes, while WT situated near the center of the fresh pool exhibited very weak SSS variability. However, two extreme situations were encountered: in the mature phase of El Niño during November 1991 to January 1992 when the fresh pool invaded the central Pacific and an increase of SSS on the WT was observed (even though surface currents were eastward) leading to negative advection of SSS (SSS increase). The other extreme situation was observed during the year 1995 when the fresh

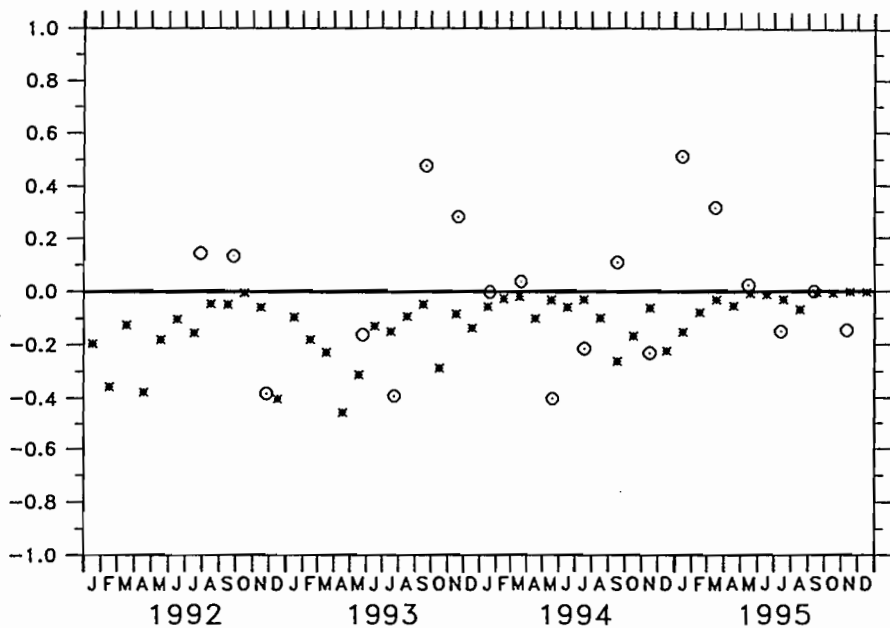


**Figure 9.** SSS time variations from TSG ( $\partial S/\partial t$ ) (open circles) and contribution of SSMI rainfall to SSS time evolution ( $-(S/H) P$ ) (stars). Both quantities are estimated at 173°E equator (in month $^{-1}$ ).

pool was confined to the far western Pacific, associated with westward currents and negative SSS advection also leading to an increase in SSS, visible on our two tracks (see Plate 2, and Figures 3 and 4).

## 5. Conclusion

We analyzed surface salinity data collected with thermosalinographs on merchant ships crossing the western tropical Pacific fresh pool along two north-south tracks (WT and ET) and on TAO moorings. Our period of observation covered the years 1992–1995, namely the 1991–1994 El Niño and the moderate 1995 La Niña. The WT was shown as being in the fresh pool most of the time, and the ET near its eastern edge where a sharp zonal SSS front was detected, induced by zonal convergence of water masses in the equatorial band. SSS experienced strong variations especially close to the equator with

episodes of high salinity (above 35.0). Our results suggest that at the scale of our study, zonal advection is the main mechanism responsible for these variations near the equator. Other possible mechanisms were evaluated but they were found to be weaker for the major abrupt changes in SSS at 1–2 month timescale. The zonal and meridional SSS fronts detected in this study emphasized the particular dynamics of the equatorial region: even if freshwater input is necessary in the long term for its formation in the western Pacific, the fresh pool location and its changes are likely clearly due to equatorial dynamics.

*Delcroix and Picaut [1998]* had emphasized marked differences in salinity distribution between the 1987 El Niño and the strong 1988–1989 La Niña. Using geostrophic surface current anomalies calculated from Geosat altimetry, they concluded that, during these two major contrasted climatic events, SSS advection by zonal current anomalies was the dominant process for SSS variability in the equatorial band. We showed in the present study that such large changes in SSS existed even during the succession of warm events in 1992–1994 and that zonal advection is the main mechanism for these variations near the equator, as by *Picaut et al. [1996]*, but for the period 1982–1989. We also explained SSS distribution in 1995 when a maximum salinity developed at the two tracks, related to the development of La Niña with the SSS zonal front migrating to the far western Pacific.

At our time scale of sampling (1–2 months), it was shown that the SSS changes described by the displacements of the zonal SSS front are in phase with maximum of atmospheric convection. *Picaut et al. [1996]* have suggested that these displacement are also correlated with zonal displacement of the warm pool and the southern oscillation index. The relative displacements of the warm pool and the fresh pool induce changes in overlying atmospheric condition and play a key role in air-sea interaction.

TSG monitoring in the fresh pool has been found fruitful for describing and understanding SSS distribution and its changes in relation with equatorial dynamics and thermodynamics. This type of data, necessary to map SSS objectively, will be associ-

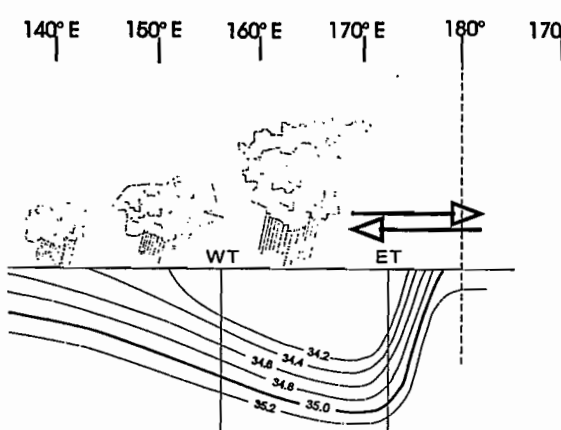


**Figure 10.** Schematic vertical view of salinity of the fresh pool along the equator. The zonal front is situated at its eastern edge. Atmospheric convection maximum is west of the SSS front and decreases westward. Vertical lines represent the two shipping lines (western track (WT) and eastern track (ET)).

ated with other oceanic data and satellite measurements in order to properly answer the question of the balance of precipitation, evaporation, and upper ocean salt flux which is fundamental for understanding air-sea coupling. Any climate coupled model must reproduce observed SSS (as well as SST) to have a correct parametrization of the hydrological and related energy fluxes. This is one of the questions that will be addressed by the future Tropical Rainfall Measuring Mission programme.

**Acknowledgments.** We are indebted to the officers and crews of the merchant ships and research vessels which participate voluntarily in the monitoring of the ocean, and to J. Grelet, B. Buisson and F. Gallois for developing the TSG system. R. Lukas, P. Freitag, and M. McPhaden were very kind to provide SSS mooring data. We also thank Mayra Pazos for her help in surface drifter processing, and Mark Ferraro for his advice in getting SSM/I files. J. Picaut, T. Delcroix, and P. Rual are acknowledged for their useful comments and discussions on this study.

## References

- Ando, K., and M. J. McPhaden, Variability of Surface Layer Hydrography in the Tropical Pacific Ocean, *J. Geophys. Res.*, **102**, 23,063–23,078, 1997.
- Cooper, N. S., The effects of salinity on tropical ocean models, *J. Phys. Oceanogr.*, **18**, 697–707, 1988.
- Delcroix, T., and G. Eldin, Observations hydrologiques dans l'océan Pacifique tropical ouest, *TDM 141*, 77 pp, ORSTOM, Noumea, New Caledonia, 1995.
- Delcroix, T., and C. Hénin, Mechanisms of subsurface thermal structure and sea surface thermohaline variabilities in the southwestern tropical Pacific during 1979–85, *J. Mar. Res.*, **47**, 777–812, 1989.
- Delcroix, T., and C. Hénin, Seasonal and interannual variations of sea-surface salinity in the tropical Pacific Ocean, *J. Geophys. Res.*, **96**, 22,135–22,150, 1991.
- Delcroix, T., and J. Picaut, Zonal displacement of the western equatorial Pacific “fresh pool,” *J. Geophys. Res.*, **103**, 1087–1098, 1998.
- Delcroix, T., G. Eldin, M. H. Radenac, J. Toole, and E. Firing, Variation of the western equatorial Pacific Ocean, 1986–1988, *J. Geophys. Res.*, **97**, 5423–5445, 1992.
- Delcroix, T., C. Hénin, V. Porte, and P. Arkin, Precipitation and sea surface salinity in the Tropical Pacific Ocean (1974–1989), *Deep Sea Res. I*, **43**, 1123–1141, 1996.
- Donguy, J. R., Recent advances in the knowledge of the tropical Pacific, *Progr. Oceanogr.*, **19**, 49–85, 1987.
- Donguy, J. R., Surface and subsurface salinity in the tropical Pacific Ocean, *Progr. Oceanogr.*, **34**, 45–78, 1994.
- Donguy, J. R., and C. Hénin, Anomalous navifacial salinities in the tropical Pacific Ocean, *J. Mar. Res.*, **34**, 355–364, 1976.
- Donguy, J. R., and C. Hénin, Hydroclimatic anomalies in the South Pacific, *Oceanol. Acta*, **1**, 25–30, 1978.
- Eldin, G., T. Delcroix, C. Hénin, K. Richards, Y. du Penhoat, J. Picaut, and P. Rual, The large scale structure of currents and hydrology along 156°E during the COARE intensive observation period, *Geophys. Res. Lett.*, **21**, 2681–2684, 1994.
- Ferraro, R. R., and G. F. Marks, The development of SSM/I rain-rate retrieval algorithms using ground-based radar measurements, *J. Atmos. Oceanic Technol.*, **12**, 755–770, 1995.
- Gouriou, Y., and J. Toole, Mean circulation of the upper layers of the western equatorial Pacific Ocean, *J. Geophys. Res.*, **98**, 22,495–22,520, 1993.
- Hansen, D. V., and P. M. Poulain, Quality control and interpolations of WOCE-TOGA drifter data, *J. Atmos. Oceanic Technol.*, **13**, 900–909, 1996.
- Hayes, S., L. Mangum, J. Picaut, A. Sumi, and K. Takeuchi, TOGA-TAO: A moored array for real time measurements in the tropical Pacific, *Bull. Am. Meteorol. Soc.*, **72**, 339–347, 1991.
- Hénin, C., Intensive measurements of sea surface temperature and salinity in the Western Pacific (1996), *Int. WOCE Newslett.*, **22**, 8–11, 1996.
- Hénin, C., and J. Grelet, A merchant ship thermo-salinograph network in the Pacific Ocean, *Deep Sea Res.*, **43**, 1833–1855, 1996.
- Hénin, C., Y. du Penhoat, M. Ioualalen, and R. Lukas, Large scale sea-surface salinity changes in the western equatorial Pacific Ocean during 1992–1994, paper presented at TOGA-95, Melbourne, Australia, April 2–7, 1995.
- Hires, R. I., and R. B. Montgomery, Navifacial temperature and salinity along the track from Samoa to Hawaii 1957–1965, *J. Mar. Res.*, **30**(2), 177–200, 1972.
- Kessler, W. S., and M. J. McPhaden, The 1991–1993 El Niño in the Central Pacific, *Deep Sea Res.*, **2**, 295–333, 1995a.
- Kessler, W. S., and M. J. McPhaden, Oceanic equatorial waves and the 1992–93 El Niño, *J. Clim.*, **8**, 1757–1774, 1995b.
- Kessler, W. S., and B. A. Taft, Dynamic heights and zonal geostrophic transports in the central tropical Pacific during 1979–84, *J. Phys. Oceanogr.*, **17**, 97–122, 1987.
- LeBorgne, R., Ch. Brunet, G. Eldin, M. H. Radenac, and M. Rodier, Campagne océanographique FLUPAC à bord du N. O. L'Atalante (23–9 au 29-10-1994). Recueil de données, *Archives Sciences de la Mer, Oceanogr. I*, 337 pp., OSTROM, Noumea, New Caledonia, 1995.
- Levitus, S., Climatological atlas of the world ocean, *NOAA Prof. Pap. 13*, 173 pp.. U. S. Gov. Print. Off., Washington, D. C., 1982.
- Lukas, R., Freshwater input to the western equatorial Pacific Ocean and air-sea interaction. in *Proceedings of US-PRC International TOGA Symposium*, pp. 305–327, China Ocean Press, Beijing, 1988.
- Lukas, R., and E. Lindstrom, The mixed layer of the western equatorial Pacific Ocean, *J. Geophys. Res.*, **96**, suppl., 3343–3357, 1991.
- McPhaden, M. J., TOGA-TAO and the 1991–92 El Niño/Southern Oscillation event, *Oceanography*, **6**, 36–44, 1993.
- McPhaden, M. J., F. Bahr, Y. du Penhoat, E. Firing, S. P. Hayes, P. P. Niiler, P. L. Richardson, and J. M. Toole, The response of the western equatorial Pacific Ocean to westerly wind bursts during November 1989 to January 1990, *J. Geophys. Res.*, **97**, 14,289–14,303, 1992.
- Picaut, J., M. Ioualalen, C. Menkes, T. Delcroix, and M. J. McPhaden, Mechanism of the zonal displacements of the Pacific warm pool: Implications for ENSO, *Science*, **274**, 1486–1489, 1996.
- Reason, C. J. C., On the effects of ENSO precipitation anomalies in a global ocean GCM, *Clim. Dyn.*, **8**, 39–47, 1992.
- Reverdin, G., D. Cayan, H. D. Dooley, D. J. Ellett, S. Levitus, Y. duPenhoat, and A. Dessier, Surface salinity of the North Atlantic: Can we reconstruct its fluctuations over the last one hundred years?, *Prog. Oceanogr.*, **33**, 303–346, 1994.
- Rochford, D. J., The surface salinity regime of the Tasman and Coral Seas, *Rep. 84*, 33 pp., Div. of Fish. and Oceanogr., CSIRO, Cronulla, Australia, 1977.
- Roemmich, D., M. Morris, W. R. Young, and J. R. Donguy, Fresh equatorial jets, *J. Phys. Oceanogr.*, **24**, 540–558, 1994.
- Shinoda, T., and R. Lukas, Lagrangian mixed layer modeling in the western equatorial Pacific, *J. Geophys. Res.*, **100**, 2523–2541, 1995.
- Sprintall, J., and M. McPhaden, Surface layer variations observed in multi-year time series measurements from the western equatorial Pacific, *J. Geophys. Res.*, **99**, 963–973, 1994.
- Sprintall, J., and T. Tomczak, Evidence of the Barrier layer in the surface layer of the tropics, *J. Geophys. Res.*, **97**, 7305–7316, 1992.
- Vialard, J., and P. Delecluse, A OGCM study for the TOGA decade, I, Role of haline stratification in the physics of the warm pool, *J. Phys. Oceanogr.*, in press, 1998a.
- Vialard, J., and P. Delecluse, A OGCM study for the TOGA decade, II, Barrier layer formation process, *J. Phys. Oceanogr.*, in press, 1998b.
- Villain, J. P., Variabilité de la salinité dans le Pacifique ouest. Amélioration du calcul de la topographie dynamique et des courants géostrophiques, in *Mémoires de stages. Série Sciences de la Mer. Océanographie Physique*, 53 pp., Centre ORSTOM de Nouméa, Nouvelle-Calédonie, 1995.
- Webster, P. J., and R. Lukas, TOGA COARE: The Coupled Ocean Atmosphere Response Experiment, *Bull. Am. Meteorol. Soc.*, **73**, 1377–1416, 1992.
- Zhang, G. J., and M. J. McPhaden, The relationship between sea surface temperature and latent heat flux in the equatorial Pacific, *J. Clim.*, **8**, 589–605, 1995.
- Zhang, G. J., V. Ramanathan, and M. J. McPhaden, Convection-evaporation feedback in the equatorial Pacific, *J. Clim.*, **8**, 3040–3051, 1995.

Y. dePenhoat, Groupement de Recherche en Goodesie Spatiale, 14 av E. Belin, 31 401 Toulouse, France.

C. Hénin, Centre ORSTOM Noumea, BP A5, 98848 Noumea Cedex, New Caledonia.

M. Ioualalen, LODYC, Univ. P. and M. Curie, boite 100, 4 Place Jussieu, 75252 Paris Cedex 05, France.

(Received November 18, 1996; revised June 9, 1997; accepted June 16, 1997.)

# Sea surface salinity changes along the Fiji-Japan shipping track during the 1996 La Niña and 1997 El Niño period

Thierry Delcroix, Lionel Gourdeau, and Christian Hénin

Groupe SURTROPAC, ORSTOM Centre, BP A 5, Nouméa, New Caledonia

**Abstract.** Sea-surface salinity (SSS) changes during the 1996 La Niña and 1997 El Niño events are analysed along the Fiji-Japan shipping track, based on 20 thermosalinograph sections. In the equatorial band, above-average SSS (35.2 to 35.4 instead of 35) were observed in 1996, consistent with a well-marked south equatorial current, an unusually-strong equatorial upwelling, and below-average precipitation (P). From January to August 1997, the SSS decreased sharply from 35.2 to 33.8 (lowest recorded monthly value over the last 20 years), compatible with a reversal of zonal current, the occurrence of equatorial downwelling, and above-average P. From September to November 1997, the SSS remained almost constant (34.2), consistent with the opposite effects of eastward current, likely bringing low saline water from the Pacific warm pool, and of evaporative cooling, vertical mixing and below-average P which all tend to increase SSS. The potential impacts of the observed SSS changes on sea level are discussed.

## Introduction

The distribution of salt in the tropical oceans and its variability are potentially important in better understanding the ocean-atmosphere coupled system. In the tropical Pacific, the average distribution of Sea Surface Salinity (SSS) is characterised by a relatively low value in the Inter Tropical and South Pacific Convergence Zones (ITCZ, SPCZ), and in the so-called warm pool in the western equatorial region where Sea Surface Temperature (SST) is over 28°C [Levitus *et al.*, 1994]. In these three areas, the low value of SSS reflects primarily the negative evaporation minus precipitation (E-P) budget resulting from light winds and high rainfall rates.

Ignoring the high-frequency variability, the SSS changes happen essentially at the seasonal time scale in the ITCZ and SPCZ, and at the ENSO (El Niño Southern Oscillation) time scale in the warm pool region [Delcroix *et al.*, 1996]. This latter region has been called also the "fresh pool" ( $SSS \leq 35$ ); its eastern edge is characterised by a marked salinity front centred around the

35 isohaline, and it separates the less saline water in the west from the more saline water in the central basin [Picaut *et al.*, 1996; Delcroix and Picaut, 1998; Hénin *et al.*, 1998]. Based on observational and modelling studies covering the pre-1996 period, these last authors demonstrated that the eastern edge of the warm and fresh pool was displaced eastward during El Niño and westward during La Niña periods, chiefly in response to zonal advection of heat and salt by anomalous currents. Such zonal displacements, in phase with the SOI (Southern Oscillation Index), are associated with changes in local mixed layer temperature and salinity, barrier layer thickness and the world's greatest tuna harvest [Ando and McPhaden, 1997; Lehodey *et al.*, 1997].

As a complement to some of the previously-cited studies, the goal of the present note is to analyse the SSS changes occurring along a shipping track running from Fiji to Japan (Figure 1). Interestingly, the 1996-97 period of study encompasses the 1996 La Niña-like event together with the first year of the strongest El Niño of the century. For comparison purpose and to help in the interpretation, the SSS analysis will be complemented by an analysis of Sea Level Anomaly (SLA), 0/700 dbar Dynamic Height Anomaly (DHA), and vertical thermal structure obtained along the same shipping track.

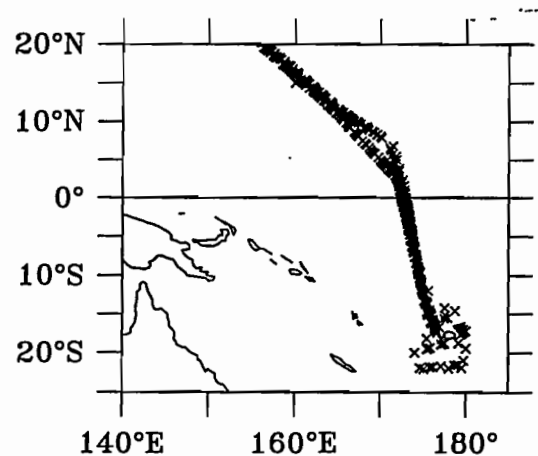
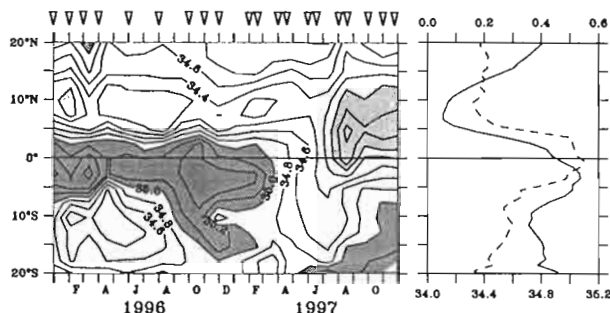


Figure 1. Location of the thermosalinograph, TOPEX/Poseidon and XBT derived measurements along the Fiji - Japan shipping track during 1996-97. The crosses denote the location of the XBT casts. The track separation within 2°N-12°N reflects that 7 out of the 20 shipping tracks call in Tarawa (2°N) and 13 in Majuro (7°N).

Copyright 1998 by the American Geophysical Union.

Paper number 98GL02320.  
0094-8534/98/98GL-02320\$05.00



**Figure 2.** Left panel: Latitude-time evolution of SSS along the Fiji-Japan shipping track. Contour intervals are 0.2. Shaded areas indicate either values above 35 or below 34. The triangles on the top represent the departure dates of the 20 southward voyages. Right panel: 1996-97 mean (full line, bottom scale) and standard deviation (dashed line, upper scale) of SSS.

## Data and processing

The SSS measurements derive from a ship of opportunity thermosalinograph network operated since 1992 from ORSTOM-Nouméa. The measurements, collected every 15 s, were obtained from SeaBird SBE-21 thermosalinograph instruments installed onboard two commercial vessels plying the shipping line Fiji-Japan (Figure 1). The SSS accuracy is about 0.01; details are given in Hénin and Grelet [1996]. The departure dates of the 20 voyages along the Fiji-Japan track during 1996-97 are reported on Figure 2; note that most 25°N-20°S voyages (lasting about 10 days) produced complete data sets, except during Oct. 1996 (8°N-2°N), Nov. 1996 (25°N-5°N, 20°S-8°S), Dec. 1996 (7°S-14°S), and Feb. 1997 (1°N-3°N). These gaps resulted either from instrumental failure or from a qualitative data validation procedure based on internal consistency and climatic limits.

The two vessels were also selected as part of the international Ship of Opportunity Program (SOP) for launching T7 eXpendable Bathymeter (XBT) probes every six hours. The T7-XBT provided temperature profiles from the surface down to 700 dbar with an accuracy of about 0.1°C. The XBT data validation relied on multiple standard deviation criteria. The temperature profiles were converted into 0/700 dbar DHA, using local mean Temperature-Salinity (TS) relation obtained from Levitus *et al.* [1994].

Gridded fields of TOPEX/Poseidon SLA ( $1^\circ \times 1^\circ$  latitude longitude by 10 days) were obtained via FTP (see the Acknowledgements). The estimated accuracy of SLA in this data base ranges from 2-4 cm; details are given in Tapley *et al.* [1994]. The SLA were sampled along the same shipping track as that of Figure 1.

For consistency, the time/space irregularly distributed SSS data, temperature profiles, and SLA data were all plotted on a regular grid using an objective interpolation scheme (Laplacian method; see Delcroix and Hénin [1991]) with a grid element size of  $1^\circ$  latitude by 1 month, neglecting the small zonal variations around the mean track between  $2^\circ\text{N}$  and  $10^\circ\text{N}$ . Both the 0/700 dbar

DHA and SLA were computed relative to the January 1996 - November 1997 period.

## Results

The latitude-time evolution of SSS along the track, as well as the 1996-97 average and its standard deviation ( $\sigma_s$ ), are shown in Figure 2. The mean value exhibits the well-known SSS minima [Delcroix *et al.*, 1996]: one around  $8^\circ\text{N}$  ( $\text{SSS} < 34.2$ ) associated with the ITCZ and the North Equatorial CounterCurrent (NECC), and the other around  $12^\circ\text{S}$  ( $\text{SSS} < 34.8$ ) associated with the SPCZ and the South Equatorial CounterCurrent (SECC). At the equator, the value of 35 indicates that the eastern edge of the warm and fresh pool was located around  $170^\circ\text{E}$  on average during 1996-97, similar to the long-term mean [Levitus *et al.*, 1994]. The strongest variability ( $\sigma_s > 0.3$ ) is trapped in the equatorial band, maximum at the equator ( $\sigma_s = 0.55$ ), as observed from cruises along  $165^\circ\text{E}$  during 1984-94 [Delcroix and Picaut, 1998].

Away from the equatorial band, the SSS evolution exhibits a well-marked seasonal cycle in the ITCZ and SPCZ. There, the SSS minima occurred at the end of the summer season of each hemisphere, mainly in relation to the P seasonal cycle [Delcroix and Hénin, 1991]. In the equatorial band the SSS evolution is much more spectacular, and can be separated into three different time periods. Firstly, during 1996 (when the SOI was weakly positive indicating a La Niña-like period) the SSS was almost constant within 35.2-35.4, i.e. above the long-term mean by about 0.2. Secondly, from January 1997 (when the SOI switched from positive to negative indicating an El Niño signal) to August 1997, the SSS decreased sharply from 35 to below 33.8. This last value is the smallest monthly-averaged SSS observed in the studied area for more than 20 years, according to the 1973-95 SSS time series in Delcroix [1998]. Thirdly, during the remaining time period, the SSS remained almost constant (34.2), well below the long-term mean value (35), while the SOI indicated the persistence of El Niño at basin scale.

Let us now turn to a qualitative discussion of the SSS changes in the equatorial band. The 1996-97 mean sea-surface topography (Figure 3) reveals the meridional boundaries of the surface zonal geostrophic currents, and in particular the mean westward-flowing South Equatorial Current (SEC) in the equatorial band. During most of 1996, a period characterised by above-average SSS, the SLA presents a tendency for a negative curvature at the equator (the SLA at the equator is lower than the SLA on each side of the equator), indicating a stronger-than-average SEC. The presence of this westward flow in the surface layer during most of 1996 is confirmed by the  $0^\circ\text{N}-165^\circ\text{E}$  TAO current measurements [McPhaden, 1993], and by the trajectories of drifting buoys in operation for the CLIVAR Surface Velocity Program [Niiler *et al.*, 1996]. (For conciseness, TAO- and SVP-derived measurements are not shown

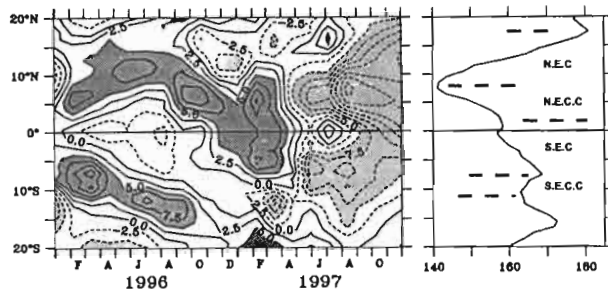


**Figure 3.** Left panel: Latitude-time evolution of the TOPEX/Poseidon derived sea level anomalies (re. Jan. 1996 - Nov. 1997) along the Fiji-Japan shipping track. Contour intervals are 2.5 cm. Shaded areas indicate either values above 5 or below -5 cm. Right panel: XBT-derived 1996-97 averaged 0/700 dbar dynamic height. Units are dyn cm. The surface zonal geostrophic currents referenced in the main text are indicated.

here; they can be found in the 1996-1997 monthly issues of the Climate Diagnostics Bulletin edited by the US Dept. of Commerce and/or at <http://nic.fb4.noaa.gov>). Furthermore, the vertical thermal structure averaged between April and August 1996 (Figure 4a) indicates the occurrence of an equatorial upwelling, with a clear rise of the 28°C isotherm from about 100 m at 5°N and 5°S to near-surface at the equator. This upwelling structure is reminiscent of a strong SEC and characteristic of a La Niña period at 170°E. Still, the precipitation (P) anomalies were below average as inferred from outgoing longwave radiation (see the Climate Diagnostics Bulletin). Hence, the above-average SSS is consistent with horizontal and vertical advection, which, given the mean horizontal and vertical salinity gradients (see Delcroix and Picaut, 1998), could conceivably bring relatively high salinity water from the east and from below, as well as with the rainfall deficit.

From January to August 1997, when the SSS decreased sharply by 1.6, the SLA (Figure 3) presents generally a tendency for positive curvature at the equator, and it is generally positive. This suggests geostrophic eastward flow anomalies as well as local downwelling. Indeed both the 0°N-165°E TAO current measurements and the drifting buoy trajectories, indicate strong near-surface eastward flows reaching as much as 60 cm/s, associated with recorded episodes of westerly winds of the order of 2-8 m/s. Furthermore, the vertical thermal structure in January-May 1997 (Figure 4b) is strikingly different from that of the previous period (Figure 4a), indicating a well-marked equatorial downwelling and a 140 m deep isothermal layer ( $T > 28^{\circ}\text{C}$ ). This downwelling structure is consistent with eastward flows, positive SLA and downwelling Kelvin waves, and it is characteristic of the onset of El Niño in the western equatorial Pacific. Contrasting with 1996, the P anomalies were above-average in the first half of 1997. Hence, the observed SSS decrease appears consistent with both horizontal and vertical advection, likely bringing relatively low-salinity water from the west and suppressing

the import of high salinity water from below, as well as with above-average precipitation.

From September 1997, when the SSS stayed almost constant (34.2), the SLA (Figure 3) decreased to reach -15 cm by November. At that time, the drifting buoy trajectories clearly indicate the occurrence of strong eastward flows in the near-surface layer, consistent with the quasi persistence of westerly winds at the 0°N-165°E mooring site. (Note that at the time of writing the 0°N-165°E TAO current measurements have not yet been recovered). The vertical thermal structure in the second half of 1997 changed drastically (Figure 4c), with a reduction of about 50 m of the thickness of the isothermal layer corresponding to the basin-scale zonal tilt of the thermocline detectable from the equatorial TAO moorings. Interestingly, by September 1997, the P anomalies shifted from positive to negative at 170°E, and the SST anomalies, which had remained nearly constant during the first half of 1997, started to cool (Figure 5). These conditions suggest that the almost-constant SSS during Sept.-Nov. 1997 could reflect the balance between eastward advection which would tend to lower SSS versus the combined effects of rainfall shortage, vertical mixing and evaporative cooling which would tend to increase the SSS.

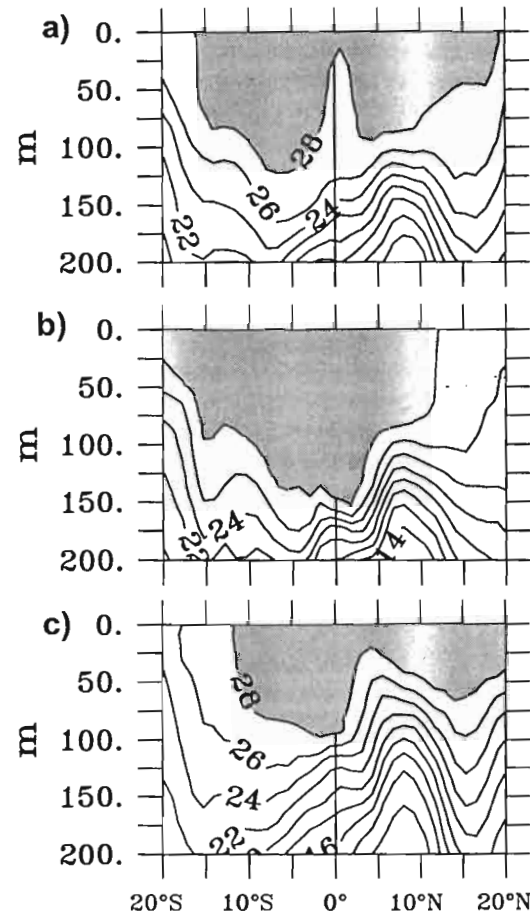


**Figure 4.** Latitude-depth distribution of the thermal structures along the Fiji-Japan shipping track, averaged over: (a) Apr. - Aug. 1996, (b) Jan. - May 1997, and (c) July - Nov. 1997. Contour intervals are  $2^{\circ}\text{C}$ , and shaded areas denote temperatures warmer than  $28^{\circ}\text{C}$ .

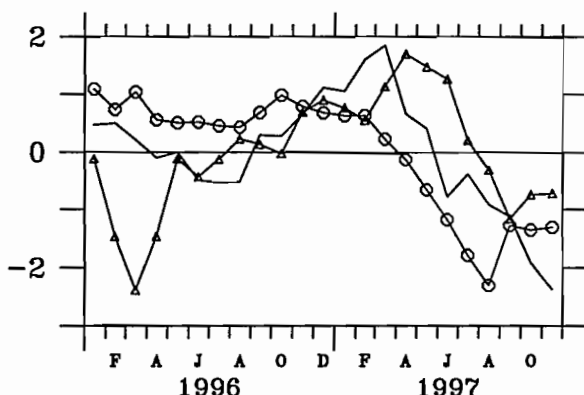


**Figure 5.** Magnitude of the 5°N-5°S averaged TOPEX/Poseidon derived sea level anomaly (full line), XBT-derived SST anomaly (triangles), and thermosalinograph-derived SSS anomaly (circles). The anomalies are relative to the Jan. 1996 - Nov. 1997 period, and they are normalised by their respective standard deviations (5.2 cm for sea level, 0.33°C for SST, and 0.46 for SSS). Note that the SSS signal discriminates the 1996 La Niña from the 1997 El Niño periods more clearly than the SST and sea level signals.

## Conclusion and discussion

To conclude, we have shown that SSS experienced drastic changes in the warm pool region, with peak to peak variations in the equatorial band of as much as 1.6 between the 1996 La Niña and the 1997 El Niño. Assuming that these SSS changes were representative of the upper 50 m, they would correspond to a change of 6 cm in sea level, all other factors being the same, a value which is of the same order of magnitude as the standard deviation of SLA derived from TOPEX/Poseidon during 1996-97 (5.2 cm; see Figure 5). The SSS changes were found qualitatively consistent with horizontal and vertical advection, as well as with precipitation, vertical mixing and evaporative cooling. Although instructive, our qualitative analysis admittedly remains to be quantitatively assessed, possibly via model results in the absence of suitable in situ measurements, provided that salinity changes would be reproduced correctly in models.

One interesting question is the potential effects of the notable observed SSS changes, as presently shown, regarding the quality of ENSO prediction in numerical models assimilating temperature and/or altimeter-derived sea level data only [Ji et al., 1995]. As discussed by Acer-Schertzer et al. [1997], the lack of salinity control in this type of models results in major discrepancies between near-surface modelled and observed currents. Such a failure is especially relevant in the western equatorial Pacific where there is a strong ENSO-related near-surface salinity signal, and where zonal advection is of main importance for ENSO mechanisms. With this contention in mind, it is clear that methods should be developed to assimilate SSS data in prediction models. Expansion of our SOP thermosalinograph network,

with real-time transmission of the measurements, is currently in progress to partly fulfil this requirement.

**Acknowledgments.** We are most thankful to the officers and crews of the M/V Pacific Islander and Coral Islander for authorising and/or facilitating installation of thermosalinographs on board. D. Varillon, C. Peignon, and L. Foucher from ORSTOM were essential in the installation and maintenance of these instruments. The TOPEX Poseidon data were provided by the C.S.R. of the University of Texas at Austin, USA. Comments from J. Picaut were appreciated.

## References

- Acer-Schertzer, C., D. Hansen, and M. Swenson, Evaluation and diagnosis of surface currents in the National Centers for Environmental Prediction's ocean analyses, *J. Geophys. Res.*, 102, 21037-21048, 1997.
- Ando, K., and M. J. McPhaden, Variability of surface layer hydrography in the tropical Pacific ocean, *J. Geophys. Res.*, 102, 23063-23078, 1997.
- Delcroix, T., and C. Hénin, Seasonal and interannual variations of sea-surface salinity in the tropical Pacific ocean, *J. Geophys. Res.*, 96, 22135-22150, 1991.
- Delcroix, T., C. Hénin, V. Porte, and P. Arkin, Precipitation and sea-surface salinity in the tropical Pacific, *Deep Sea Res.*, 43, 1123-1141, 1996.
- Delcroix, T., and J. Picaut, Zonal displacement of western equatorial Pacific "fresh pool", *J. Geophys. Res.*, 103, 1087-1098, 1998.
- Delcroix, T., Observed surface oceanic and atmospheric variability in the Tropical Pacific at seasonal and ENSO time scales: a tentative overview, *J. Geophys. Res.*, in press, 1998.
- Hénin, C., Y. du Penhoat and M. Ioualalen, Observations of sea-surface salinity in the western Pacific fresh pool: large scale changes during 1992-1995, *J. Geophys. Res.*, 103, 7523-7536, 1998.
- Ji, M., A. Leetmaa, and J. Derber, An ocean analysis system for seasonal to interannual climate studies, *Mon. Weath. Rev.*, 123, 460-481, 1995.
- Lehodey, P., M. Bertignac, J. Hampton, A. Lewis, and J. Picaut, ENSO and tuna in the western Pacific, *Nature*, 389, 715-718, 1997.
- Levitus, S., R. Burgett, and T. P. Boyer, *World Ocean Atlas 1994, Vol. 3, Salinity, NOAA Atlas*, 97 pp., Natl. Environ. Satell. Data Inf. Serv. 3, U.S. Dep. of Commer., Washington, D.C., 1994.
- McPhaden, M., TOGA-TAO and the 1991-93 El Niño Southern Oscillation event, *Oceanogr.*, 6, 36-44, 1993.
- Niiler, P., D. Hansen, D. Olson, P. Richardson, G. Reverdin, Y. du Penhoat, and G. Cresswell, The Pan-Pacific surface current study: lagrangian drifter measurements: 1988-1994, *J. Geophys. Res.*, submitted, 1996.
- Picaut, J., M. Ioualalen, C. Menkes, T. Delcroix and M.J. McPhaden, Mechanism of the zonal displacements of the Pacific Warm Pool, implications for ENSO, *Science*, 274, 1486-1489, 1996.
- Tapley, B., D. Chambers, C. K. Shum, R. J. Eanes, and J. C. Ries, Accuracy assessment of the large-scale dynamic ocean topography from TOPEX/Poseidon altimetry, *J. Geophys. Res.*, 99, 24605-24617, 1994.

T. Delcroix, L. Gourdeau, and C. Hénin, Groupe SURTROPAC, ORSTOM centre, BP A 5, Nouméa, New Caledonia. (e-mail: delcroix@noumea.orstom.nc)

(Received April 8, 1998; revised June 22, 1998; accepted June 30, 1998.)

# **Thermo-haline variability of the western tropical Pacific during 1995-1998 : on the erosion/reconstitution of the fresh pool.**

(Submitted to *Geophys. Res. Lett.*)

Mansour Ioualalen & Christian Henin

*Institut de Recherche pour le Développement, IRD, Nouméa, New-Caledonia.*

## **Abstract**

The thermohaline variability of the western tropical Pacific is investigated during the period 1995-1998 along three transects, with data derived from the international Ship Of Opportunity Programme (SOOP). The water masses crossing these transects are studied chronologically with the support of the estimate atmospheric forcing and fresh water budget. It is shown how the Pacific equatorial fresh pool can be eroded through westerly wind forcing and reconstructs itself with fresh water input below intense convective zones and outside of the westerlies' influence. At the end, the fresh pool is confined in a more limited region. These low density waters within a more confined region might require less wind momentum (present in the process) to be shifted back and forth along the equatorial wave guide, eventually leading to El Niño event.

## Introduction

The sea surface salinity (SSS) climatology of the equatorial Pacific is subject to characteristic contrasts; in the eastern-central Pacific are observed high salinity waters ( $SSS > 35$  psu) due to a strong easterly wind activity, yielding to a deficit of fresh water through equatorial upwelling and a prevalence of evaporation over precipitation [Delcroix et al., 1996]; in the western Pacific, the presence of the warm pool and the convergence of winds force a fresh water input within the ascending branch of the Walker circulation.

These two characteristic water masses are separated by a zonal salinity front observed at  $172^{\circ}\text{W}$  during the FLUPAC oceanographic cruise along the equator in October 1994 [LeBorgne et al., 1995, Eldin et al., 1998], and by Sprintall and McPhaden (1994) at  $165^{\circ}\text{E}$  with historical data. Having gathered equatorial current fields derived from observations and models, Picaut et al. (1996, 1999) suggested that this salinity front is directly associated to a convergence of water masses. They found that this salinity front oscillates within the equatorial band at interannual time scale in phase with the southern oscillation index, SOI, mainly through a zonal advection process. West of the salinity front and within the warm pool, lies the fresh pool composed by low density waters and which is often insulated from the bottom of the thermal layer by the barrier layer, BL, (Lukas, 1988) where the vertical salinity gradient controls the density stratification. Following Vialard and Delecluse (1998a, 1998b) who performed sensitivity tests with OPA ocean general circulation model, the BL seems to play a role in the dynamics of ENSO: it forces the derived sharp mixing layer to trap most of the wind momentum and thus amplifies the surface currents, such that the warm/fresh pool can easily oscillate in the equatorial wave guide, dragging/dragged-by the active zone of atmospheric convection through complex air-sea interaction processes. Further, they recovered that the heat exchange at the sea surface can be modified in presence of a BL. This is because the entrainment cooling can be inhibited: in presence of a negative net surface heat flux, one can observe an inversion of temperature at the bottom of the mixing layer and eventually an entrainment heating can occur.

For these reasons the variability of the SSS in the western Pacific is an interesting issue to study. Such a study has been performed by Hénin et al. (1998) for the period 1992-1995. The authors have shown how the thermosaligraph sampling routes can be accurate in describing this large scale variability by validating the data with those of moorings; they also showed how the position of the salinity front can be a useful index in

monitoring ENSO signal. We propose to extend this study up to 1998. This period is interesting because it covers a complete La Niña/El Niño/La Niña cycle. In this study, the evolution of the fresh pool and the salinity front is investigated through observations.

### Data processing

The need for a better knowledge of sea surface salinity distribution in the tropical oceans was evidenced during the 10 years of the TOGA programme (1985-1994). In order to improve the original "meteorological bucket" method of sampling, IRD (Institut de Recherche pour le Développement, former ORSTOM) has developed a network of thermosalinometers (TSG) installed onboard commercial vessels (Hénin and Grelet, 1996). High frequency sampling (every 15 sec) and recording of the median value for every 5 min resulted in quite accurate monitoring of the SSS and the sea surface temperature (SST). The instruments (SBE-21 manufactured by Seabird Electronics Inc., Bellevue, USA) provided an accuracy of 0.02 in SSS and 0.2 to 0.3 °C in SST (when TSG instrument is close to intake water cooling system).

TOA (Thermal Ocean Array) instrumented moored buoys provided thermal distribution in the equatorial band for the 0-500m upper layer (McPhaden, 1993) and Temperature profiles (0-700m) are obtained from the international Ship Of Opportunity Programme (SOOP) using merchant ships equipped with XBT systems.

In this study, we have selected data from the main shipping routes in the tropical western Pacific, during the 1995-1998 period, operated by IRD in Noumea (New-Caledonia), i.e. from New-Caledonia and Fiji toward Hong-Kong, Korea and Japan.

Three polygons of about 10° of extension in longitude have been filled with available TSG data, XBT and TAO moored data (Fig 1). The first polygon, the WW-track, is centered at 145°E at the equator and is mainly supplied by the Hong-Kong/New-Caledonia shipping line; the second polygon, the WE-track, is centered at 156°E at the equator and is mainly fed by the Korea-Japan/New-Caledonia line; the third polygon, the EE-track, is centered at 173°E at the equator and is supplied by the Japan/Fiji shipping line.

The latitude-time SSS contour (Fig.2) plotted with TSG data presents gaps, especially for the WW- and WE-tracks due to instrumental failures or/and to absence of voyages. The EE-track is the best sampled with a total of 30 sections for the 1995-1998 period, while approximately 20 sections describe the two western tracks. The associated

latitude-time SST contour (Fig 3) is plotted with surface data provided by the XBTs and TAO array which are better time-space distributed and more accurate than SST from TSG instruments.

### ~~Discussion and conclusion~~

In figure 2 are plotted the time-latitude evolution of the SSS along the three selected shipping tracks. Relatively low salinity waters ( $\text{SSS} < 34.2$ ) appear generally (i) around  $8^\circ\text{N}$  due to the presence of the Inter Tropical Convergence Zone, ITCZ, and (ii) around  $12^\circ\text{S}$  under the influence of the South Pacific Convergence Zone, SPCZ. The seasonal cycle is well marked at these latitudes (mainly in the EE-track) and a minima of SSS is observed at the end of the summer season of each hemisphere (Delcroix and Hénin, 1991) associated to maxima of precipitations.

Within the equatorial band, from March 1995, a tongue of salty waters ( $> 35$ ) reaches the EE-track and remains at that longitude during two years. The southern oscillation index (SOI) is overall positive during this La Niña period. These high salinity waters, limited at their western edge by a salinity front, reach the WE-track 4-5 month later and seem to have attain their westerly incursion limit since this salty tongue is not detected in the WW-track.

This zonal shift of the salinity front is in agreement with results of Picaut *et al.* (1996) and Hénin *et al.* (1998) who found that zonal advection is prominent in the heat and salinity budget within the equatorial band. The same process starts again by the end of 1998 during the 1998/1999 La Niña. In the CAC bulletin, wind fields from CDAS/Reanalysis indicate a persistent westerly intrusion of the trade winds from May 1995 to December 1996 mainly between the WE track and the EE-track. The trade winds are favourable to the westerly shift of the salinity front through a reinforcement of the south equatorial current. They are also favourable to the erosion of the fresh pool through unusual equatorial upwelling in the far western Pacific region and strong loss of latent heat leading to high evaporation.

After that period, a persistent westerly wind event (WWE) whose core propagates easterly occurs, as far as the EE-track until October 1997. Vialard and Delecluse (1998b) computed the effects of a westerly wind burst (WWB) on the BL with the OPA/OGCM: as observed by Lukas and Lindström (1991), they found that the wind momentum penetrates into the BL and thus erodes the BL via a deeper turbulent mixing. This yields to upward

intrusion of saltier waters. Beside this erosion/destruction of the BL in the WWE region, they observe an eastward propagation of the thicker BL toward the salinity front, probably due to a downwelling kelvin wave generated by the WWB. This mechanism applies in our observations since we observe an erosion of the fresh pool between the WE-track and the EE-track where the core of the WWE is located. Moreover, between the two La Niña periods (1996/97, and from end of 1998), the fresh pool is observed only at the EE-track, east of the WWE core where the BL has moved to, following Vialard and Delecluse (1998b). Following Hénin *et al.* (1998), after the October 1996-June 1997 WWE, we should have observed the eastward displacement of the fresh pool and the zonal salinity front on the two tracks because it was located west of the WW-track before these events. We however can observe the fresh pool only in the EE-track: this is because, while crossing eastward the WE-track, the fresh pool and the intensity of the salinity front are eroded by the WWE and the fresh pool is reconstituted between the WE and EE tracks, where the WWEs are not as intense as westward. OLR estimates in the CAC bulletin indicate high precipitations all over the western equatorial Pacific, west of the date line, i.e. over the three tracks, during the same period as the WWE. These precipitations are favourable to the reconstitution of a BL and thus of the fresh pool but this reconstitution can be efficient only outside the WWE region (east of WE-track). A WWE may easily advect the fresh/warm pool eastward, and eventually give rise to an El Niño event [Picaut *et al.*, 1996, 1999, Hénin *et al.* 1998], but in the contrary it can inhibit this shift because it erodes the low density fresh/warm pool, which thus would require more wind momentum to be shifted eastward. In the period we consider, this contradiction is removed because the WWE probably limited the zonal extension of the fresh pool since its reconstitution occurs in the region of precipitations where the WWE are not so active. Thus the restrained fresh pool would require less wind momentum to be shifted eastward and one can expect that the zonal eastward currents within the WWE region can be redistributed eastward through zonal current advection and Kelvin wave propagation. The small-size fresh pool would then be "pushed" eastward through zonal transport and advection. This would not be in contradiction with the rapidity at which the 1997/98 El Niño developed. As far as the the zonal salinity front is concerned, one can expect that it will be enhanced when the low salinity waters get closer to the eastern salinity waters.

In their computations, Vialard and Delecluse (1998b) found that, locally, in a WWB region, there is a deepening of the mixing layer because of the deeper penetration of

the wind momentum yielding to a negative SST anomaly through an entrainment cooling. East of the WWB region, where the thicker BL propagates to, there might be a positive SST anomaly because the thick BL tends to inhibit the entrainment cooling of the surface water and eventually generates an entrainment heating with a temperature inversion near the bottom of the mixing layer. In figure 3, is reported the SST distribution along the three XBT tracks. A decrease in SST is observed at the WE-track within the equatorial band, from January 1997 (at the beginning of the WWE), with a minimum of SST occurring during the July-October period. Then the SST recovers larger values at the end of the WWE (from November 1997). The WWE core reaches later the EE-track (July 1997), and during this time lag, i.e. April 1997 to July 1997, a maximum of SST is observed in the 7°S-2°S band; therefore, low-salinity/high-SST waters appear and prevail during this time lag. We can suggest that the warm/fresh pool has been reconstructed during this lag time, between the WE-and the EE-track. The limited extension of the new fresh pool might have played a crucial role in the development of the 1997/1998 El Niño event. It can be of interest to do further tests with general circulation models reproducing the 1997/1998 event: for example, what would be the response if one extends artificially in space the fresh pool prior to the triggering of the 1997/1998 El Niño event?

---

*Acknowledgments.* The authors would like to acknowledge with thanks David Varillon, Jean-Marc Ihily, Luc Foucher and Pierre Waigna for their efforts in monitoring the IRD TSG-XBT network in Nouméa, Yvette Raguenes (Thermal Subsurface Data Center, Ifremer-Brest) for kindly providing XBT temperature profiles and the PMEL for TAO buoys data. Finally the authors are undebtful to crews of the numerous M/Vs involved in the TSG-XBT network for their constant help.

.....  
M. Ioualalen and C. Henin, Institut de Recherche pour le Développement, BP. A5, 98848 Nouméa Cedex, New-Caledonia.

## References

- Delcroix, T., L. Gourdeau and C. Hénin, Sea surface salinity changes along the Fiji-Japan shipping track during the 1996 La Niña and the 1997 El Niño period, *Geophys. Res. Lett.*, vol. 25, NO. 16, 3169-3172, Aug. 15, 1998.
- Delcroix, T., and C. Hénin, Seasonal and interannual variations of sea-surface salinity in the tropical Pacific ocean, *J. Geophys. Res.*, 96, 22135-22150, 1991.
- Delcroix, T., C. Hénin, V. Porte, and P. Arkin, Precipitation and sea-surface salinity in the tropical Pacific ocean, *Deep Sea Res., Part I*, 43, 1123-1141, 1996.
- Eldin, G., M. H. Radenac, and M. Rodier, Physical and nutrient variability in the upper equatorial Pacific associated with westerly wind forcing and wave activity in October 1994, *Deep-Sea Res.*, 44, 1783-1800, 1997.
- Hénin, C., and J. Grelet, A merchant ship thermo-salinograph network in the tropical Pacific, *Deep-Sea Res.*, 43, 1833-1855, 1996.
- Hénin, C., Y. du Penhoat and M. Ioualalen, Observations of sea-surface salinity in the western Pacific fresh pool : Large scale changes during 1992-1995, *J. Geophys. Res.*, 103, 7523-7536, 1998.
- LeBorgne, R., C. Brunet, G. Eldin, M. H. Radenac, and M. Rodier, Campagne océanographique FLUPAC à bord du N. O. L' Atalante (23/9 au 29-10 1994), Recueil de données, *Archives Sciences de la mer, Océanogr.*, 1, 337pp, ORSTOM, Nouméa, New-Caledonia, 1995.
- Lukas, R., On the role of the western Pacific air-sea interaction in the El Niño/Southern Oscillation phenomenon, *Proc. U.S. TOGA Western Pacific, Air-Sea Interaction Workshop, Nololulu, HI, U.S., TOGA*, 43-69, 1988.
- Lukas, R., and E. Lindström, The mixed layer of the western equatorial Pacific ocean, *J. Geophys. Res.*, 96, 3343-3457, 1991.
- McPhaden, M., TOGA-TAO and the 1991-93 El Niño Southern Oscillation event, *Oceanog.*, 6, 36-44, 1993.
- Picaut, J., M. Ioualalen, C. Menkes, T. Delcroix, and M. J. McPhaden, Mechanism of the zonal displacements of the Pacific Warm Pool, implications for ENSO, *Science*, 274, 1486-1489, 1996.
- Sprintall, J., and M. J. McPhaden, Surface layer variations observed in multiyear time series measurements from the western equatorial Pacific, *J. Geophys. Res.*, 101, 22 513-22 533, 1994.
- Tapley, B., D. Chambers, C. K. Shum, R. J. Eanes, and J. C. Ries, Accuracy assessment of the large scale dynamic ocean topography from TOPEX/Poseidon Altimetry, *J.*

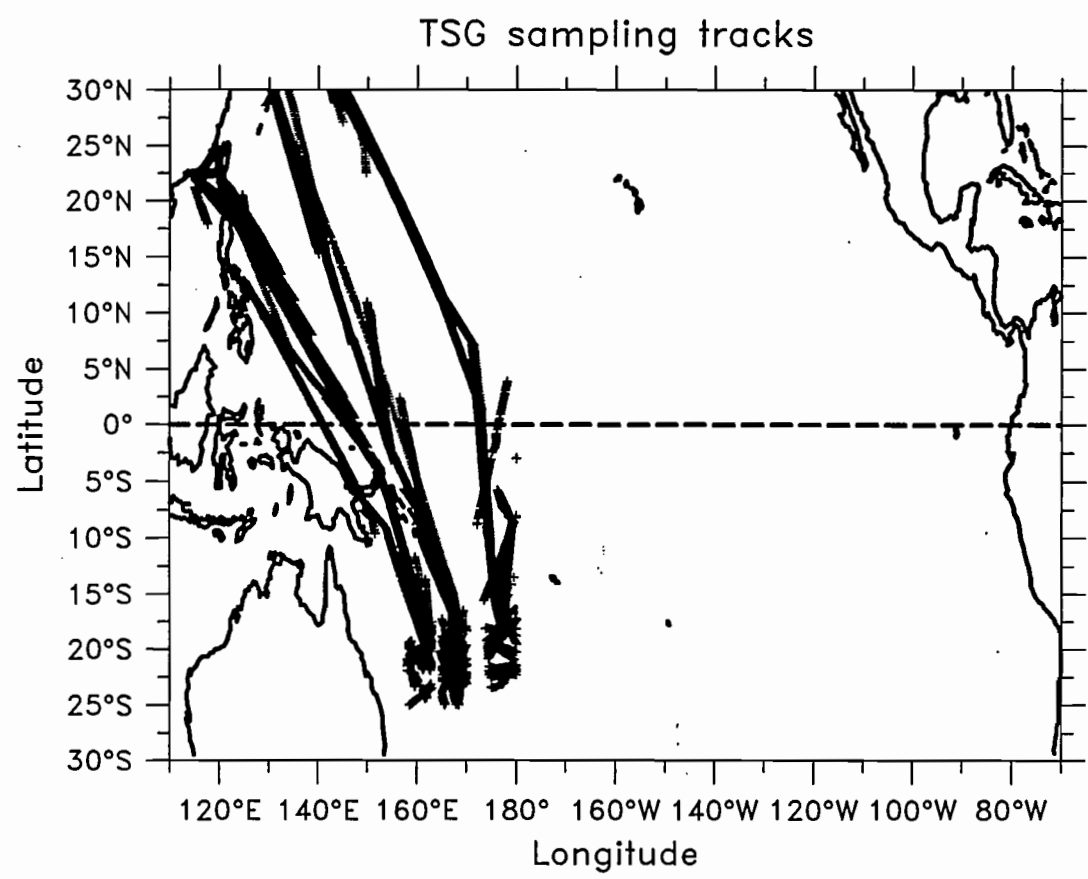
*Geophys. Res.*, 99, 24605-24617, 1994.

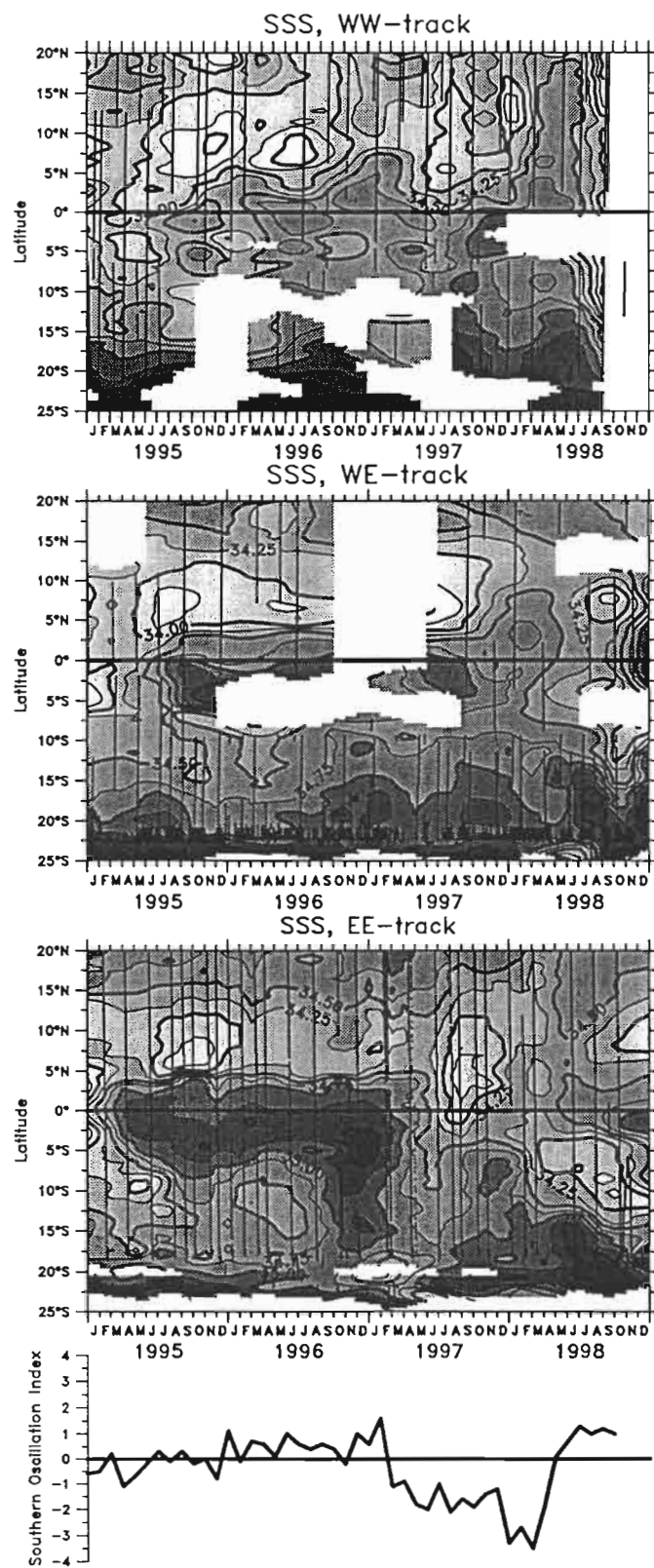
Vialard, J., and P. Delecluse, An OGCM study for the TOGA decade. Part I : Role of salinity in the physics of the western Pacific fresh pool, *J. Phys. Oceanogr.*, 28, 1071-1088, 1998a.

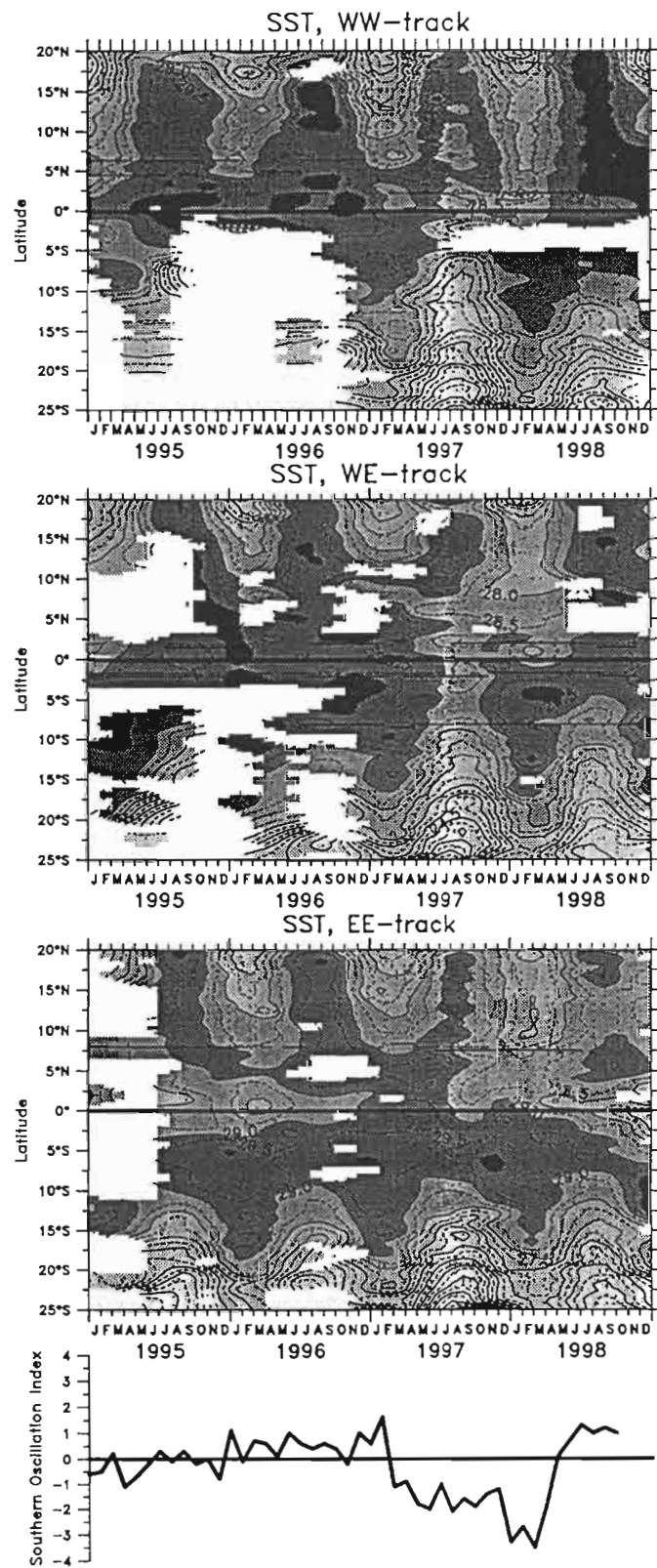
Vialard, J., and P. Delecluse, An OGCM study for the TOGA decade. Part II : Barrier-layer formation and variability, *J. Phys. Oceanogr.*, 28, 1089-1106, 1998b.

## FIGURE CAPTIONS

- Figure 1. Selected sampling tracks ( $10^{\circ}$  of expansion in longitude): the WW-, WE- and EE-tracks cross the equator near respectively  $145^{\circ}\text{E}$ ,  $156^{\circ}\text{E}$  and  $173^{\circ}\text{E}$ .
- Figure 2. Time-latitude sea surface salinity measured with thermosalinographs, along the three sampling tracks; segments represent TSG data points. (Bottom) SOI over the same period..
- Figure 3. Time-latitude sea surface temperature measured with XBT probes and TAO mooring sensors, along the three sampling tracks; plus signs (+) represent XBT launches. (Bottom) SOI over the same period.







# **Stations côtières de Nouvelle-Calédonie et variabilité thermique : Mise en Evidence d'un Upwelling Côtier**

Christian Hénin  
*Centre IRD (ex-ORSTOM)*  
*Nouméa*

**DRAFT (Mai 1999)**

## **INTRODUCTION ET OBJECTIFS**

La Nouvelle-Calédonie est située dans le Pacifique sud-ouest siège de structures océanographiques et météorologiques très particulières :

i) la zone de convergence des vents du Pacifique Sud (ZCPS) qui s'étend de la Nouvelle-Guinée aux îles Samoa et jusqu'en Polynésie Française est constituée de la rencontre des deux systèmes d'alizés du Pacifique Sud :

- les alizés générés par l'anticyclone de l'Ile de Pâques et
- les alizés générés par l'anticyclone de Norfolk.

Cette zone de convergence est située au nord de la Nouvelle Calédonie qui est en général soumises aux alizés de Norfolk.

ii) la grande gyre anticyclonique dont le centre se trouve légèrement au nord est de la Nouvelle-Calédonie qui est ainsi baignée par une circulation océanique permanente dirigée vers l'est. Ce qui constitue un des paradoxes de la région océanique de la Nouvelle Calédonie où la circulation océanique générale est opposée au vent dominants que sont les Alizés de sud-est (Henin et al, 1984)

iii) la Nouvelle-Calédonie est située en bordure sud de la Warm Pool dont on sait qu'elle est le réservoir de chaleur mondial du système couplé océan-atmosphère et dont les déplacements sont liés à la variabilité climatique interannuelle.

Les anomalies de type ENSO (El Nino / Southern Oscillation) étant associées à des modifications de position et d'intensité de ces structures il résulte de la position géographique de la Nouvelle-Calédonie que celle ci est fortement concernée par ces fluctuations climatiques (Donguy et Hénin, 1980; Delcroix et Lenormand, 1997).

Le Pacifique sud-ouest a été le siège de campagnes océanographiques depuis une cinquantaine d'années qui ont permis de décrire la situation océanographique moyenne (Daniel et al, 1995). Cependant le nombre et la couverture spatiale de ces campagnes sont malheureusement insuffisants pour décrire et étudier la

zone économique de la Nouvelle-Calédonie en particulier la variabilité temporelle des structures océaniques.

Afin de disposer d'une observation continue de l'environnement océanique, des réseaux d'observations systématiques par navires de commerce et par des stations côtières ont été ainsi mis en place par les océanographes du centre ORSTOM de Nouméa (Donguy et Hénin, 1976; Hénin et Grelet, 1996; Hénin, 1997).

-Un réseau d'observation océanographiques par navires de commerce a été mis en place dès 1969 par les océanographes de l'ORSTOM. Il permet de suivre l'évolution temporelle de la température de la couche 0-700m (sondes XBT / Expendable Bathymographs), et de la salinité de surface (thermosalinographies automatiques). La couverture autour de la Nouvelle-Calédonie bénéficie d'une distribution satisfaisante des mesures à partir de Nouméa en direction de l'Australie, de la Nouvelle Zélande, du Japon, du Vanuatu, des îles Fiji et de la Polynésie Française.

Ces observations ont permis la mise en évidence d'une différence systématique de température et de salinité superficielles entre les eaux du large de la côte est et celles la côte ouest de la Nouvelle Calédonie (Hénin et al, 1984; Delcroix et Lenormand, 1997) suggérant des mécanismes océaniques particuliers, voire une circulation différente de part et d'autre de la Nouvelle Calédonie. Une série de campagnes de mesures directes de courant de surface entreprises à bord du N.O. Vauban de l'ORSTOM ont conduit Hénin et al (1984) à fournir une première hypothèse : ils proposent un schéma de circulation de surface dépendant des conditions de vent avec toutefois un courant côtier quasi-permanent observé le long de la côte Est dirigé vers le sud-est, baptisé « Courant du Vauban ». Ce courant expliquerait la présence d'eaux chaudes et dessalées originaires du nord (Vanuatu) alors que la côte ouest serait baignée par des eaux plus salées et plus froides originaires de la mer de Tasman et soumise à l'influence des alizés de Norforlk. Ces observations très coûteuses en temps navire n'ont pu être entreprises que pendant une période limitée dans le temps (3 années) et dans la partie sud-est de la Nouvelle-Calédonie uniquement. Seuls des lâchers de bouées dérivantes autonomes permettraient de poursuivre les études sur la circulation superficielle autour de la Nouvelle-Calédonie.

-Depuis 1958 des observations journalières de la température de surface de la mer ont été entreprises à l'Anse Vata dans le lagon sud-ouest de Nouvelle-Calédonie (et depuis 1977 des mesures journalières de la salinité de surface). Malgré les imprécisions dues à la variation diurne de la température et des influences des précipitations côtières, ces observations ont permis la mise en évidence de l'impact du phénomène El Nino sur la région (Delcroix et Lenormand, 1997). Parmi les nombreux facteurs qui modifient la température et la salinité hauturière on peut citer l'influence des petits fonds sur le réchauffement diurne et sur l'évaporation due au vent, des apports d'eaux douces par ruissellement et précipitations locales, la stratification verticale etc....

Après avoir installé en 1967 une seconde station manuelle au Phare Amédée (une observation journalière) en bordure de la passe de Bouari, plus représentative des conditions océaniques il a été décidé d'améliorer la surveillance océanographique en automatisant à partir de 1991 la mesure de la

température et de la salinité (financement CORDET) puis d'étendre le réseau de stations côtières en Nouvelle-Calédonie (financement ZoNéCo /1994-1998)

C'est ainsi que nous disposons à l'heure actuelle d'un réseau de stations côtières automatiques (13) et manuelles (2) qui nous fournissent des données de température (15) et de salinité (2) de surface à une fréquence d'échantillonnage variant de 15 minutes à 24 heures (Rivaton, 1996; Hénin , 1997; Nangard, 1998). Ces stations sont principalement situées sur le pourtours de la Nouvelle Calédonie à l'extérieur du récif barrière fixés sur la pente récifale à une profondeur de 10-12 mètres (Fig 1). En raison du brassage vertical des eaux la température observée est celle de la couche de surface. La mise en place de stations complémentaires en divers sites situés à l'intérieur du lagon sud-ouest (Fig 2) a été guidée par le souci de disposer d'observations de longue durée de l'environnement marin dans une région au fort potentiel de développement urbain, touristique et industriel.

Le réseau des stations côtières nous permet de disposer à ce jour de données nouvelles et continues dans le temps permettant d'améliorer la connaissance de la variabilité thermique régionale.

Nous avons choisi dans ce travail de considérer principalement les données de température superficielles fournies par les stations côtières automatiques pour entreprendre l'étude de la variabilité côtière. Les observations de salinité de surface, de la température de la couche 0-700m des eaux du large, et du vent côtier permettront de compléter la description de la variabilité océanique et nous permettront de formuler des hypothèses sur les mécanismes responsables de cette variabilité.

## DISCUSSION

Notre réseau d'observations côtières automatiques nous permet de considérer la variabilité thermique selon des échelles de temps très variées allant de la journée à plusieurs années.

### Variabilité interannuelle :

Nous utiliserons les données de la période 1993-1998 de la station de référence installée à la Fausse Passe de Uitoé (Fig 3). Il est remarquable de constater qu'il existe une très forte variabilité aussi bien de la température d'été (maximum atteignant 26.5°C en février 1994 et 28.5°C en février 1998) que de la température d'hiver (minimum variant de 22°C pendant les mois de septembre 1992, 1993, 1994, 1996 et 1997 à 23.5°C en septembre 1998).

L'impact du phénomène ENSO sur les eaux océaniques bordant la Nouvelle Calédonie explique cette variabilité interannuelle de la SST. Jusqu'en 1994 l'index d'oscillation australe (SOI, Fig 4) négatif correspondait à une situation El Nino c'est à dire d'eaux chaudes équatoriales déplacées vers le Pacifique central laissant plus à l'ouest et en zone tropicale une anomalie thermique négative en particulier dans le Pacifique sud-ouest. En 1996 un indice SOI positif correspond à une situation La Nina modérée accompagnée d'un réchauffement des eaux du Pacifique sud-ouest. Pendant la période comprise entre mars 1997 et mai 1998 la mise en place du Nino « du siècle » est associée à une anomalie négative de la température dans notre région,

immédiatement suivie d'un basculement vers un état La Nina qui explique les eaux particulièrement chaudes en hiver austral 1998.

Ces mesures automatiques de la température réalisées au cours de la période de six années (1993-1998) nous permettent ainsi de confirmer une forte variabilité interannuelle, associée au phénomène climatique ENSO, de la température des eaux océaniques entourant la Nouvelle-Calédonie (Delcroix et Lenormand, 1997)

### **Variabilité diurne :**

L'échantillonnage haute densité (une mesure toutes les 15 minutes) des stations côtières automatiques nous permet également d'évaluer la variabilité diurne qui est presque essentiellement causée par le réchauffement solaire, maximal lorsque le soleil est au zénith. La température maximale se produit aux environs de 13-14 heures locales (Fig 5). L'amplitude de la variation diurne dépend également de plusieurs facteurs tels que l'ensoleillement (couverture nuageuse), l'action du vent (évaporation), l'état de la mer (du également à l'action du vent et influant sur le mélange vertical), la saison (réchauffement plus important en été qu'en hiver....), la profondeur de la mesure, l'épaisseur de la couche d'eau du site (large, lagon profond, lagon de petit fond, fond de baie, etc...), les courants de marée etc....

Pour estimer l'amplitude de la variation diurne nous utilisons l'écart type journalier du signal. En première approximation le signal étant proche d'une fonction sinusoïdale de type,  $SST = A \sin(wt + \theta)$ , l'écart type est proportionnel à l'amplitude A.

Station	Prof mesure		Ecart type été (°C) (dec-mars)	Ecart type hiver (°C) (juin-aout)
Uitoe	11m	Extérieur	0.3 à 0.4	0.04
Boulari	10m	Extérieur	0.3 à 0.4	0.07
Dumbea	10m	Extérieur	0.3	
Amedee	3m	Lagon faible fond	0.2 à 0.4	0.2 à 0.3
Ponton	4m	Lagon faible fond	0.4	0.1
Réc Prony	7m	Lagon profond	0.1 à 0.2	0.1
Nouville	13m	Baie profonde	0.1	0.08
Anse Vata	2m	faible fond	0.3 à 0.4 (sept)	0.2
Chaleix	2m	Baie faible fond	0.4	0.3
Cap Goulvain	10m	Extérieur	0.2 à 0.3	0.07
Goro	12m	Extérieur	0.3 à 0.4	0.1 à 0.2
Poindimie	12m	Extérieur	0.1 à 0.2	0.1

Table 1 :Ecart type journalier de la température observée aux stations côtières de Nouvelle-Calédonie.

L'amplitude observée est très variable d'un site à un autre et selon la saison (Table 1). De plus les facteurs évoqués ci avant n'ayant pas été évalués il est impossible d'estimer l'importance de chacun. Néanmoins ces résultats bruts amènent des informations sur la diversité du comportement thermique des eaux côtières et lagonaires de Nouvelle-Calédonie

### **Variabilité de plusieurs jours**

Une autre échelle de variabilité de la température a été considérée aux différentes stations côtières aussi bien à l'extérieur du récif barrière qu'à l'intérieur du lagon. C'est d'ailleurs celle qui est peut être la plus originale

et qui a certainement une influence notable aussi bien sur le fonctionnement des lagons que la distribution des masses d'eaux autour de la Nouvelle-Calédonie.

Des chutes brutales de la température de l'ordre de 3 à 5°C apparaissent, la température se maintenant à des valeurs basses pendant 7 à 10 jours puis reprenant assez rapidement sa valeur initiale. Ce phénomène a été observé depuis 1993 à Uitoé surtout pendant l'été (Fig 3). Les autres stations extérieures au lagon de la côte ouest de la Nouvelle Calédonie (Boulari, Dumbea et Cap Goulvain) présentent une variabilité tout à fait semblable (Fig 6). Le phénomène possède de ce fait une extension spatiale conséquente ( 200 km séparent Boulari du Cap Goulvain).

On ne décèle pas de type de chutes brutales de la température à la station de Poindimié sur la côte est (Fig 7). La température observée à la station de Goro au sud de la côte est est plus variable mais nous verrons ci-après qu'elle n'est pas corrélée aux variations de température de la côte ouest. On peut ainsi supposer que les mécanismes responsables de la variabilité thermique côtière sont différents au large des côtes est et ouest de Nouvelle-Calédonie.

Plusieurs hypothèses peuvent être considérées pour expliquer le mécanisme responsable de ce refroidissement .

- i) une advection d'eau froide nécessiterait des courants de surface de plus de 20 noeuds pour amener des eaux de température semblable se trouvant vers le nord de la Nouvelle-Zélande. Hypothèse à rejeter bien entendu.
- ii) un refroidissement des eaux par évaporation due au renforcement du vent est également à rejeter car il ne pourrait pas excéder quelques dixièmes de degré Celcius.

iii) l'hypothèse qui semble la plus envisageable est celle d'un upwelling côtier généré par le vent. Les structures thermiques observées au large par les XBT (Fig 8) et les données des campagnes de recherche attestent d'une stratification thermique marquée en été austral entre la surface ( $T > 27-28^{\circ}\text{C}$ ) et 120 m de profondeur ( $T = 21 \text{ à } 23^{\circ}\text{C}$ ). Une remontée rapide vers la surface des eaux expliquerait l'amplitude de la chute de température (3 à 5°C ). Le moteur de cet upwelling serait l'Alizé qui est parallèle à la côte de Nouvelle Calédonie. En effet, la théorie d'Ekman explique le développement d'un upwelling côtier lorsque la côte est à droite du lit du vent dans l'hémisphère sud et une plongée des eaux de surface lorsque la côte est à gauche du vent.

Une observation attentive des données du vent observé sur l'îlot Amédée, près de la barrière récifale et caractéristique du vent côtier du sud-ouest de la Nouvelle Calédonie entre novembre 1993 et mai 1994 nous permet de constater qu'il y a une relation entre le renforcement de la composante du vent le long de la côte et les observations d'upwelling à la fausse passe de Uitoé (Fig 9). La chute brutale de température de l'eau se produit lorsque la composante moyenne journalière du vent se renforce et dépasse 6m/s

Afin de pouvoir mieux apprécier les relations entre vent et refroidissement nous avons réalisé des tests statistiques entre les composantes parallèle et perpendiculaire à la côte du vent observé au Phare Amédée d'une part et le

refroidissement exprimé par l'anomalie de température delta-T d'autre part. Delta T est la différence entre la température moyenne du jour J, et la température moyenne sur le mois encadrant le jour J. L'utilisation de la valeur moyenne journalière permet de nous affranchir de la variabilité diurne et de celle due aux courants de marée.

La corrélation entre la composante du vent parallèle à la côte et delta-T à Uitoé est manifeste. Nous avons utilisés les données de vent et de température sur environ cinq années (1962 jours), aussi bien en hiver qu'en été. La Fig 10 nous montre que la corrélation à Uitoé est de 0,41 avec un décalage d'une journée. Au Cap Goulvain le calcul réalisé sur 435 jours donne une corrélation de 0,45 avec un retard de une journée également. Cette corrélation atteint 0,52 à Uitoé si on considère une période d'été austral (239 jours entre septembre 1997 et mai 1998). En revanche aucune corrélation significative n'a été décelée avec les données de Poindimié et encore moins avec celles de Goro. Enfin aucune corrélation existe entre la composante du vent perpendiculaire à la côte et l'anomalie thermique. La Fig 11 représentant la corrélation entre les anomalies thermiques delta-T du Cap Goulvain celles des autres stations de la côte ouest nous suggère une propagation du signal de l'upwelling vers le sud le long de la côte ouest (Cap Goulvain vers Uitoe, Dumbea et Bouari)

Un test de sensibilité sur un modèle linéaire simple à deux couches océaniques forcé de façon homogène sur le domaine néo-calédonien par le vent observé au Phare Amédée de 1993 à 1995 confirme des mouvements verticaux importants de la thermocline au large de la côte ouest et une relative stabilité au large de la côte est.

En conclusion nous exprimons l'hypothèse d'un upwelling côtier généré par le vent. Sa signature sur la température de surface est manifeste sur la côte ouest lorsque l'Alizé dépasse une intensité moyenne journalière de 6m/s. Un traitement des données des capteurs IR des satellites NOAA, réalisé par le LATICAL (Laboratoire de traitement d'Images Calédonien) de l'année 1998 a permis d'estimer l'amplitude spatiale du phénomène. La situation du 16 janvier 1998 (Fig 12) repérée par un refroidissement très net aux stations côtières de la côte ouest (Fig 3 et 6) montre que l'extension du refroidissement au large s'étend jusqu'à une quarantaine de kilomètres au large de la côte sud-ouest de Nouvelle Calédonie tandis que la température le long de la côte est reste élevée.

## Influence sur le lagon.

A l'intérieur du lagon sud ouest de Nouvelle-Calédonie le réseau d'observations automatiques est relativement bien distribué spatialement (intérieur récif barrière /à Amedee et à la Fausse-Passe de Uitoe /, partie centrale du lagon / Récif du Prony/ ,littoral / Anse-Vata, Nouville, Chaleix/ ). Cependant les appareils posés sur le fond sont installés dans des configurations très diverses : baies ou récif et profondeurs de quelques mètres à Chaleix, Anse Vata, Amedée, Ponton et 10-12 mètres au Récif du Prony et à Nouville. La Figure 13 présente l'évolution de la température à certaines de ces stations.

Dans l'hypothèse d'un upwelling côtier du au vent le long de la côte ouest, la Fig 14 montre qu'il existe une corrélation entre l'anomalie thermique du large (delta-T de Uitoe) et celle des divers points observés du lagon. Elle varie de 0.90 à proximité immédiate du récif barrière (Ponton), à 0.55 à l'Anse Vata et au phare Amédée par petits fonds sans retard (une traînée du signal est toutefois décelable). En revanche la température des eaux plus profondes du lagon est corrélée à celle du large avec un retard de 3 à 6 jours, respectivement pour le Récif du Prony et à Nouville. Nous devons préciser que les corrélations ont utilisé des données de durées variables selon les stations y compris les mesures obtenues en hiver pendant lequel la signature en température de l'upwelling côtier, s'il existe, n'est pas marquée. Ainsi le lagon est directement concerné par ce phénomène d'upwelling côtier le long de la côte ouest. Les eaux de surface du lagon et celles proches du récif réagissent très rapidement alors que les eaux plus profondes du lagon sont concernées avec un retard notable de plusieurs jours. Les courants de marée favorisent le renouvellement des eaux du lagon par celles du large.

Dans la partie sud-ouest du lagon ce travail montre que l'upwelling côtier intéresse le lagon, les eaux même profondes du lagon subissant l'influence du large.

Le lagon bordant la partie centrale de la côte ouest de Nouvelle-Calédonie étant très étroit et peu profond dans sa partie centrale on peut supposer que l'influence de l'upwelling côtier sur le lagon est immédiat.

Dans la partie nord du lagon calédonien où des observations continues n'existent pas on peut supposer que l'upwelling est présent car l'Alizé est encore plus intense. Cependant le signal thermique pourrait y être plus réduit car le gradient vertical de température des eaux du large est plus faible (Fig 8). La largeur du lagon situé au nord de la Grande Terre laisse supposer que les eaux du large de la côte ouest envahissent le lagon mais qu'il subit également l'influence les eaux de la côte est par l'action de courants de marée. L'implantation de stations côtière pourrait répondre à cette interrogation.

## Mise en évidence

La température étant un bon marqueur de l'upwelling en été uniquement on peut envisager d'utiliser d'autres indices. Le vent étant le moteur de

l'upwelling des remontées d'eaux profondes peuvent se produire même en hiver sans qu'il soit accompagné de signal décelable en température.

-la *salinité* est maximale en subsurface vers 100 à 200 mètres de profondeur au large de la Nouvelle Calédonie. L'upwelling remonte ainsi vers la surface de eaux plus salées. Les précipitations locales et l'apport d'eau douce par les rivières réduisent cependant très fortement la salinité du lagon et des eaux côtières et perturbent le signal d'upwelling en salinité. Les données disponibles sont encore fragmentaires (les seules observations de la salinité en automatique à Uitoé extérieur et manuelle journalière à l'Anse Vata et au Phare Amedee). On peut cependant y voir des variations intéressantes de type upwelling à la fausse Passe de Uitoe sur la Fig 15 entre novembre 1993 et mai 1994. Les diminutions de température associées à l'upwelling correspondent à des augmentations de salinité pour les événements particuliers de décembre 1993, mi- et fin janvier, début et fin mars et fin avril 1994. Les mesures continues de salinité de surface aussi bien par stations côtières que par navires de commerce sont de ce fait développées dans le cadre des programmes de recherche de l'IRD.

-les *sels nutritifs* augmentent avec la profondeur et pourraient lorsque des teneurs élevées sont mesurées en surface être un indicateur de l'upwelling. Seules des mesures régulières réalisées dans le lagon et à l'extérieur du lagon pourraient permettre d'étudier une productivité accrue du lagon liée à l'upwelling.. Lors des campagnes historiques (radiale Saint-Vincent) entreprises par les océanographes du centre ORSTOM de Nouméa aucune observation de température en continu n'était réalisée parallèlement en des stations côtières et nous ne pouvons pas les situer en relation avec un upwelling éventuel. En revanche lors de futures campagnes côtières ou lagonaires il pourrait être envisagé de comparer les valeurs en sels nutritifs selon que le réseau d'observation en place par stations côtières indique qu'on est ou non en période d'upwelling. Il faudra cependant rester très prudent car les sels nutritifs sont par nature non conservatifs car dépendant de l'activité biologique. De plus le ruissellement et l'apport des rivières modifie largement leur distribution dans le lagon et à la côte.

Ce type d'upwelling côtier observé le long de la côte ouest de Calédonie est comparable à l'upwelling décrit par Dorman et Palmer (1981) le long des côtes de Californie. Selon ces auteurs il existe deux échelles d'upwelling : un upwelling qui s'étend jusqu'à 200 km au large de la côte de Californie présent du printemps à l'automne et un upwelling local qui apparaît plusieurs fois l'été sous l'action des vents locaux. Les observations faites pendant la période 1967-1976 établissent que sa durée moyenne est de 9 à 15 jours et la chute de température de 4 à 9 °C. Le critère signifiant selon eux de cet upwelling côtier généré par les vents : chute de température de 3°C et une durée d'au moins 6 jours. Brunks et al (1981) ont étudié un upwelling situé à 15°C le long des côtes du Pérou et montrent que l'upwelling atteint environ une profondeur de 100m.

L'upwelling côtier de Nouvelle-Calédonie présente ainsi des caractéristiques relativement typiques.

## Impacts

Parmi les impacts du phénomène d'upwelling côtier présent en général le long de la côte ouest et absent le long de la côte est, la prédominance des

alizés pourrait expliquer en partie la différence de SST et même de SSS de part et d'autre de la Nouvelle Calédonie. Henin et al (1984) avaient émis l'hypothèse d'un apport d'eaux dessalées et chaudes par le courant côtier du Vauban se dirigeant vers le sud-est. La mise en évidence par ce travail de l'upwelling côtier de la côte ouest permet de proposer un mécanisme supplémentaire pour expliquer la différence entre les masses d'eaux de surface. Il en résulte des possibilités d'affrontement, de juxtaposition de masses d'eaux d'origine différentes (Est et Ouest) mais également entre les eaux du large et les eaux côtières upwellées. La Figure 12 montre que le refroidissement côtier est observé assez loin de la côte sud-ouest le 16/01/1998, des fronts thermiques horizontaux de surface étant situés à une distance d'environ 40 km de la côte.

Ces gradients thermiques, indices d'affrontement de masses d'eaux différentes sont des zones potentiellement riches pour la pêche; leur suivi et leur prévision permettrait d'améliorer l'exploitation des ressources marines vivantes autour de la Nouvelle-Calédonie.

Un autre domaine où la connaissance, ou encore mieux, la prévision des refroidissements thermiques pourrait être de première importance est l'industrie aquacole. Il a en effet été remarqué (Cyrille Goirant, Ifremer, comm personnelle) que les épisodes de mortalité des élevages de crevettes appelé Syndrome 93 correspondait à des chutes brutales de température des bassins d'élevage. L'upwelling ayant un effet immédiat dans les lagons de la côte ouest où se situent les élevages de crevettes, son action sur la température des bassins alimentés par l'eau du lagon est évidente. La gestion des fermes aquacoles pourrait tenir compte de la température des eaux côtières observées en temps réel et de celle qui serait prévisible par un modèle simple de prédiction prenant en compte les observations en temps réel du vent côtier.

Dans le domaine de l'étude de la trajectoire des dépressions et cyclones tropicaux ce mécanisme d'upwelling côtier peut être également considéré. Ces perturbations météorologiques qui conditionnent de nombreux secteurs d'activités économiques (agriculture, élevage, tourisme, pêche etc....) abordent la Nouvelle-Calédonie par le nord suivant une trajectoire en général nord-sud. Les vents de secteur est associés aux dépressions situées au nord, sont forts et génèrent un upwelling côtier très marqué. La température des eaux de surface est alors abaissée très sensiblement le long de la côte ouest et restent élevées le long de la côte est. La dépression à la recherche d'eaux chaudes aura tendance à longer la côte est de la Nouvelle-Calédonie. Si la dépression traverse la chaîne centrale tout en s'affaiblissant elle aura tendance à s'écartez de la côte ouest à la recherche d'eaux plus chaudes. On trouve dans les statistiques de trajectoires de cyclones publiées par Météo-France des indices qui confortent cette hypothèse.

## CONCLUSION

Les stations côtières automatiques ont permis de faire progresser la connaissance de la variabilité thermique des eaux bordant la Nouvelle-Calédonie. L'upwelling côtier, mis en évidence par cette étude, étant essentiellement induit par les alizés il est primordial de connaître la distribution des vents et sa variabilité. Les observations régionales classiques et celles plus récentes obtenues par les techniques satellitaires (ERS-1 depuis 1991) confirment le régime d'alizés dont le noyau est centré vers 18°S et une variabilité saisonnière surtout marquée au sud par l'apparition de vents d'ouest en juillet-aout et par des dépressions et cyclones tropicaux qui intéressent tout le territoire de décembre à mars-avril.

La station météo automatique du Phare Amédée qui transmet les données horaires nous permet d'avoir une vision fine du régime du vent le long de la côte ouest. C'est ce type d'observations associées à celles des stations côtières qui seules permettront de prédire et suivre l'upwelling côtier à une échelle temporelle de quelques jours à 10 jours.

D'autre part il est bien établi que l'étude du climat mondial ne peut progresser que par des observations continues des paramètres océanographiques et météorologiques réalisées sur tout le globe. Les stations côtières de Nouvelle-Calédonie participent à cet effort de recherche dont les retombées régionales et locales ne sont plus à démontrer.

## REFERENCES

Daniel J., R. Grandperrin, C. Hénin, F. Rougerie, 1995. Un demi-siècle d'Océanologie ORSTOM dans le Pacifique Sud. *La Revue Maritime*. N°440, décembre 95, 4ème trimestre 95, pp 65-105.

Delcroix Th, C. Hénin, 1989 : Mechanisms of subsurface thermal structure and sea-surface thermohaline variabilities in the southwestern tropical Pacific during 1979-85. *Journal of Marine Research*, 47, 777-812

Delcroix T., O. Lenormand, 1997. ENSO signals in the vicinity of New-Caledonia, south-western Pacific. *Oceanologica Acta*, 20, N°2, 1-11.

Donguy JR, C. Hénin, 1976 : La surveillance continue des conditions de surface de l'océan par des navires non spécialisés. *La Mer. Bulletin de la Societe Franco Japonaise d'Oceanographie*. Tome 4, N°3-4, pp 159-160.

Donguy JR, C. Hénin, 1980 : Climatic teleconnections in the south western Pacific with the El Niño phenomenon. *Journal of Physical Oceanography*. Vol 10, N°12, pp 1952-1958.

Hénin C., JM Guillerm, L.Chabert, 1984. Circulation superficielle autour de la Nouvelle-Calédonie. *Océanographie Tropicale*, 19 (2), 113-126

Hénin C., J. Grelet, 1996, A Merchant Ship Thermosalinograph Network in the Pacific Ocean. *Deep Sea Resarch*, Vol 43, Iss 11-12, pp 1833-1855

Hénin C., 1997, Surveillance thermohaline de la ZEE en 1994-1995 et 1996. *Archives, Ed ORSTOM Nouméa, Série Sciences de la Mer*, N°9, 15 pp

Nangard S, 1998, Les stations côtières. Rapport de Stage, *Rapport de Stage, Ed ORSTOM Nouméa, Série Sciences de la Mer, Oceanog. Phys.* 17 pp

Rivaton A., 1996, Gestion des données côtières et océaniques sous SGBD ORACLE dans le cadre du programme ZoNéCo. Mém. Stages. Sci. Mer, Oceanog. Phys., ORSTOM Nouméa, 82p.

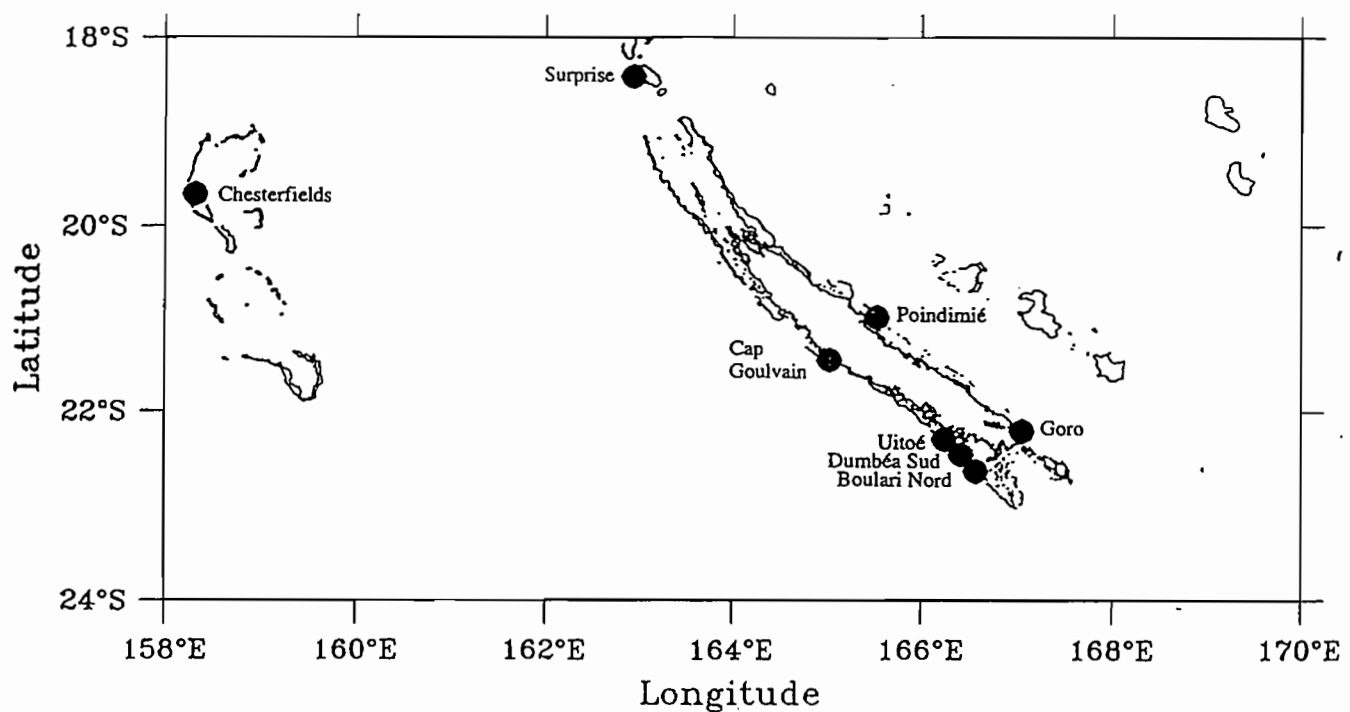


Figure 1 : Stations côtières automatiques de Nouvelle-Calédonie

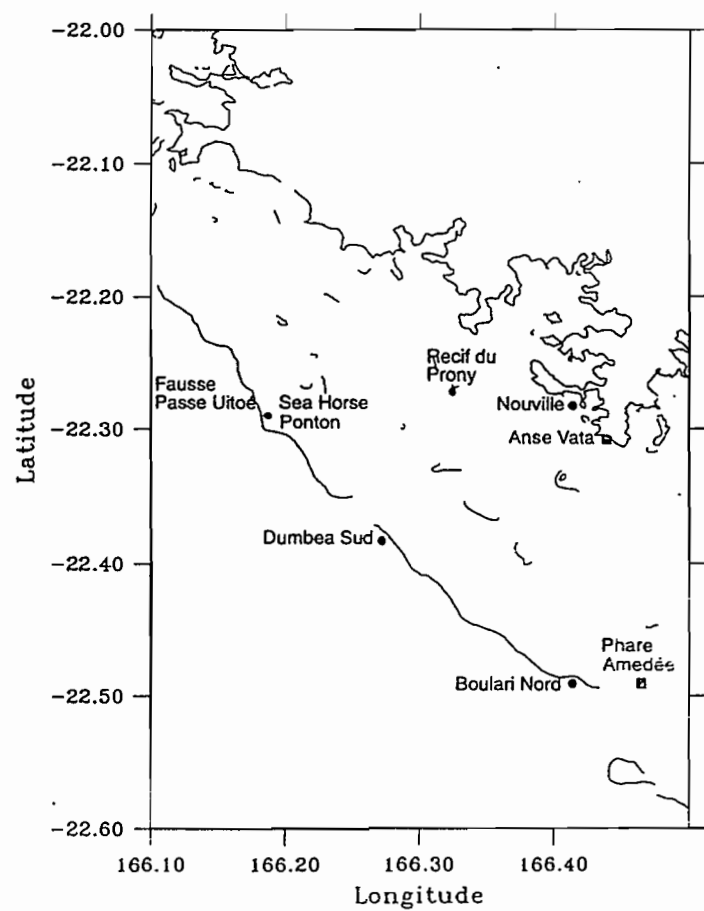


Figure 2 : Stations côtières automatiques  
du lagon sud-ouest de Nouvelle-Calédonie

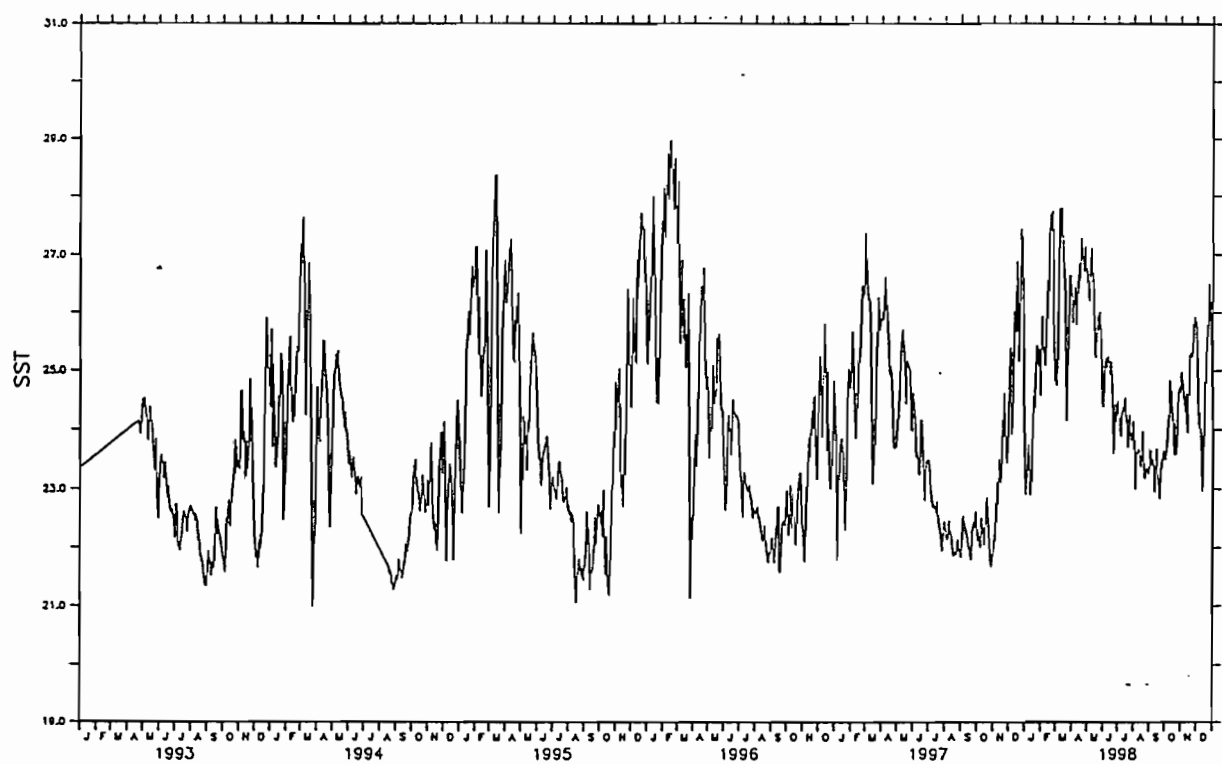


Figure 3 : Température de surface à la station  
de la fausse-passe de Uitoé de 1993 à 1998.

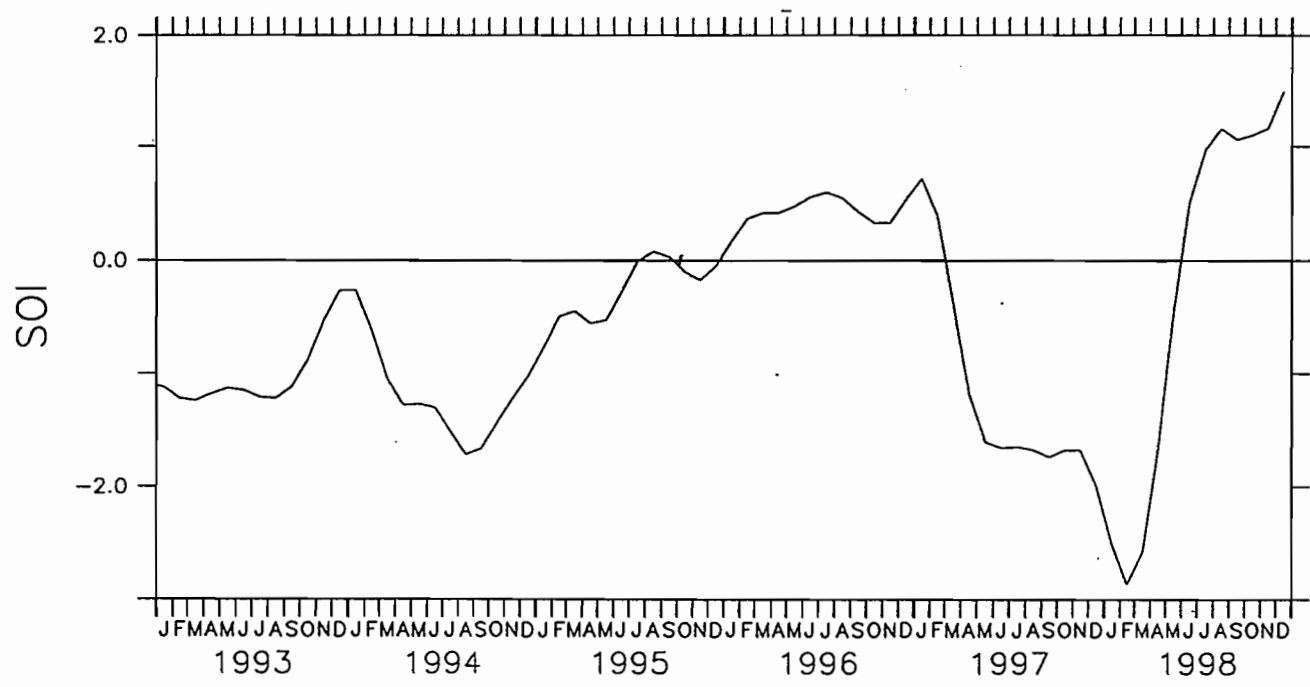


Figure 4 : Indice d'oscillation australe (SOI)

*SST Chaleix fevrier 1991*

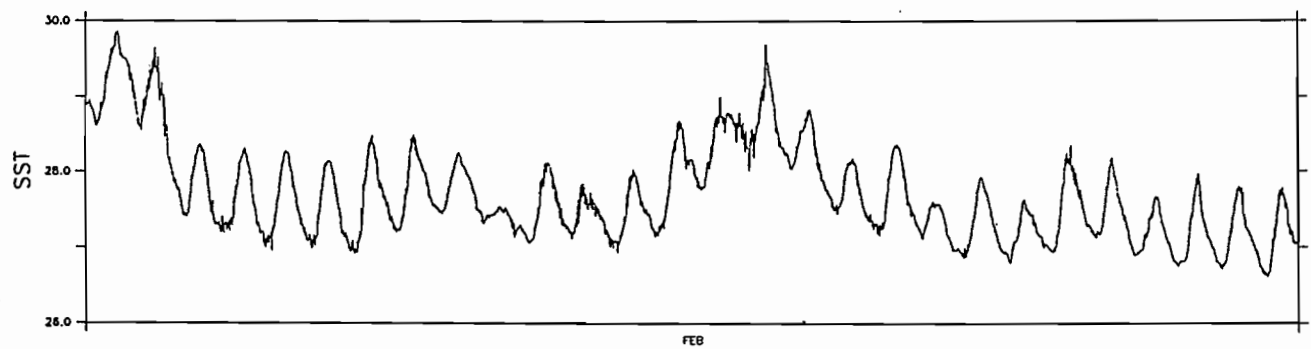


Figure 5 : Température de surface dans le lagon  
à la station Chaleix en février 1991.

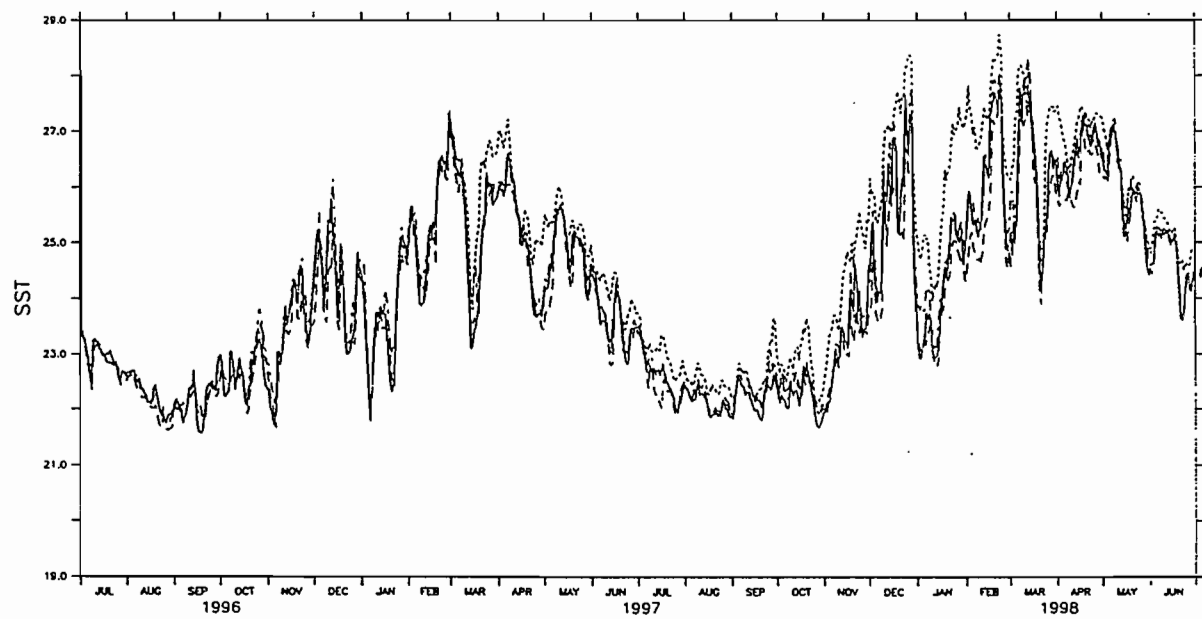


Figure 6 : Température de surface aux stations  
de la côte ouest (Boulari, Dumbéa, Uitoé, Cap Goulvain)  
de juillet 1996 à juin 1998.

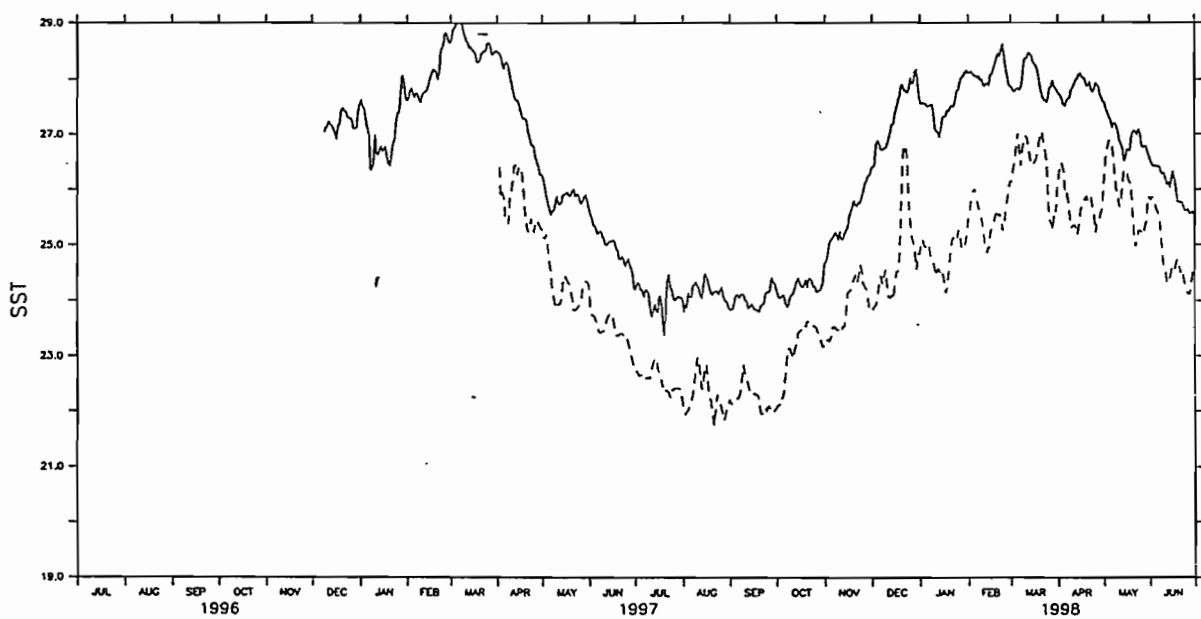


Figure 7 : Température de surface aux stations  
de la côte est (Poindimié et Goro) de juillet 1996 à juin 1998.

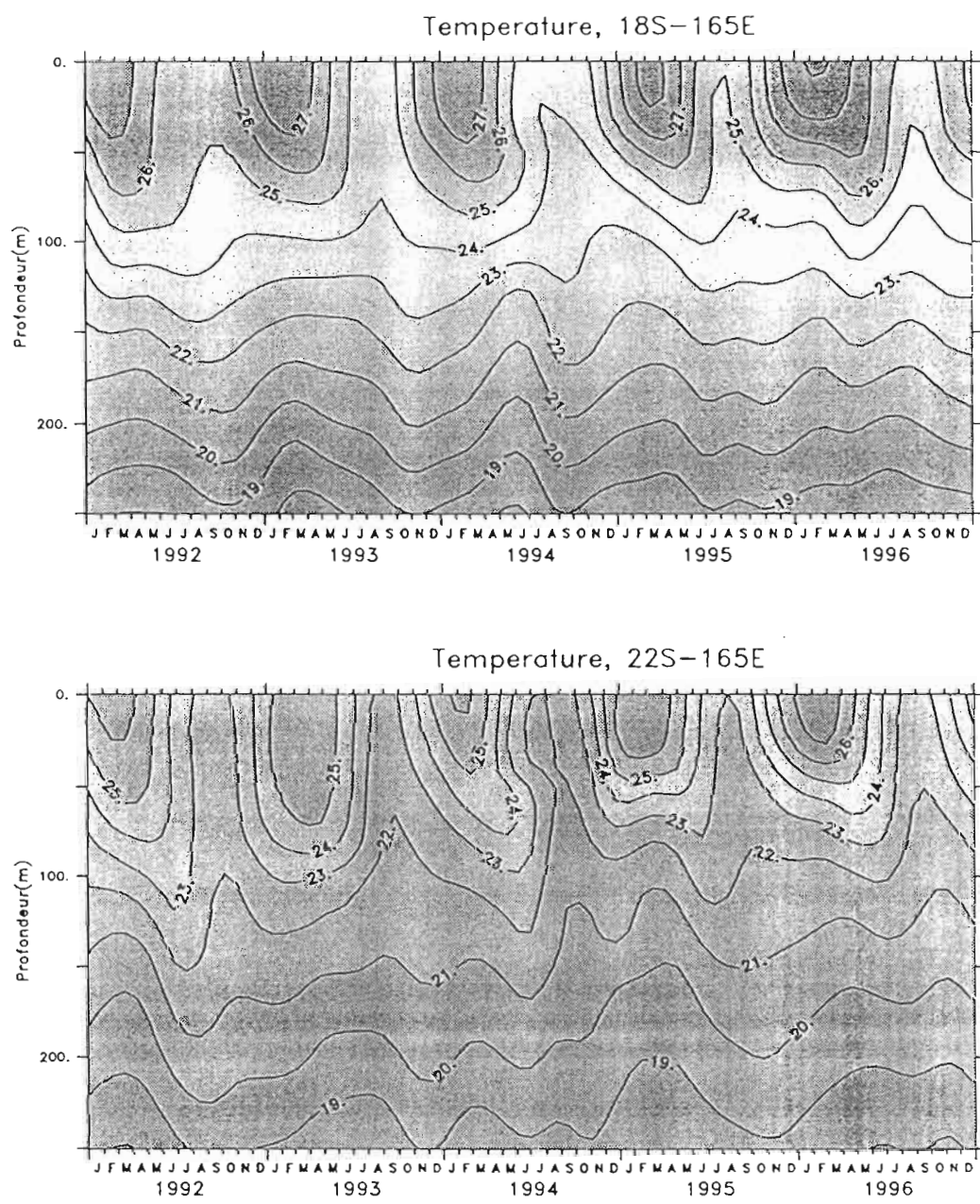


Figure 8 : Evolution temporelle de la structure thermique  
de la couche 0-250m au large  
de la Nouvelle-Calédonie (haut : 18°S - 165°E, bas 22°S - 165°E)

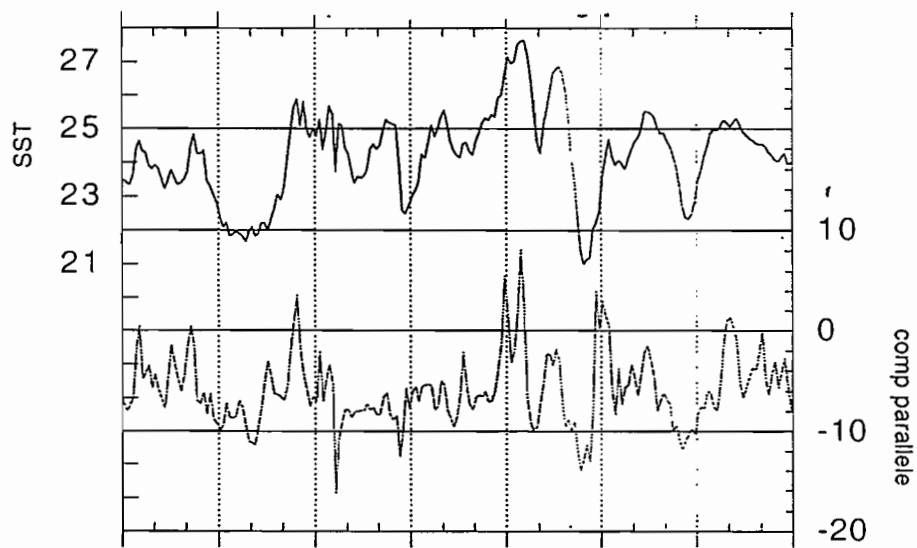


Figure 9 : Observations de la température (Uitoé)  
et de la composante du vent parallèle à la côte (Phare Amédée)  
de novembre 1993 à mai 1994.

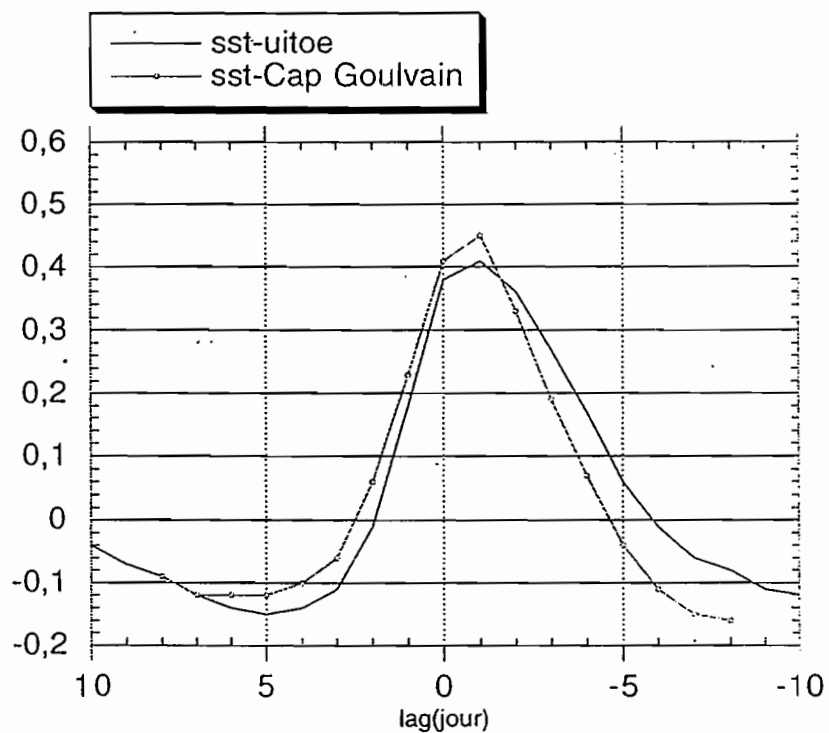


Figure 10 : Corrélation entre la composante du vent parallèle à la côte (Phare Amédée) et delta-T à Uitoé (1) et au Cap Goulvain (2)

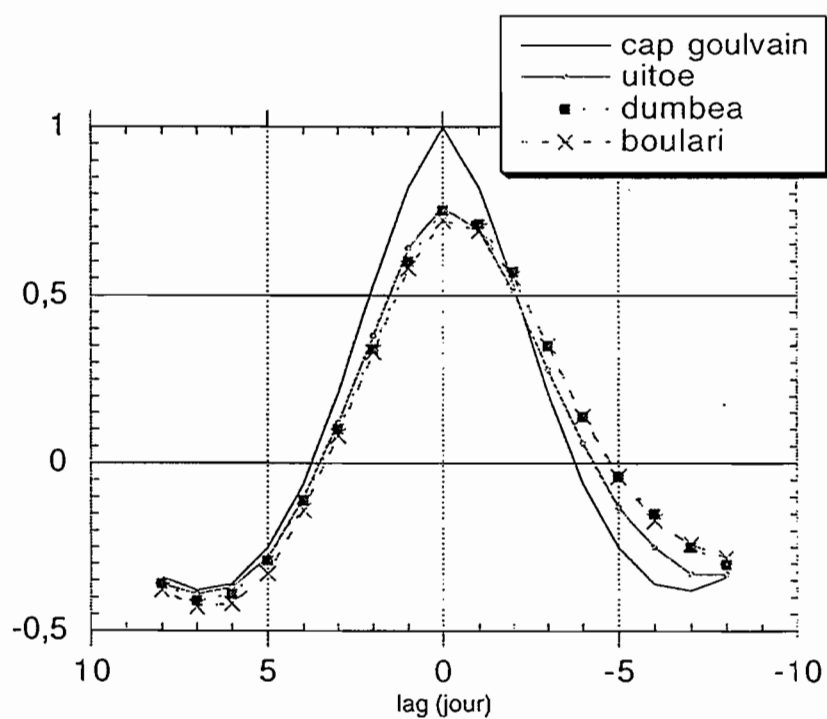


Figure 11 : Corrélation entre delta-T au Cap Goulvain et delta-T au Cap Goulvain (1), à Uitoé (2), Dumbéa (3) et Boulari (4)



Figure 12 : Température de surface du 16 janvier 1998  
issue du traitement IR par le LATICAL.



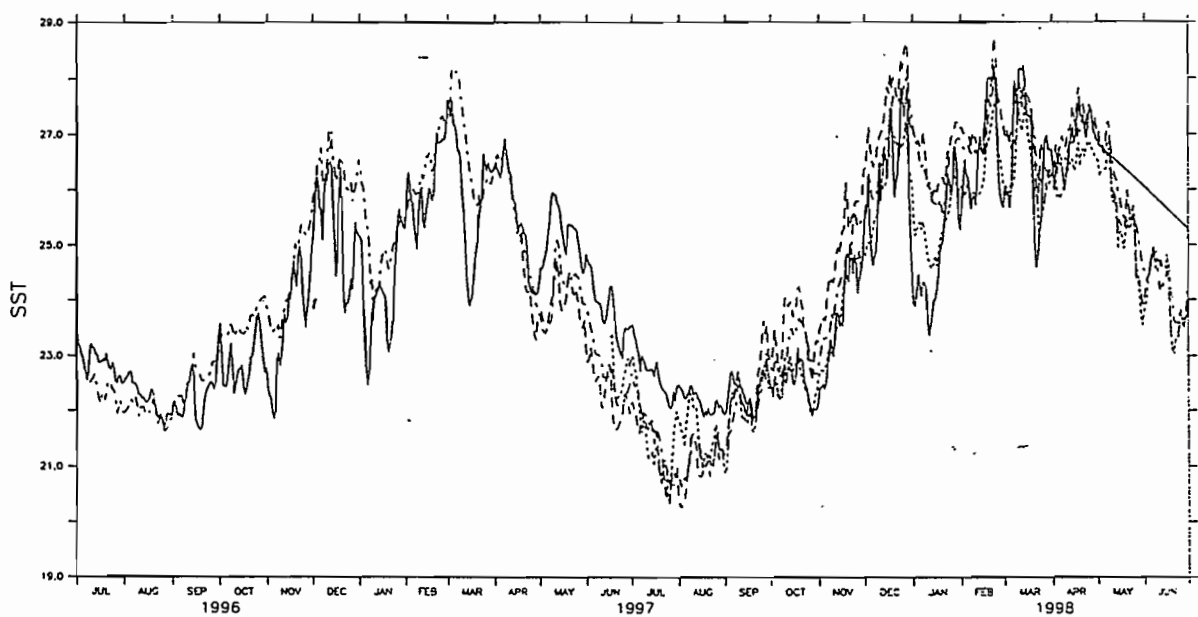


Figure 13 : Température de surface aux stations  
du lagon sud-ouest (Ponton, Phare Amedee, Anse Vata, Récif du Prony)  
de juillet 1996 à juin 1998.

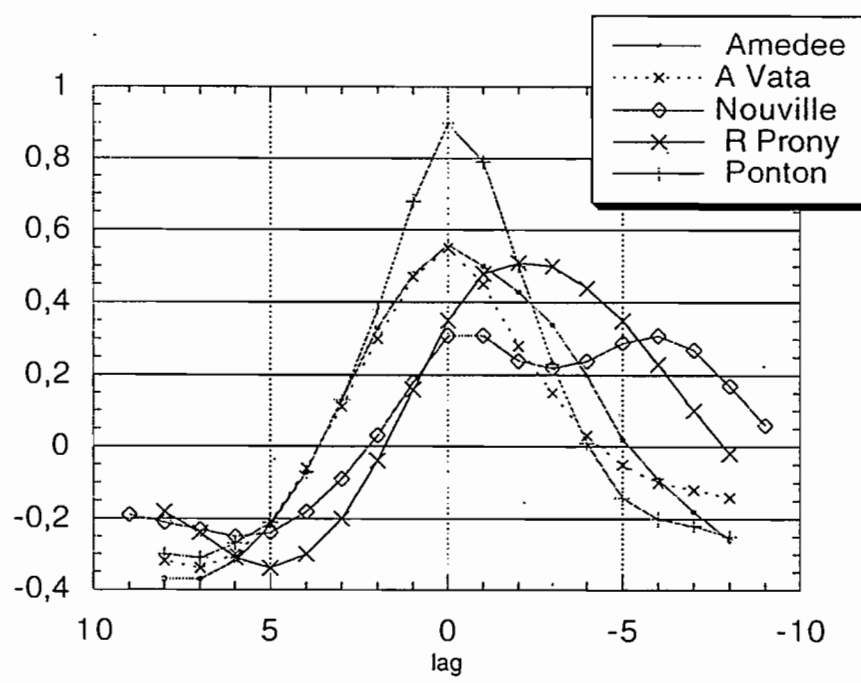


Figure 14 : Corrélation entre delta-T  
à la fausse passe de Uitoé  
et delta-T au Ponton (1), à Anse Vata (2), Nouville (3) et Récif du Prony (4)

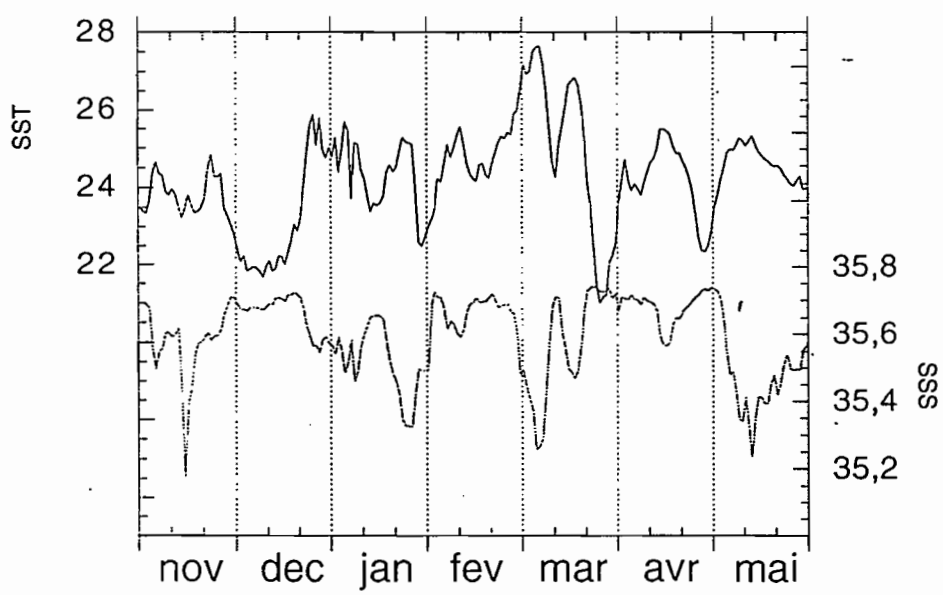


Figure 15 : Observations automatiques  
de la température et de la salinité  
à la fausse passe de Uitoé de novembre 1993 à mai 1994.

